# The dynamic nature of amyloid-beta protein aggregation and its association to Alzheimer's disease

Sílvia Vilaprinyó Pascual

Programa de doctorat en Química Orgànica

Universitat de Barcelona

# The dynamic nature of amyloid-beta protein aggregation and its association to Alzheimer's disease

Sílvia Vilaprinyó Pascual

Tesi doctoral dirigida per:

Prof. Ernest Giralt Lledó

Universitat de Barcelona
Facultat de Química
Departament de Química Orgànica

Dra. Natàlia Carulla Casanovas

IRB Barcelona
Programa de Química
i Farmacologia Molecular



Barcelona 2015

*A tots vosaltres,*
*sou la canya!*

*A en Gerard,*
*al papa i a la mama,*
*a l'avi i a la iaia.*

Success is not final, failure is not fatal:
it is the courage to continue that counts.

---

*Winston Churchill*

# Agraïments

Amb aquesta memòria tanco cinc anys de la meva vida. Cinc anys plens, intensos, durs, a vegades tristos però sobretot bonics. Com no pot ser d'altra manera, tinc molt a agrair, perquè un dels millors regals que m'enduc d'aquesta etapa és cadascuna de les persones que ha contribuït a fer això possible.

Vull agrair en primer lloc als meus codirectors, l'Ernest i la Natàlia. A l'Ernest, per donar-me la magnífica oportunitat de treballar durant aquests anys en el seu laboratori. Li agraeixo en particular la seva visió global, polièdrica i serena, tant en ciència com a nivell personal. A la Natàlia, indubtablement. Ja durant el meu Passa l'Estiu el Parc (estic parlant de l'estiu del 2008!) em va captivar el teu rigor, la teva paciència, la teva passió per les coses ben fetes, la teva persistència. Un dia em vas recordar que la ciència és una cursa de fons, que simplement es tracta de no defallir perquè la feina ben feta no té fronteres ni té rival. Després de tot plegat et puc dir en veu alta que sí, és així, no en tinc cap dubte Natàlia! Gràcies pel teu suport i per totes les oportunitats que m'has donat.

A l'Eva, per la teva amabilitat i eficiència, no sé què faríem tots plegats sense tu. No em vull oblidar dels membres del meu TAC: en Miquel Pons, en Toni Planas i la Marta Vilaseca. Agraeixo els vostres comentaris crítics i constructius. Aprofito per donar les gràcies a tota la *troupe* d'Espectrometria de Masses: la Marina, la Mireia i la Mar. Sou un equip fantàstic i heu sigut un gran suport en cadascuna de les idees esbojarrades que us hem proposat. I ja que estem en el paràgraf dels col·laboradors, també hi han de constar en Lluís i la Daniela, el bio-amyloid team. Gràcies per la vostra simpatia i per prestar-vos sempre a treballar plegats. També vull recordar a la Carmen de microscòpia electrònica, te deseo lo mejor en tu nueva etapa por tierras holandesas.

A l'amyloid team, la meva família científica. A la Montserrat, recordes quan vam començar juntes la nostra peripècia científica amb la ditxosa Aß? Des d'aquell setembre de 2010 hem compartit moltes vivències científiques i personals, en ocasions de decepció o tristesa, però sobretot d'alegria i amb moltes ganes de lluitar i tirar endavant. M'alegro molt haver-te tingut al meu costat. Saps, encara que a vegades sembla que només plogui, l'endemà acaba sortint el sol. O cal que us ho recordi a tu i a en Francesco? Montsi, no em perdràs de vista fàcilment, ens queda molt per celebrar! A la Roberta, la Mazzu, la *mia piccola*. Gracias por tu paciencia, por tus ganas de trabajar, por tu apoyo, por ser mi alter ego cuando yo no podía estar en el laboratorio, por escucharme y aguantarme, eres una gran amiga. Ya sabes

que tampoco te voy a perder la pista, ¿cuándo vengo yo a Italia? A l'Aurelio, un altre que ha hagut d'aguantar la mandona de la Sílvia; gràcies per suportar-me, espero haver-t'ho posat mitjanament fàcil. Crec que vam fer un gran equip amb la Roberta. Això sí, has llegit el correu en el que et convido a la defensa de la meva tesi? Com no vinguis et cantaré les quaranta! A en Martí, el cul inquiet que mai para. La teva alegria i energia s'encomanen, els meus ànims i millors desitjos per la tesi. A en Bernat, el bibliògraf andante, quin crack. Trobo a faltar el teu pragmatisme, la teva sinceritat i sobretot les teves ressenyes bibliogràfiques, ja fossin de contingut científic o sobre les batalletes dels autors. M'alegro que la teva etapa al CRG estigui sent profitosa.

Continuo pel POP i ara Iproteos team, capitanejat per la Tere. A en Jesus, llàstima que haguem compartit poc temps com a veïns de taula, t'agraeixo els consells de futur i la paciència amb els meus histerismes en període d'escriptura. A en Roger, gràcies pels ànims i el *pressing* per posar-me a escriure. Al final no vaig trobar l'ordinador a la pica, però sí a l'escriptori de casa nit i dia. A la Núria, l'alter ego de la Mendi, sempre amb un somriure i disposada a ajudar. Et desitjo molta sort en el futur. A l'Abraham, el *fiestero destroyer*, el ciclista incansable. Encara estic al·lucinada quan et vaig veure arribar amb la bici a Rupit. Felicitats casi-doctor! A Monica, por tu afabilidad y simpatía, eres una trabajadora incansable. ¡Ánimos con la POP y la expresión recombinante de proteínas! Marta, Mendi, si m'ho permeteu us tinc un lloc reservat més endavant.

A qui li dedico un paràgraf sencer per petició expressa és a l'Albert. Ja pensaves que m'havia oblidat de tu! Bé, és que estrictament no ets un Iproteos, només a temps parcial. De fet, això implica que ja podem dinar a la mateixa taula oi? Ara ja no hi ha excusa, que tenim motius a celebrar! Et volia agrair la teva simpatia, les teves paraules sempre justes, el teu suport, el teu detallisme. Ets un gran.

A la Txell, el timó del BBB team. M'has ensenyat que la vida no és esperar a que passi la tempesta, sinó a aprendre a ballar sota la pluja. Per a mi has sigut i ets un exemple de lluita constant, procurant sempre no perdre el somriure. Gràcies pels molts dinars que hem compartit, pels teus consells i per arrancar una riallada d'on calgui. A la Núria Bayó, per les moltes converses sobre tech transfer, sobre tal biotech o tal altra, sobre aquell esdeveniment de BioCat o de CataloniaBio… Llàstima que no vam fer el seminari de gestió de projectes, és una espineta que tindré clavada.

Vull fer una menció especial al postdoc team. A Macarena, ¡qué mujer! Me encanta y te agradezco tu desparpajo, tu simpatía, tu elegante ironía y tu generosidad. Y si faltaba pedir algo más, encima dominas de anticuerpos, modelos celulares, HPLC, cinética enzimática, expresión y purificación de proteínas… ¿hace falta que siga? A Laura Nevola, otra crack. Eres una gran científica, con todas sus letras. Te auguro y te deseo un gran futuro tanto en ciencia (aunque sea en el *dark side*) como en el cine. ¡Oye, aún estoy esperando ver tu corto! A Daniele, qué tio. Bajo amenaza escribo que voy a echar de menos que me chinches o que me preguntes qué tal me va la tesis. ¡Felicidades por tu bodorrio! Espero que Perú os fascine tanto como a mí. Este team también tiene que incluir a Sol, a Rubí y a Miguel y a la Zuri. El lab300 no es el mismo desde que os fuisteis.

A tots els peques, per bé que alguns ja rondàveu per aquest món quan jo encara no havia nascut. A la Júlia, digna successora d'organització d'esdeveniments, et cedeixo el testimoni si no és que el tenies ja. A en Pol, també conegut com a Jean-Pol *horarios*. Quin tio! A la Cris Diaz, una treballadora infatigable. A la Sonia, per la teva afabilitat. A l'Ester, et desitjo molta sort en el futur! A la Mar, l'*alegría de la huerta* amb el permís de la Macarena. A en Salva, ja saps que no deixaràs mai de ser en Pulpito. M'encanta la teva simpatia i les teves ganes d'arrencar somriures, no ho perdis, ets un crack. A la Fuster, quina una! Gironina havies de ser. Ep, això no vol dir res dolent, no te'm posis farruca. Llàstima que hem coincidit en una de les etapes més intenses del meu doctorat, et desitjo molta sort en el teu. Quan dius que muntem el Salvame Deluxe català?

Evidentment, a en Benjamí. Saps que ja hem celebrat les bodes de plata? Es diu ràpid. Ara què faré sense tu? M'ha fet molt feliç veure que aquests últims cinc anys han servit per apropar-nos una miqueta més, ara espero no perdre't el rastre. Doctor Oller, t'auguro un futur brillant en ciència o en el que et proposis, és el mirall en el que tots ens volem reflectir.

A Ale, Alessandra, la Mela. Ya lo sabes, *mi manche*. Compartimos uno de los mejores años de mi doctorado, por no decir el mejor. Recuerdas las fiestas en casa de Mariano o Giulio, las excursiones a Cadaqués y otros rincones de Catalunya, el viaje a Salerno, el concierto de Mando Diao… ¡Cuántos buenos recuerdos! Y por muchos años más, ahora solo falta escoger la siguiente capital europea.

Indiscutiblement, a tot el Grupo G. Començo per en Pep, l'espatlla en la que tantes vegades m'he recolzat, les orelles que tantes vegades m'han escoltat, les paraules que tantes vegades m'han aconsellat i, òbviament, el pepchero en el que tantes

vegades he penjat l'abric! Ets de les persones més bondadoses, divertides i alegres que he conegut, ets un amic en majúscules. I quantes vegades t'he dit que feu bona parella amb l'Adri? Cuida-la, que no te la mereixes. A en Vila, el meu samurai. Et trobem massa a faltar, el Grupo G ja no és el que era i jo em penedeixo de no haver anat mai als mítics piknics electrònics. Saps, últimament m'ha sortit un tic: allà als volts de les 7 de la tarda el ratolí sembla que apunta cap a Spotify esperant que soni Imagine Dragons, recordes? I al loro, aviat ens tindràs rondant pels carrers de NY! A la Cris, no ens enganyem, la més jove de tots plegats. Quina energia, quin cul inquiet! Per a mi també ets un exemple d'esperit de superació: encara al·lucino que fa uns anys tinguessis la teva pròpia perruqueria i que a dia d'avui estiguis al peu del canó d'un laboratori de química. T'agraeixo en particular les converses que hem compartit a la cafeteria esmorzant, les teves abraçades els dies que em veies apagada o trista i el teu detallisme. A Laura, la Mendi, la perica, la chica que baila salsa, mailof. No sabes cuánto hecho (ay perdón, echo) de menos que me hagas de macho, sólo me gusta contigo mi amol (guiño guiño). Han sido cinco años de muchas risas, batallas contra enzimas, clases de salsa dentro y fuera de Mojito, cotilleos, cortados con espumita, mediodías al sol (¡qué lagartas!), confidencias, consejos y, en definitiva, de una gran amistad. A ver si algún día se me pega un poco de tu estilo, de tu castellano *made in* RAE, de tu empeño y capacidad de trabajo, de tu simpatía, de tu detallismo y de tu generosidad. ¡Eso sí, tu puntualidad no por favor! Finalment, a la Marta, per escoltar-me i aconsellar-me com ningú, què hauria fet sense tu! Admiro el teu afany de superació, la teva empenta, la teva força moral i la teva capacitat per sobreposar-te a les circumstàncies. Marta, ets molt forta i tens un cor que no t'hi cap al pit! Ja saps que l'expressió és figurada, no literal. També voldria agrair-vos a tu i en Pau deixar-me compartir amb vosaltres un dels dies més importants a les vostres vides. Sou una parella fantàstica, sou un gran equip!

No em vull deixar els Albericios: la Judit Tulla, la Judith, l'Helena, en Jan, en Markus, l'Ivan, l'Anais, en Pau, la Carol… Y a Juan, ¿a quién chincharé ahora? ¿A quién saludaré a las 9 de la mañana un domingo en el lab? També han de constar els alumni del lab300: l'Anna-Iris (quina crack!), en Bernat Guixé, en Peterini, la Marta Pelay, la Laia Miret, en Xavi Just, la Janire, l'Adriana, l'Andrey, en Michael, en Giacomo.

Els IRBDocs han sigut uns magnífics companys de camí, hem compartit cinc anys ofegant les penes i celebrant les alegries en bona companyia. A en Giulio, per saber-nos escoltar i aconsellar mútuament, per compartir els moments de dificultat i d'alegria, per deixar-me refugiar quan ho he necessitat. M'alegro molt per totes les

coses bones que t'estan passant. A Giorgia, por tu sonrisa incansable, tu alegría y tu energía positiva. Gracias en especial por este último año de casas rurales, vermuts, calçotadas, GioJoSi's y body pump's. ¡Te aprecio un montón! A Pablo, mi caballero de la armadura oxidada. Siento haber sido a veces dura contigo, eres una gran persona. A Lorena Pereira, por ser una fuente de inspiración y d'*empenta*. Sin duda, eres la superwoman del siglo XXI. No m'oblido d'en Mariano, la Lore i l'Eulàlia. The last but not (at all) the least, to Arzu and Ilker. You are a great couple, always so generous, so big-hearted, so caring, and with the right words to say. I want to thank you for all these years you have always been by my side! I am missing you guys.

También quiero recordar a tres personas a las que no veo muy a menudo, pero de quien espero haberme ganado su amistad. Estas líneas son para Jessi, Ágata y Joana. Vull fer constar els meus Riera's preferits, l'Àlex i la Sílvia. Us he promès massa cafès que no he complert, però no he sigut tan mala amiga oi? Sort pel futur, siguem on siguem. Recordo amb molt de carinyo a l'Anna Montaner, que ja m'han dit que has tornat a començar el doctorat, ànims! No voldria oblidar-me dels companys del PhD Symposium, així com tampoc d'en Paco, de l'Angeles i de la Maria. També vull deixar per escrit la simpatia i l'amabilitat que sempre han caracteritzat la Patricia Nadal i la Leyre.

From my research stage in Cambridge, I would like to acknowledge first the kindness of Professor Dobson, thank you for hosting me and for your time. I would also like to acknowledge Karen for being such an efficient and wonderful secretary. Many thanks to the people at the Klenerman and Knowles groups. Specifically, I would like to thank Nadia, Anna, Paolo and Johnny for your mentorship. Anna, I enjoyed so much the lunch we shared at your college, thank you! I also recall the friendliness of Wilson and Julien. No me olvido de mis primeros compañeros de piso: Alex, Mónica y la tierna Carmela. Després ja vaig conèixer la Núria, en Nacho, en Jordi, l'Anna, l'Arun i tinc un record particular d'en Volker. Voldria agrair especialment les moltes tardes, birres, sopars i converses compartides amb en Pau i l'Ares, sou uns grans amics. Queda pendent la trobada a Barcelona, no me n'oblido! Por último, quería agradecer el apoyo y el cariño de David. Sin ti no hubiera sobrevivido mis últimas tres semanas en Cambridge. Gracias por tu paciencia, por tu tiempo y por tu respeto, eres una gran persona. Espero no perderte la pista.

Als amics de sempre. A la Marilu, ay perdón María, ¿o te puedo llamar Chu? ¡Qué mujer! Ya sabes cuánto te admiro y cuánto tengo que aprender de ti. No sé cómo agradecerte nuestros Santa Anna's, nuestros Paninos Silvestre's, nuestros paseos por

Sarrià… Ah y que me hayas venido a buscar tantas veces al PCB! Eres una grandísima amiga, nunca me has fallado. Que sea por muchísimos años más, estemos donde estemos. Quiero que sepas que no tengo ninguna duda que lo que te propongas lo conseguirás, ¡a por todas! A Joang, porque a pesar de la intermitencia en nuestras quedadas, seguimos siempre ahí. Me alegro mucho por tus éxitos empresariales, qué crack. Ah y cásate ya con Núria, que Chu y yo queremos ir de bodorrio. A Pamela, porque a pesar de la distancia y de que nos vemos sólo una vez al año, me alegra un montón estar en contacto contigo. Ánimos con el doctorado y muchísimas felicidades por tu próxima boda. ¡Te mereces alguien que te cuide tanto como Carles!

A la Gabriela i a la Irena, les meves amigues de tota la vida. Últimament no ens veiem amb la freqüència que voldríem, però quan ens veiem és com si no haguessin passat els dies o els mesos. Gaudeixo molt de les quedades al cine o al teatre, no ho perdem si us plau! Gabriela, ànims amb els teus projectes, no defalleixis. Irena, sort amb el doctorat, encara que sé que no la necessites, ets una treballadora infatigable.

A les noies, a cadascuna de vosaltres pel vostre suport durant tot aquests anys i per saber que puc contar amb vosaltres. Hem crescut juntes, hem compartit viatges, confidències i consells, cadascuna fent el seu camí. En aquests últims cinc anys hem viscut grans moments plegades com ara el casament de la Hai (quines ploreres d'emoció!), sempre al costat les unes de les altres. No ho podem perdre, encara menys ara que sembla que vindran bones notícies una darrera de l'altra! A la Blanca, per la teva rauxa i pel teu seny. A la Hai, pel teu entusiasme i pel teu rigor. A la Carla, per la teva entrega i per ser tan quadriculada (m'encanta!). A la Deutch, la nostra empresària gironina amb l'outfit perfecte sempre apunt i les ganes de festa sota la pell. A la Hoti, per ser el nostre pardalet. A l'Eli, pel teu afany de superació i per poder comptar amb tu encara que estiguis a 6500 km de distancia. Gràcies noies!

A en Miki perquè amb els bons i els mals moments has contribuït a que sigui la persona que sóc a dia d'avui.

A la família, la Vilaprinyó-del Perugia i els Clapés. Voldria fer una menció especial a la Graupe i a la Lourdes per donar suport a la família en els moments més difícils i a l'Ana Maria por cuidar tan bien del avi y prepararme las mejores cremas de calabacín.

Ja per acabar, vull agrair per sobre de tot el suport incondicional dels meus avis, del meu germà i dels meus pares. A la iaia, perquè eres única i no saps quant et trobem a faltar. A l'avi, per transmetre'm la més pura serenitat i estimació. A en

Gerard, perquè ets el pilar en el que tots ens recolzem. Al papa, per aferrar-se a la vida quan tocava. I a la mama, per tenir una paciència infinita i suportar la pesada de la seva filla.

# Index

# Abbreviations

| | |
|---|---|
| A | Alanine |
| AA | Ammonium Acetate |
| AD | Alzheimer's Disease |
| APP | Amyloid Precursor Protein |
| APS | Ammonium Persulfate |
| Aß | Amyloid-Beta Protein |
| BE | Back Exchange |
| $Ca^{2+}$ | Calcium Cation |
| CD | Circular Dichroism Spectroscopy |
| CL | Cross-Linked |
| CSF | Cerebrospinal Fluid |
| cTCCD | Confocal Two-Color Coincidence Detection |
| CV | Column Volumes |
| D | Dimer |
| DMSO | Dimethyl Sulfoxide |
| Dnp | 2,4-Dinitrophenyl |
| DTT | Dithiothreitol |
| ESI-IM-MS | Ion Mobility coupled to ESI-MS |
| ESI-MS | Electrospray Ionization Mass Spectrometry |
| F | Phenylalanine |
| FA | Formic Acid |
| fAD | Familial AD |
| FE | Forward Exchange |
| G | Glycine |
| GdnHSCN | Guanidinium Thiocyanate |
| HCl | Hydrochloric Acid |
| HDX | Hydrogen-Deuterium Exchange |
| Hp | Heptamer |
| Hx | Hexamer |
| icv | Intracerebroventricular |
| IDE | Insulin Degrading Enzyme |
| IM | Ion Mobility |
| IMAC | Ion Metal Affinity Chromatography |
| IPTG | Isopropyl ß-D-1-Thiogalactopyranoside |
| ISF | Interstitial Fluid |
| K | Lysine |
| $K_m$ | Michaelis-Menten Constant |
| LC-HRMS | Liquid Chromatography High Resolution Mass Spectrometry |
| LDH | Lactate Dehydrogenase |
| LMW | Low Molecular Weight |
| LMW_CL | LMW Cross-linked |
| LTD | Long Term Depression |
| LTP | Long Term Potentiation |
| M | Monomer |
| m/z | Mass to Charge Ratio |
| Mca | (7-Methoxycoumarin-4-yl)Acetyl |
| MD | Molecular Dynamics |
| $Me_2S$ | Dimethyl Sulfide |

| | |
|---|---|
| MTT | 3-(4,5-Dimethylthiazol-2-yl)-2,5-Diphenyltetrazolium Bromide |
| $NaN_3$ | Sodium Azide |
| NFT | Neurofibrillary Tangles |
| $NH_4I$ | Ammonium Iodine |
| NMR | Nuclear Magnetic Resonance |
| O | Octamer |
| P | Proline |
| Pt | Pentamer |
| PBS | Phosphate-Buffered Saline |
| PET | Positron Emission Tomography |
| PICUP | Photo-Induced Cross-Linking of Unmodified Proteins |
| PK | Proteinase-K |
| $PrP^c$ | Cellular Prion Protein Receptor |
| $P_{fd}$ | Fully Deuterated Species |
| $P_{pd}$ | Partially Deuterated Species |
| R | Arginine |
| ROS | Reactive Oxygen Species |
| RP-HPLC-PDA | Reverse-Phase High Pressure Liquid Chromatography coupled to Photodiode Array Detector |
| RT | Room Temperature |
| $Ru(bpy)_2^{3+}$ | Tris(2,2'-Bipiridil)-Dichlororuthenium(II) Cation |
| S | Serine |
| sAD | Sporadic AD |
| SAR | Structure-Activity Studies |
| SDS | Sodium Dodecyl Sulfate |
| SDS-PAGE | SDS Polyacrylamide Gel Electrophoresis |
| SEC | Size Exclusion Chromatography |
| SICM | Scanning Ion Conductance Microscopy |
| SM fluorescence | Single Molecule Fluorescence Microscopy |
| sNMR | Solution NMR |
| SPPS | Solid-Phase Peptide Synthesis |
| Sub-CMC | Concentration Lower than Critical Micellar Concentration |
| Supra-CMC | Concentration Higher than Critical Micellar Concentration |
| Te | Tetramer |
| TEM | Transmission Electron Microscopy |
| TFA | Trifluoroacetic Acid |
| Tg | Transgenic |
| ThT | Thioflavin T |
| TIRF | Total Internal Reflection Fluorescence |
| Tr | Trimer |
| Tris·HCl | Tris(Hydroxymethyl) Aminomethane Hydrochloride |
| Tris·base | Tris(Hydroxymethyl) Aminomethane |
| u | Atomic Mass Unit |
| $v_{max}$ | Maximum Initial Velocity of Substrate Degradation |
| WT | Wild Type |

| | | | |
|---|---|---|---|
| XTT | 2,3-Bis-(2-Methoxy-4-Nitro-5-Sulfophenyl)-2H-Tetrazolium-5-Carboxanilide | $^{35}$Met | 35-Methionine |
| | | $^{35}$MetO | 35-Methionine Sulfoxide |
| Ω | Collisional Cross-Section | | |

# Introduction

## Alzheimer's disease

Amyloid diseases comprise around 50 disorders characterised by the misfolding and aggregation of proteins into insoluble amyloid deposits in specific organs or tissues. These deposits are made up of misfolded proteins arranged in a cross ß-sheet structure, in such a way that they are able to bind the histochemical dye Congo Red.[1] Among the aforementioned disorders, some are neurodegenerative such as Parkinson's disease, amyotrophic lateral sclerosis, prion diseases or Alzheimer's disease (AD).

AD is a chronic and progressive brain disorder that accounts for 60-70% of the cases of diagnosed dementias. Symptomatically, AD patients are first unable to retain recent memories, and their pathology devastatingly evolves to a full cognitive and functional impairment.[2] 5% of AD cases are associated to familial mutations that advance disease onset before the age of 60, and they are classified as early-onset AD or familiar AD (fAD). The remaining cases are idiopathic in origin, being grouped as sporadic AD (sAD). In sAD, the prevalence is doubled every 5 years after the age of 65, being age the main risk factor.[3] In 2011, there were 35 million AD patients around the globe and the numbers are expected to triplicate by 2050 due to the rising life expectancy.[4] With such alarmingly increasing social and economic burden, AD has become one of the top first public health priorities worldwide.

Back in 1906, Dr. Alois Alzheimer described for the first time AD neuropathology in a 51-year-old woman. The patient had suffered over the last 5 years a progressive loss of memory, and a decline of time and spatial orientation.[5] Post-mortem examination of her brain revealed atrophic areas and the presence of spherical deposits and neurofibrillary pathology. This histopathology was the consequence of neuronal loss, and accumulation of extracellular amyloid deposits and intracellular neurofibrillary tangles (NFTs). Importantly, these three elements are still currently the three diagnostic hallmarks of AD.

More than thirty years ago, the scientific community started to uncover the molecular mechanisms underpinning AD. Analysis of extracellular deposits showed that they were mainly composed of a short protein named amyloid-beta protein (Aß),[6,7] whereas NFTs were made up of abnormally hyperphosphorylated tau, a microtubule-stabilizing protein.[8] These two findings raised two confronted hypothesis on the possible AD causative agent, namely the amyloid hypothesis[9] and the tau hypothesis.[10] Nowadays, it is widely accepted that tau phenotype arises downstream Aß,[11] with tau being an effector in Aß neurotoxicity[12] (see Appendix A).

## Amyloid-beta protein and the amyloid cascade hypothesis

Aß is the metabolic product of two aspartyl proteases over a membrane protein named amyloid precursor protein (APP).[13] Sequential action of ß- and γ-secretase over APP releases Aß to the extracellular matrix. γ-secretase cleavage is not specific and many Aß alloforms are produced, ranging from 37 up to 43 amino acids.[14] The most abundantly produced is the 40 amino acids variant, known as Aß40, whilst the most strongly linked to AD neuropathology is Aß42, which has two additional amino acids at the C-terminus.[15] Aß is also produced lifelong in healthy people, presumably exerting antimicrobial activity.[16] It is the aberrant processing of the protein that triggers its accumulation and self-assembly, first into intermediate and transient oligomer species, that evolve into protofibrillar structures that ultimately yield the fibrils deposited in amyloid plaques (Figure I1).

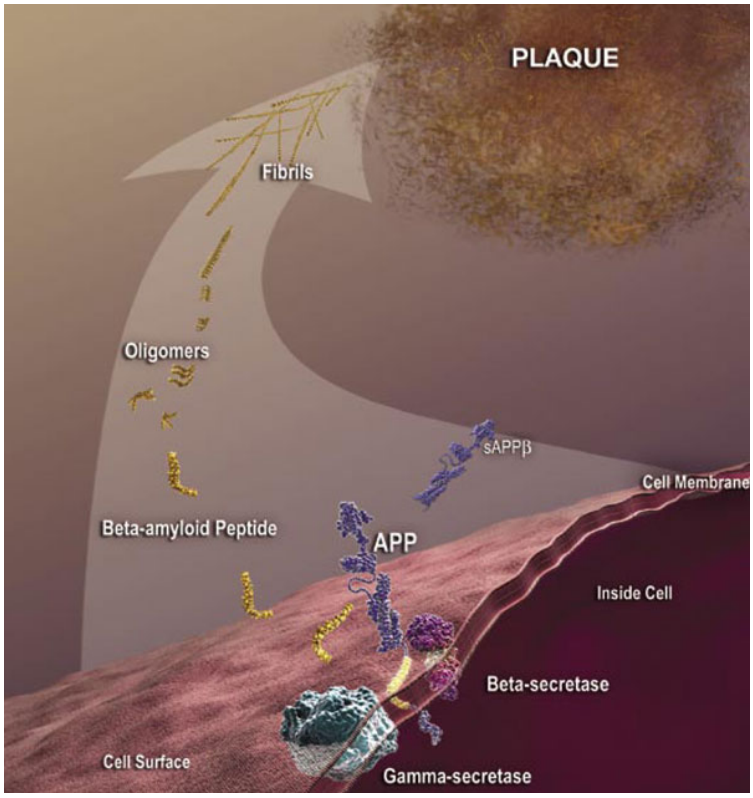


***Figure I1.*** *Schematic representation of Aß formation by sequential cleavage of ß- and γ-secretases over APP. Aberrant processing of Aß triggers its accumulation and self-assembly up to the fibrils, which are the main component of amyloid plaques. The image is copyright from the National Institute of Health (NIH).*

Many evidences support the central role of Aß in AD,[17] even though the exact link to the observed neurotoxicity is still unknown. These evidences come from genetic studies, transgenic mouse models and biochemical assays. First, all AD-linked mutations in fAD are associated to Aß, none of them to tau or other proteins.[3] Mutations in APP gene, flanking or inserted in Aß region, enhance Aß production and/or aggregation; mutations in presenilins – γ-secretase catalytic sites – shift APP processing towards the formation of Aß42, the more aggregation-prone alloform.

Moreover, APP gene is located in chromosome 21 and AD neuropathology is invariably seen in Down's syndrome, originated from trisomy precisely in chromosome 21. Second, transgenic mice bearing human APP gene develop plaque deposition and behavioural abnormalities, reproducing some human AD phenotypes.[18] Other models expressing the allele ε4 of human ApoE, a major AD risk factor, also develop plaque deposition. Third, synthetic Aß preparations have been extensively shown to be toxic to neurons both *in vitro* and *in vivo*, and their intracerebroventricular (icv) injection in human APP transgenic mice advance plaque deposition.[19]

At first, amyloid plaques were believed to be the causative agents in AD.[20] However, subsequent studies revealed that plaque count correlated weakly to cognitive deficits,[21,22] and other reports claimed that patients displaying plaque deposition didn't have any AD clinical symptom.[23] By contrast, the soluble Aß pool was a good predictor for patient cognitive impairment.[21,22] Consistently, soluble Aß should be able to diffuse much easily than fibrils around the brain and into synapses to exert their toxic effect.[1] The quest to elucidate the identity and the mechanism by which this soluble Aß exerts neurotoxicity is underway.

## Biomarkers and Therapeutics

Biomarkers are fundamental tools for clinical diagnosis of diseases as well as to monitor their progression. Biomarkers are also key assets in patient selection in clinical trials and their subsequent follow-up during the length of the study. Recently, the scientific community agreed in two Aß-centric biomarkers for AD: (i) positive signals in positron emission tomography (PET) imaging of plaques with radioactive Aß binding ligands, and (ii) low Aß42 concentration or Aß42:Aß40 ratio in cerebral spinal fluid (CSF).[24] Both biomarkers are convergent, they appear 10 years before any symptom and they display 85-95% sensitivity and specificity for prodromal and dementia stages.[25] AD diagnosis at stages when there are no evident clinical symptoms is fundamental since alterations in Aß metabolism and plaque deposition are occurring years before cognitive deficits appear.[26,27]

Nonetheless, there is still need for standardization of protocols and both Aß biomarkers present important drawbacks. First, PET imaging has a high economic cost and requires the production of radioactive ligands on-site – due to their short lifetimes – in cyclotron facilities, which are scarce. Second, CSF extraction involves lumbar puncture which is an invasive procedure for patients and requires specific training for physicians.[24] Currently, there are proteomic studies in the search for

additional CSF biomarkers[25] or blood-borne metabolites[28] specific to AD, which might also bring insights into other concurrent pathological events.

Nowadays, there are only four drugs in the market directed to AD.[29] The four of them are symptomatic, which transiently improve cognition, behaviour and functional state. Donepezil, Rivastigmine and Galantamine are cholinesterase inhibitors that enhance cholinergic transmission, which has been weakened by the loss of cholinergic neurons featured in AD. Memantine is an antagonist of N-methyl-D-Aspartate receptor whose mechanism of action is through the reduction of glutamate excitotoxicity at the synapse.

Disease-modifying pharmaceuticals have been designed based on three main therapeutic approaches: (i) decreasing Aß production by inhibition or modulation of ß- and γ-secretases, (ii) enhancing Aß clearance by active or passive immunotherapy, and (iii) tackling alternative pathologic pathways.[30] So far, none of the designed molecules that have undergone clinical trials have succeeded in reaching the market.[31] Drugs halting Aß production have failed because of their low inhibitory activity or because the inhibition of secretases prevented the cleavage of other vital substrates, deriving in detrimental side-effects.[32] Therefore, current research aims to develop molecules with higher selectivity for inhibition of APP processing. Several reasons have been reported to account for the failure of immunotherapeutic approaches developed to date. Either (i) because the selection of patients in the clinical trials was not accurate enough, (ii) because their disease stage was far too advanced for immunotherapy to improve their cognitive and functional performance, (iii) because of undesired side-effects such as autoimmune meningoencephalitis or brain edema,[33] or (iv) because of lack of target engagement.[34] Therefore, adequate selection of patients and of antibodies is required for future positive results in immunotherapy. Finally, alternative therapeutic approaches rely on the direct inhibition/modulation of Aß or tau aggregation. There are few promising candidates such as Methylthionimium, a tau aggregation inhibitor currently in phase III clinical trials.[30]

## The complexity underlying Aß aggregation

Aß-directed strategies are eminent in AD therapeutic interventions. In fact, many efforts have been devoted to the elucidation of the Aß neurotoxic structure(s) for proper design and targeting of therapeutic agents. However, such quest has been an enormous challenge to structural biologists due to the highly heterogeneous and

dynamic nature of Aβ aggregation. Multiple aggregation pathways are accessible and selected depending on the current physiological conditions and the presence of specific cofactors.[35,36] This is simply reflected by the huge variety of neurotoxic oligomers from various sources that have been reported to date: ADDLs,[37] protofibrils,[38] amylospheroids,[39] sodium dodecyl sulphate (SDS)-stable dimers and trimers from cell cultures,[40] Aβ*56,[41] SDS-stable dimers from AD brains,[42] dodecamers,[43] and annular protofibrils.[44]

Traditional structural biology techniques such as X-ray crystallography and solution nuclear magnetic resonance (NMR) cannot be applied, since Aβ oligomers do not form crystals and large multimers tumble too slowly for NMR. The *in vitro* characterization of each of the aggregation states sampled by Aβ requires the complementary use of several biochemical and biophysical techniques, informative of all primary, secondary, tertiary and quaternary structures.[35] Differences among these techniques comprise the applicability along the aggregation process, the ability to differentiate coexisting populations, the capacity to overcome the dynamics of the system and the concentration required to perform the assays. For instance, low molecular weight species have been characterised by size exclusion chromatography (SEC),[45] chemical cross-linking coupled to SDS polyacrylamide gel electrophoresis (SDS-PAGE) analysis,[46] ion mobility coupled to electrospray ionization mass spectrometry (ESI-IM-MS)[43,47] or solution NMR.[48] Structural models of fibrils[49] have been built upon constraints obtained from X-ray fiber diffraction,[50] electron cryo-microscopy[51] or solid state NMR.[52-54] Complete picture of the whole Aβ aggregation process have been taken by single molecule fluorescence microscopy (SM fluorescence),[55] hydrogen-deuterium exchange (HDX) coupled to MS,[56,57] or using specific chemical probes[58] such as thioflavin T.[36]

Nonetheless, most of these aforementioned structural analyses of Aβ aggregation overlook a fundamental parameter which is the intrinsic dynamism of this process. The classical linear relationship between structure and activity is not solid enough to dissect Aβ aggregation and its link to neurotoxicity. Instead, we propose the triad structure-dynamics-activity as the most reliable approach to uncover the (transient) structure of Aβ neurotoxic oligomer(s). The focus of the remaining Introduction will be on structural techniques that also provide information on the dynamics of the aggregation process. This analysis will give rise to a review article: Vilaprinyó-Pascual S.; Carulla N. Tackling the dynamic nature of amyloid-beta protein aggregation, *in preparation*.

## Approaches to tackle Aß dynamics

The first consideration with respect to the study of Aß aggregation process is the source from which the peptide has been obtained. Brain derived Aß is extremely limited and concerns on the degree of purity and homogeneity have arisen because of its origin and the extraction procedures developed so far.[59] Because of these limitations, *in vitro* approaches rely on Aß produced by solid-phase peptide synthesis (SPPS) or from recombinant DNA technology.[35,59,60] On the one hand, Aß SPPS is very challenging due to the high hydrophobicity of the sequence and its high tendency to aggregate, even on resin. The consequent amino acid deletions, racemizations and oxidations have been partially overcome by innovative methodologies.[61-63] On the other hand, few successful reports on recombinant Aß production have been described to date, some of which do not strictly generate the wild type sequence.[64,65] Of note, the minute impurities generated in SPPS of Aß have been claimed to bias Aß aggregation, whereas the extremely homogenous recombinant Aß has been pointed to provide a more accurate description of the process.[65,66] Besides, *in vitro* studies have basically focussed on recombinant or synthetic Aß40 and Aß42 alloforms, whereas *in vivo* Aß pool also contents minor variants ranging from 37 to 43[67] amino acids long and N-termini truncated forms, all of which might also be phosphorylated, oxidated or nitrosilated to some extent.[14,68] Furthermore, there is a current wave of criticism on the lack of consensus on sample preparation and standardization, which may explain the huge variety of neurotoxic oligomers described and the many alternative toxic pathways reported to date (see Appendix A).[69,70]

Taking into account these considerations, the dynamic nature Aß aggregation has been studied *in vitro* by a specific set of techniques, namely ESI-IM-MS, chemical crosslinking, solution NMR (sNMR), SM fluorescence and HDX. In general terms, these techniques afford the determination of the stoichiometry, the relative population, and the shape of Aß multimers at particular aggregation stages as well as their molecular interactors, with a high temporal resolution.

### ESI-IM-MS

ESI-IM-MS is a powerful emerging technique which allows the simultaneous determination of size, relative population and shape of a heterogeneous mixture of covalent and/or non-covalent multimers and conformers.[71] Particularly, ion mobility (IM) allows the separation of species according to their collisional cross-section, providing an additional dimension where multimers and/or conformers of identical

mass to charge ratio (m/z) are effectively separated. This collisional cross-section is informative of overall shape and molecular size, delivering structural insights to the analysed molecules[43,47,72,73] which can be rationalised through molecular dynamics simulations.[47,74] Furthermore, ESI-IM-MS is ideal to the study of highly dynamic and transient molecular systems such as Aß aggregation, since sample is analysed in the extremely short millisecond time frame. Importantly, ESI-IM-MS studies have been directed to the characterization of Aß oligomers formed at early stages of aggregation. This is due to highly hydrophobic and heterogeneous nature of the species formed along the process, which ultimately preclude their ionization and detection.

The first ESI-IM-MS studies on early Aß oligomerization started a decade ago and throughout the years conflicting results have been obtained. Bernstein *et al*[72] showed that filtered synthetic Aß42 solutions were composed of monomers up to tetramers, hexamers and dodecamers, whereas Aß40 proceeded only through monomer up to tetramer.[43] Moreover, they showed that Aß40 was able to block the reported Aß42 oligomerization pattern yielding mixed 2:2 Aß40:Aß42 tetramers.[75] A few years after, recombinant Aß40 studies undertaken with a much more sensitive mass spectrometer allowed the serial detection of monomers up to hexadecamers, and different conformers thereof.[47] The work developed in our group has revealed that both synthetic Aß40 and Aß42 oligomerise through a similar pathway mainly through monomers up to tetramers, as well as low populated pentamers and hexamers.[76] It is probably the lower sensitivity of our mass spectrometer that has precluded the detection of the higher molecular weight species reported in Kloniecki *et al*.[47] Remarkably, our work is in disagreement to that reported by Bernstein *et al*.[43] In all three lines of research, the obtained structural restraints were used as inputs for molecular dynamics simulations to get a structural model for the detected oligomers.[47,74,76]

## Chemical cross-linking

Chemical cross-linking generates a covalent bond between susceptible residue side chains that are close in space due to non-covalent interactions and/or transient contacts. This methodology coupled to MS has been extensively used to gain structural information of non-covalent complexes, since cross-linked residues provide distance constraints to build molecular models.[77] In general, cross-linkers are molecular handles with two reactive groups on either end that attach to reactive side chains such as amino groups, thiols and carboxylic acids of the interacting domains or

proteins. Photo-induced crosslinking of unmodified proteins (PICUP) benefits from side chains reactivity under extremely oxidative conditions without the need of a molecular handle, implying that no modification of the native sequence is required to perform such cross-linking.[78] Importantly, PICUP overcomes Aß dynamics by freezing the system as the chemical reaction takes place in the second timescale. Besides, it has been implemented to the study of Aß aggregation at the earliest stage[46,79,80] since cross-linking efficiency decays with oligomer size. The reason is that each additional peptide molecule requires the formation of at least one covalent bond.

Bitan *et al*[46] got insights on the initial oligomerization pathways of synthetic Aß40 and Aß42 by means of the PICUP reaction and subsequent analysis by SDS-PAGE, which provided information on the stoichiometry and the relative populations of the different coexisting species. They concluded that both alloforms undergo different initial pathways, since Aß40 was a mixture of monomers up to tetramers, whereas Aß42 displayed a distribution up to octamers being the pentamers and hexamers the most abundant forms. They stressed that this distinct distribution explained their different connection to neurotoxicity. Further work on cross-linked Aß40 oligomers showed that toxicity increased with oligomer size.[81] Importantly, SDS-PAGE is an electrophoretic technique widely used to characterize Aß, although it has been lately claimed to induce the formation of artefactual oligomers.[82-84] The work presented in this thesis (see Chapter 2) brings clear evidences that SDS-PAGE analysis of cross-linked species provides misleading results.[76] This analysis also demonstrates that both alloforms undergo similar initial aggregation pathways.

## Solution NMR

sNMR provides information on the secondary, tertiary and quaternary protein structures with atomic resolution. However, this technique has seldom been applied to assess Aß aggregation because the large assemblies that are formed along the process tumble too slowly to be detected. Moreover, it requires high concentrated solutions of $^{15}N$, $^{13}C$ and/or $^{2}H$ labelled protein. In spite of that, Clore *et al* developed the dark-state exchange saturation transfer NMR experiments, which are able to address the transient contacts between NMR visible monomers and large invisible protofibrilar species at the millisecond time scale.[48,85] This is possible thanks to the broad differences in transverse relaxation rates (inversely proportional to size) between the free and bound monomeric states and the ability to selectively saturate the longitudinal magnetization of the large invisible species. This saturation is transferred to the free monomeric state by chemical exchange, yielding attenuation

of its NMR signals. Hence, kinetic information on the monomer-protofibril interaction can be derived by successive 2D NMR spectra recording at different saturation offsets. These studies have shown that around 3% of free monomer transiently binds to protofibrils[86] through the mid-region or the C-terminus of the peptide and that no other low molecular intermediate oligomer intercedes to achieve such contact. Moreover, transverse relaxation rates are larger for Aß42 than for Aß40, meaning Aß42 assembles into invisible bigger species consistent with its higher propensity to aggregate.[87]

## Single Molecule Fluorescence microscopy techniques

SM fluorescence has emerged as a new toolset to study size and distribution of fluorophore-labelled Aß oligomers at very low concentrations similar to physiological conditions.[55] SM techniques provide the direct visualization of oligomer species with a high spatial and temporal resolution, which allows the detection of sparse populations which could potentially be the neurotoxic species. They could not have been detected to date because their presence is blurred by the averaged population measures obtained through other biophysical and biochemical techniques. Technical improvements have enabled monitoring molecular events happening in the millisecond time scale, allowing the characterization of the highly dynamic Aß aggregation process.

SM techniques include SM photobleaching, confocal two-colour coincidence detection (cTCCD), fluorescence integrated intensity, single particle tracking and super-resolution fluorescence imaging. SM photobleaching is based on the sequential bleaching of the fluorophores present in a given fluorescent spot recorded by total internal reflection fluorescence (TIRF) or confocal scanning geometry. If fluorescence intensity is plotted over time, each photobleaching step corresponds to a single fluorophore, that is to say a single monomer; hence, oligomer stoichiometry corresponds to the sum of each photobleaching step.[88,89] cTCCD is a confocal microscopy based technique in which half of Aß molecules are labelled with a fluorophore distinct to the fluorophore of the other half.[90] Coincident bursts are ascribed to oligomers and their stoichiometry determined by normalization of fluorescence intensity. Fluorescence integrated intensity and single particle tracking have been devoted to the study of Aß-cell membrane and/or Aß-membrane receptor interactions by means of TIRF.[91-94] Oligomer size is determined through normalization of fluorescence intensity in fluorescence integrated intensity, and through diffusion coefficients derived from two-dimensional trajectories in single particle tracking.

Finally, super-resolution fluorescence imaging has allowed access to *in cell* recording of Aß aggregation with a resolution down to 20-30 nm.[95,96] This has been achieved by sequential stochastic photoswitching of individual fluorophores over time, in such a way that close-by fluorophores are temporally resolved, and subsequent size and shape of Aß aggregates determined.

SM photobleaching[88,89] studies are consistent with cTCCD measures[90] in that early stage Aß aggregation accumulates mostly monomers up to trimers and a small proportion of bigger species. Fluorescence integrated intensity has shown that cell membrane catalyses the formation of larger Aß species compared to the distribution reported in solution,[93] while single particle tracking has reported confinement and colocalization of Aß dimers and trimers with specific neuronal membrane receptors such as cellular prion protein receptor ($PrP^c$).[91,92,94] Super-resolution fluorescence imaging has monitored in a neuronal cell line the endocytic uptake of exogenously-administered Aß and its progressive intracellular condensation into amyloid structures.[95,96]

## Hydrogen-Deuterium exchange coupled to NMR or MS

HDX is an isotopic labelling technique for protein structural analysis which gives insight into protein folding pathways, protein conformers, protein motions and protein-ligand/protein-protein interactions.[97] Backbone amide hydrogens are rapidly exchanged to deuterons when proteins are solubilised in $D_2O$, unless they are intra-/inter-molecularly hydrogen-bonded or inaccessible to solvent due to their incorporation in stable elements of structure.[98] Exchangeable hydrogens from side chain functional groups also readily exchange under these conditions because they are not involved in secondary, tertiary or quaternary structures, implying they are unable to provide structural information. HDX can undergo acid or basic catalysis in a pH- and temperature-dependent fashion, thus HDX exchange rates are carefully tuned by controlling these two experimental conditions. Analysis of isotopic labelling is performed by NMR, which delivers individual residue exchange rates thanks to the invisibility of deuterons, or MS, since hydrogens and deuterons differ in one unit of mass.[97] Compared to NMR, MS analysis requires lower amount of sample, enables the study of larger proteins, resolves coexisting populations and affords single residue resolution if it is coupled to proteolytic digestion or MS/MS approaches. Control of isotopic labelling time allows monitoring molecular events occurring at different time scales.[97] On the one hand, pulsed HDX assays imply the exposure of proteins to $D_2O$ for a brief interval of time such that it allows monitoring protein conformational

changes or determining folding pathways. On the other hand, in continuous HDX, proteins are labelled for various periods of time to characterize their structure and dynamics under equilibrium conditions.

The use of HDX allowed the determination of the backbone amide hydrogens involved in Aß fibril and Aß oligomer structure.[99-102] Innovative approaches using pulsed HDX coupled to MS further derived dynamic information on the whole Aß aggregation process. Three ensembles with distinctive exchange pattern were identified to progressively populate Aß40 and Aß42 aggregation, one of whom correlated with neurotoxic events.[56] Moreover, the mid-region of the peptide was spotted to be the first to be structured along the aggregation process, followed by the C-terminus and the N-terminus.[57] Dynamics of Aß fibril population was also gathered by means of continuous HDX labelling, confronting the longstanding belief that fibrils were the inert end product of Aß aggregation.[103] MS analysis of labelled fibrils over time depicted two definite isotopic populations, in which the more structured population decreased in as much the less structured population increased. Such bimodal isotopic distribution reflected that the molecules comprising fibrils, detached from any available fibril end, fully exchanged all backbone amide protons and came back again to the structured fibril; this molecular event was named *molecular recycling*.[103,104] Further description and discussion on this topic will be the focus of Chapter 1.

In the present thesis, Chapter 1 will be devoted to the use of continuous HDX coupled to MS to address the nature of the species in equilibrium with fibrils through *molecular recycling*. Chapter 2 will focus on the use of PICUP as a tool to freeze low molecular weight oligomer dynamics, to enable the determination of their stoichiometry. Molecular models of these oligomers will be built upon structural restraints gathered through their study by ESI-IM-MS and circular dichroism.

# Objectives

The first objective of this thesis was to determine the nature of the recycling species within Aß amyloid fibrils.

The secondary goals to answer the first main objective were the following:

- To optimize fibril preparation to enhance molecular recycling within Aß fibrils
- To express, purify and characterize active insulin degrading enzyme

The second objective of this thesis was to characterize early Aß aggregation states.

The following secondary goals were defined to accomplish this second main objective:

- To obtain chemically well-defined cross-linked low molecular weight Aß oligomers
- To isolate cross-linked low molecular weight Aß oligomers
- To structurally characterize cross-linked Aß dimers and trimers
- To evaluate the neurotoxicity of cross-linked Aß dimers
- To assess the seeding capacity of cross-linked Aß40 oligomers in Aß aggregation

# Chapter 1.

# The nature of the recycling species within Aß amyloid fibrils

## Context

As stated in the Introduction, two decades ago amyloid plaques were claimed to be the neurotoxic agents in AD.[20] However, subsequent studies revealed that the severity of the disease did not correlate to the amount of amyloid burden, but to the soluble Aß pool.[21-23] Hence, amyloid fibrils were then considered to be the inert end product of Aß aggregation. However, further histological and *in vitro* evidences supported the description of amyloid fibrils as a potential reservoir of neurotoxic oligomers. First, neurons immediately adjacent to plaques were shown to be dead,[105] and the ones located within their area of influence exhibited altered electrophysiological properties,[106] distorted neurites,[107] and loss of dendritic spines[108] and synapses.[109] Second, measurement of brain interstitial fluid (ISF) Aß levels sampled by microdialysis in living mice[110] revealed that there was a stable pool of soluble Aß42 in aged transgenic mice displaying plaque deposition, even upon γ-secretase inhibition. In contrast, inhibition of the secretase prompted a decrease in soluble Aß38 and Aß40. This metabolic fingerprint was specific to mice possessing brain amyloid plaques, meaning soluble Aß42 was most probably supplied by amyloid fibrils. Furthermore, *in vitro* studies showed that fibril fragmentation enhanced cytotoxicity[111] and that homogenous population of fibrils were in equilibrium with soluble Aß species.[103] Both studies reported that fibrils were undergoing what has been described as *molecular recycling*, that is Aß molecules in fibril ends dissociate and re-associate back to any available end (Figure 1.1A).[103,104]

In this context, it is fundamental to address which is the nature of these *recycling* species. In order to answer this question, a viable approach[40] is to take advantage of the selectivity of insulin degrading enzyme (IDE), a mammalian 114 kDa zinc metallopeptidase selective for Aß monomer only.[112] IDE biological function is associated to the hydrolysis of a variety of regulatory short peptides such as insulin and glucagon, and it has been identified as one of the major Aß-degrading enzymes *in vivo*. The selectivity of IDE for monomeric Aß was postulated through structure elucidation of the enzyme in complex with Aß by means of X-ray crystallography.[113,114] Upon interaction, the amino and carboxy-terminal domains of IDE form a small catalytic chamber which can only fit polypeptides <50 amino acids long, precluding the hydrolysis of Aß oligomers larger than the individual monomer. Besides, additional consistent reports showed the selective removal of the monomer band in SDS-PAGE analysis of a mixture of low molecular weight oligomers and monomers incubated with IDE.[40,115]

Some of the results presented in this chapter have been obtained with the contribution of Dr. Raquel Garcia from the Protein Expression Unit (IRB Barcelona) and Dr. Marina Gay and Dr. Marta Vilaseca from the Mass Spectrometry Core Facility (IRB Barcelona).

## Results

### 1. Molecular recycling within Aß amyloid fibrils

Molecular recycling was first described in an SH3 domain of the R-subunit of bovine phosphatidylinositol-30-kinase, a generic model of amyloid formation.[104] The experimental design (Figure 1.1) was based on continuous HDX monitored through MS. Later on, it was extended to the study of Aß amyloid fibrils.[103]

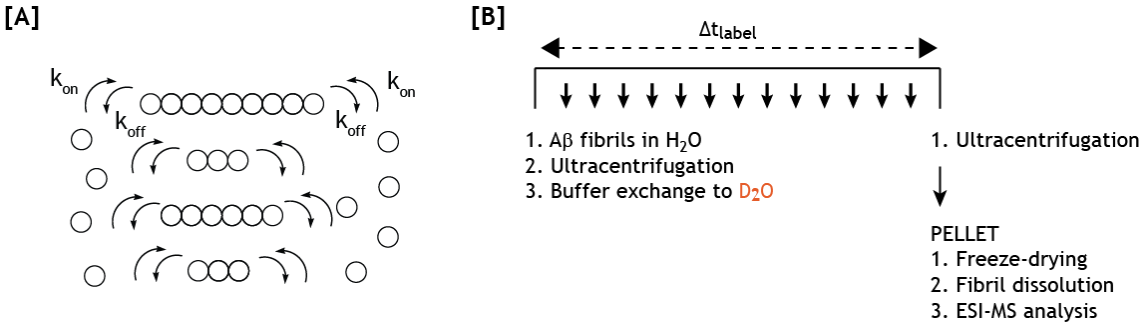


***Figure 1.1.*** *Molecular recycling within Aß amyloid fibrils.* **[A]** *Molecular recycling mechanism for a distribution of fibrils.* **[B]** *Experimental design of the HDX experiment.*

Briefly, Aß40 and Aß42 fibrils were prepared in a buffer at physiological pH (50 mM ammonium acetate (AA), 1 mM Tris(hydroxymethyl)aminomethane (Tris), 0.01% sodium azide ($NaN_3$) pH 7.4 at room temperature (RT)) (Figure 1.1B). After selection by ultracentrifugation,[116,117] fibrils were exposed to deuterated buffer for different periods of time. After different exchange times ($\Delta t_{label}$), fibrils were again ultracentrifuged, and the resulting pelleted fibrils were freeze-dried to quench exchange. Dissolution of the pelleted fibrils in a dimethyl sulfoxide (DMSO) based buffer broke them down into their constituent monomers while preserving the exchange information.[118] The HDX profile of these monomers was then analysed by electrospray ionization mass spectrometry (ESI-MS), a technique able to simultaneously detect and characterize different populations of molecules with different degrees of exchange.[97]

The mass spectra exhibited two well-resolved peaks, meaning there were two distinct isotopically labelled populations (Figure 1.2A). The lower mass peak had exchanged 20.7 (Aß40) and 23.0 (Aß42) backbone amide protons (Figure 1.2B),

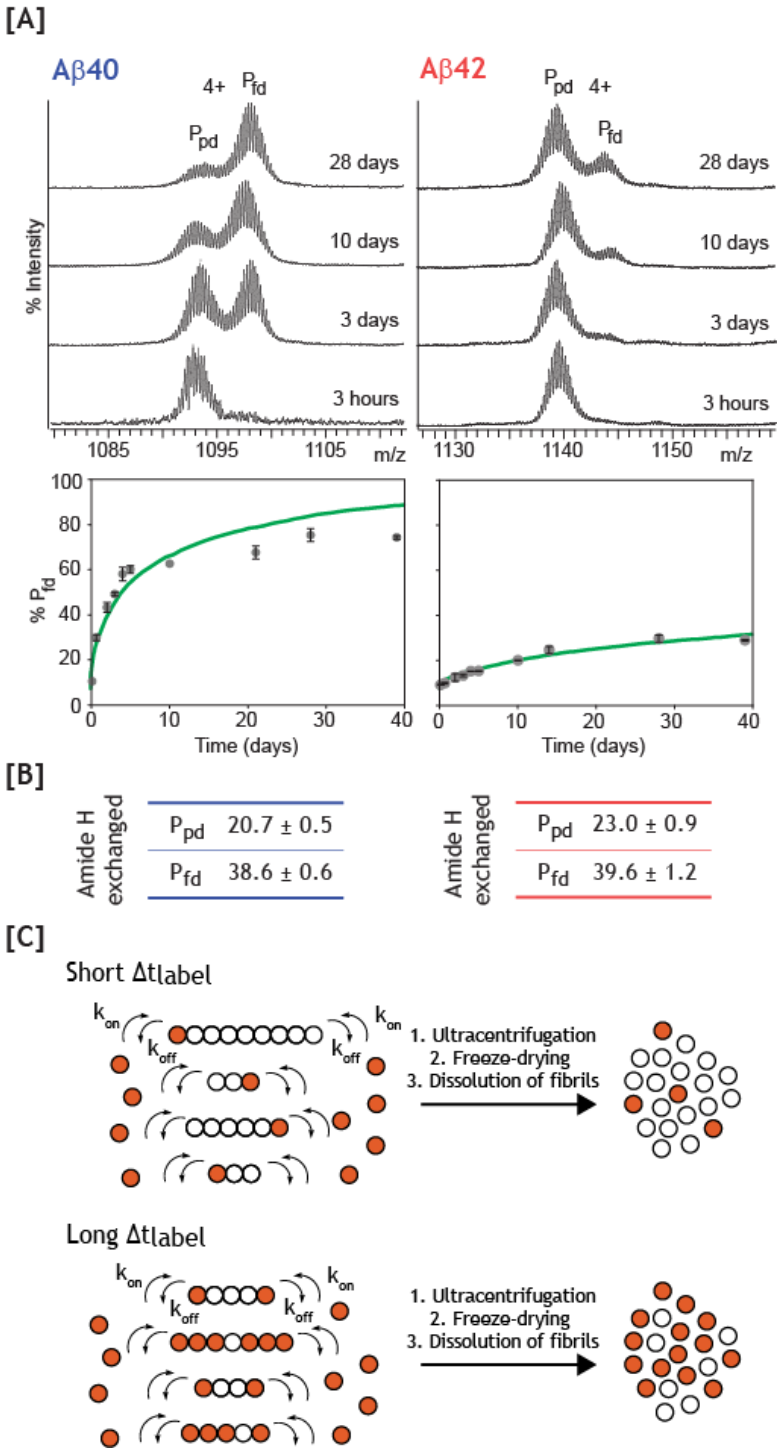


***Figure 1.2.*** *Molecular recycling within Aß amyloid fibrils.* **[A]** *Mass spectra showing the relative populations of* $P_{pd}$ *and* $P_{fd}$ *species after different times of exchange. Plot of the relative fraction of* $P_{fd}$ *as a function of time. Reproduced from Sánchez* et al.[102] **[B]** *Number of backbone amide protons exchanged in* $P_{pd}$ *and* $P_{fd}$ *populations. Aß40 and Aß42 depicted in blue and red, respectively.* **[C]** *Molecular recycling mechanism at different exchange times. The molecules that have not yet dissociated from the fibrils in white, and those that have dissociated and subsequently reincorporated after complete exchange in orange.*

consistent with the HDX exchange pattern of Aß molecules set in cross-ß sheet in amyloid fibrils.[119] This population was named partially deuterated species, $P_{pd}$. The higher mass peak had exchanged 38.6 (Aß40) and 39.6 (Aß42) backbone amide protons out of the 39 (Aß40) and 41 (Aß42) available (Figure 1.2B). Hence, this population had undergone full exchange and was referred to as fully deuterated species, $P_{fd}$. Over time, the intensity of $P_{fd}$ increased in as much the intensity of $P_{pd}$ decreased. Since there were no intermediate peaks, the model that best fitted the

data implied that the molecules comprising fibril ends dissociated, fully exchanged all backbone amide protons and reincorporated back to any available fibril end (Figure 1.2C). This model was consistent with EX1 exchange mechanism (see Box 1) whereby HDX occurs faster than Aß molecules re-associate to fibril ends. Finally, the increase in $P_{fd}$ species over time was attributed to the longer timespan for molecules to *recycle* (Figure 1.2C). Interestingly, Aß42 fibrils were shown to inherently undergo molecular recycling to a lower extent than Aß40 fibrils (Figure 1.2A).

### Box 1. Hydrogen-Deuterium Exchange

HDX is an isotopic labelling technique for protein structural analysis which is informative of protein folding pathways, protein conformers, protein motions and protein-ligand/protein-protein interactions.[97] Backbone amide hydrogens are rapidly exchanged to deuterons when proteins are solubilised in $D_2O$, unless they are intra-/inter-molecularly hydrogen-bonded or inaccessible to solvent due to their incorporation in stable elements of structure.[98] Hydrogens from side chain functional groups also readily exchange under these conditions, but they are unable to provide structural information because they are not involved in secondary, tertiary or quaternary structures. The kinetic constant ($k_{exch}$) that governs the exchange of a proton[120] is described as follows:

$$k_{exch} = k_{acid}[D^+] + k_{basic}[OD^-] + k_{water} \qquad \text{(Equation 1)}$$

As reflected in equation 1, HDX can undergo acid or basic catalysis. The associated kinetic constants are pH- and temperature-dependent, so that overall $k_{exch}$ rate is carefully tuned by controlling these two experimental conditions. In water-based buffers, basic catalysis (Figure 1.3) is predominant form pH 3 onwards.

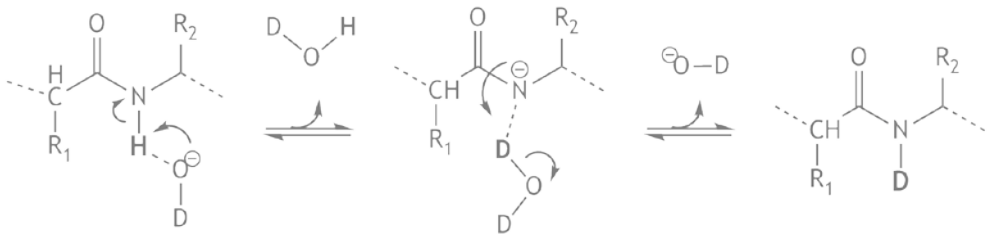

***Figure 1.3.*** *Mechanism underlying base-catalyzed HDX in backbone amide proton positions*

In a structured site, the overall mechanism of backbone amide protons HDX is represented by fluctuation of exchange sites between incompetent/closed or competent/open states[121]:

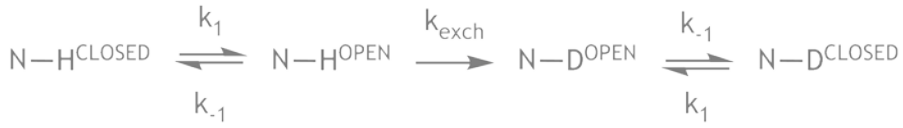


***Figure 1.4.*** *General kinetic mechanism governing HDX in structured sites*

Once in the open state, proton exchange kinetics is determined by $k_{exch}$, as detailed in equation 1. If the fluctuation between the two states is much faster than the proton exchange ($k_{-1} >> k_{exch}$), HDX is under EX2 regime whereby exchangeable positions acquire deuterons progressively as a function of the oscillation between open and closed states. In contrast, EX1 mechanism is based on proton exchange occurring largely faster than the conversion between open and closed states ($k_{exch} >> k_{-1}$) such that all exchangeable positions acquire deuterons when they switch from the closed to the open states for the first time.

Analysis of isotopic labelling is performed by NMR, which delivers individual residue HDX exchange rates thanks to the invisibility of deuterons, or MS, since hydrogens and deuterons differ in one unit of mass.[97] Compared to NMR, MS analysis requires lower amount of sample, enables the study of larger proteins, resolves coexisting populations and affords single residue resolution if it is coupled to proteolytic digestion or MS/MS approaches.

## 2. Strategy to assess the nature of the recycling species

The determination of the nature of the recycling species is fundamental taking into account that fibrils have been suggested to be a potential reservoir of neurotoxic species. In order to achieve this objective, we sought to take advantage of IDE's selectivity for monomeric Aß. The approach we designed was based on the same experimental setup described in Section 1, but introducing IDE simultaneously to the exposure of fibrils to deuterated buffer. We hypothesized two extreme situations in which the recycling species could be monomeric or oligomeric only (Figure 1.5). Hence, if the recycling entity would be a monomer, fewer or no recycling would be

observed as the recycling entity would be degraded by the enzyme before its reincorporation to the fibril. Conversely, if the recycling species would be an oligomer, the recycling process would not be altered.

Importantly, to assure that all monomeric Aß released from the fibrils would be degraded by IDE, we planned to introduce IDE in stoichiometric amounts (instead of catalytic amounts) relative to the critical concentration of soluble Aß. Moreover, in order to reduce the concentration of this soluble Aß in equilibrium with the fibrils, we decided to generate fibrils with ten times less amount of peptide.

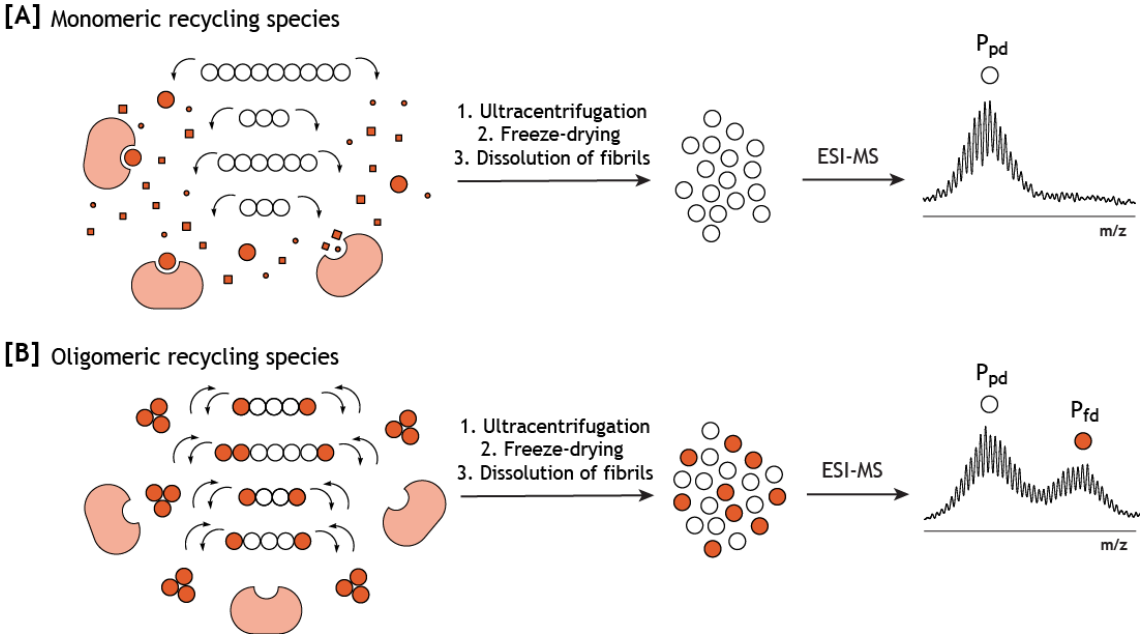


***Figure 1.5.*** *Determination of the nature of the recycling species. We envisaged two extreme situations:* **[A]** *if recycling species would be monomeric only, IDE would degrade them and* $P_{fd}$ *species peak would not be seen in the mass spectra;* **[B]** *if recycling species would be oligomeric only, the enzyme would not be able to hydrolyse them and the two isotopically labelled populations would be observed in the mass spectra.*

## 3. Optimization of fibril preparation to enhance molecular recycling

IDE proteolytic activity is very sensitive to temperature and time. The enzyme remains active and stable for up to a month at 4ºC,[122] but loses function in two weeks at RT. This implied there was a mismatch between active IDE timespan and the time frame of the experimental setup to assess molecular recycling within Aß fibrils. In order to address this mismatch, we attempted to enhance molecular recycling by increasing the number of fibril ends,[104] that is mechanically disrupting fibrils by sonication to generate a distribution of shorter fibrils.

The sonication procedure was adapted from Arimon *et al*, where they used a fine tip ultrasonicator to obtain a narrow distribution of short fibrils from mature Aß fibrils.[123] We initially applied the sonication procedure to the fibrils obtained as described in section 1 (50 mM AA, 1 mM Tris, 0.01% $NaN_3$ pH 7.4 at RT).

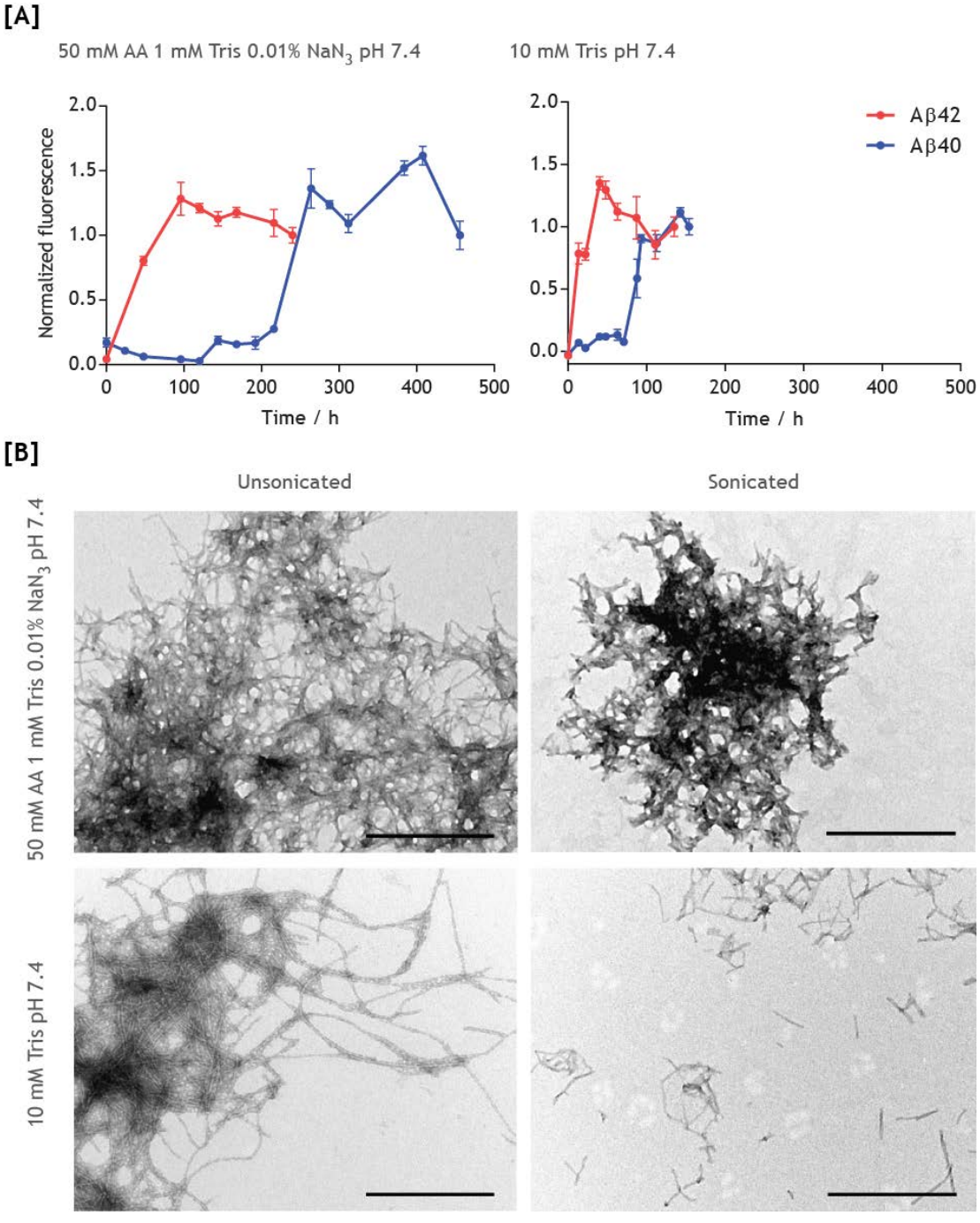


***Figure 1.6.*** *Examination of fibril formation conditions.* **[A]** *ThT binding assay fluorescence profile of Aß40 (blue) and Aß42 (red) fibril formation under the two different experimental conditions.* **[B]** *On the left, TEM micrographies of mature Aß fibrils prepared under two different experimental conditions. On the right, the resulting sonicated fibrils. Scale bar corresponds to 200 nm.*

Fibril formation was assessed through thioflavin T (ThT) binding assay (Figure 1.6A, left) - ThT is a small molecule that emits fluorescence upon binding to amyloid fibrils (see Appendix B). Once formed, their morphology was assessed by transmission electron microscopy (TEM). Fibrils were organised into dense bundles of long filaments distributed one on top of the other (Figure 1.6B, top left). Controlled sonication didn't yield shorter individual fibrils, instead we obtained trimmed fibrillar bundles (Figure 1.6B, top right). Longer sonication times only destroyed fibril ultrastructure. Consequently, we decided to apply fibril formation conditions used in Arimon *et al*, this is 10 mM Tris pH 7.4 at 37ºC.[123] Under these new conditions, fibrils were formed more than threefold faster (Figure 1.6A, right) and TEM images showed they were distributed as long individual filaments with nicely defined ultrastructure (Figure 1.6B, bottom left). More importantly, application of sonication procedure yielded homogeneously shorter fibrils (Figure 1.6B, bottom right).

In all, fibril formation under 10 mM Tris pH 7.4 at 37ºC was three times faster than in the initial conditions and it yielded nicely defined fibrils with fine structure. Their sonication following established procedures provided a distribution of shorter fibrils of about 100 nm in length.

### 4. Expression, purification and characterization of IDE

Once fibril preparation was optimised, we set to express, purify and characterize IDE. We sought to obtain recombinant IDE to take advantage of its reported selectivity between monomeric and oligomeric Aß.

In collaboration with Dr. Raquel Garcia from the Protein Expression Unit (IRB Barcelona), we obtained pOPINE[124] plasmid containing Met42-Leu1019 human IDE hexahistidine-tagged construct. Expression trials showed optimal IDE production was attained through transformed B834 E. Coli cells induced by isopropyl-1-thio-ß-D-galactopyranoside (IPTG). Next, we implemented a previously published purification protocol[122] which in our hands yielded impure IDE. Through optimization of ion metal affinity column (IMAC) gradient, we obtained highly pure protein (Figure 1.7A), which was only active if IMAC buffer contained reducing agents. In fact, IDE has been reported to be thiol-sensitive as it possesses 13 cysteines, two of whom need to form a disulphide bridge and the remaining need to be free, to obtain the active enzyme.[125] Last SEC step was carried out without any reducing agents so that on-column folding afforded active IDE. Interestingly, our in-house produced IDE displayed a higher specific activity than the commercial enzyme from R&D systems (Figure 1.7B).

The objective of expressing and purifying IDE was to ultimately achieve selectivity between monomeric Aß versus oligomers. Even though this selectivity had already been claimed, none of the reported studies provided direct evidence of the extent of such selectivity using properly characterised Aß.[40,113,115] In this context, we sought to provide further evidence of this selectivity to determine its precise scope. This was imperative since we did not expect the recycling species to be very large as they displayed an almost full deuteration pattern.

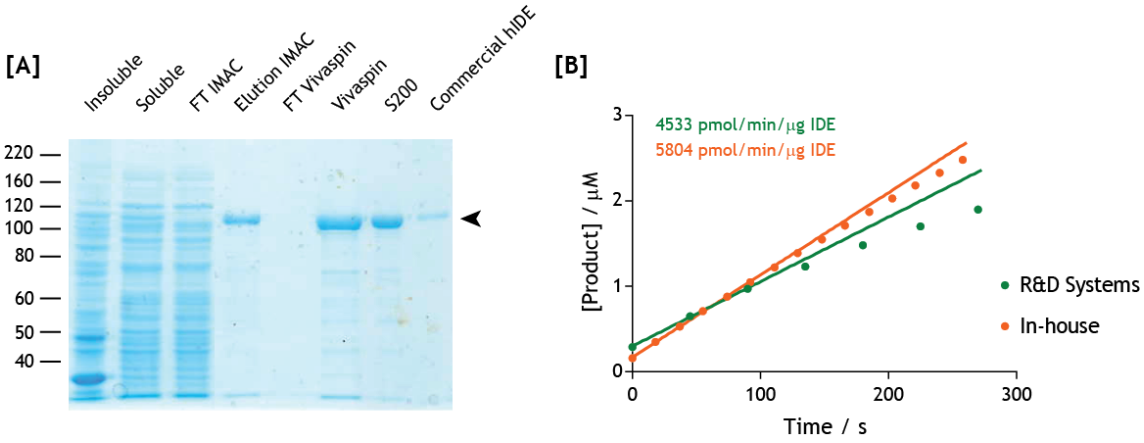


***Figure 1.7.*** *Expression, purification and characterization of IDE.* **[A]** *SDS-PAGE of the different IDE purification steps. The band corresponding to the enzyme is indicated with an arrowhead.* **[B]** *Enzymatic activity plot of product formation over time. Comparison of specific enzymatic activity of in-house produced IDE (orange) and commercial IDE (green). Enzyme specific activity values indicated on top.*

In order to prove this selectivity, we prepared cross-linked low molecular weight Aß40 oligomers, including intact monomer up to cross-linked tetramer (Figure 1.8A, lane 1 – see Chapter 2). Incubation with slightly substoichiometric amounts of IDE and subsequent analysis through SDS-PAGE showed cross-linked dimers, trimers and tetramers resisted IDE proteolytic activity (Figure 1.8A). In contrast, monomeric Aß40 band progressively disappeared over time, displaying degradation fragments of ~2 kDa at short time points, which completely disappeared at longer incubation times. To the best of our knowledge, this is the first direct evidence that IDE is unable to cleave the smallest Aß oligomers including dimers up to tetramers.

Next, we set to characterize Aß-IDE kinetic system. We chose Aß40 peptide to perform this characterization because it has a lower aggregation propensity than Aß42, and we used catalytic amounts of IDE since it is one of the premises of the classical Michaelis-Menten framework.[126] A substrate-enzyme kinetic study implies the determination of the following parameters: (i) the maximum initial velocity of substrate degradation ($v_{max}$) which is the maximum initial velocity that will be

achieved due to enzyme saturation; (ii) the Michaelis-Menten constant ($K_m$), which is the substrate concentration at which the substrate degradation initial velocity is half the maximal, and it reflects the thermodynamic constant of affinity of substrate and enzyme. The kinetic rates of the system can be derived from these two parameters. Overall, the fundamental Michaelis-Menten plot relates the dependence of substrate degradation initial velocity versus substrate concentration at a given enzyme concentration. However, this relation can only be drawn if preceding plots of substrate consumption over time achieve full depletion of the substrate at long times.

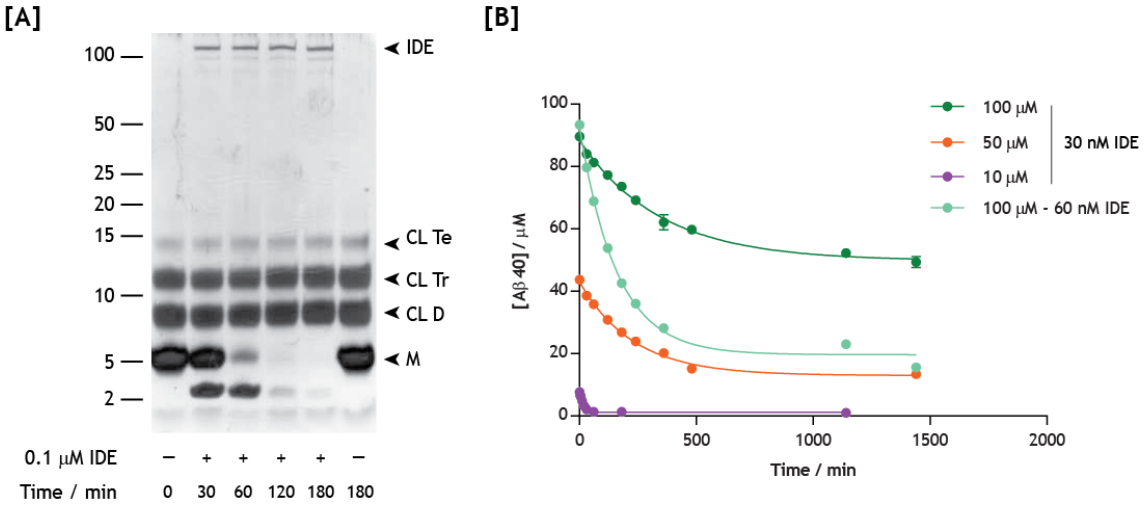


***Figure 1.8.*** *IDE characterization.* **[A]** *SDS-PAGE of cross-linked Aβ40 low molecular weight oligomers with IDE at increasing sampling times. The bands corresponding to IDE, Aβ40 monomer (M), cross-linked dimer (CL D), trimer (CL Tr) and tetramer (CL Te) are indicated with arrowheads.* **[B]** *Aβ degradation plots incubated at 30 and 60 nM IDE at several initial Aβ concentrations. One phase exponential decay curves have been adjusted to mean values of triplicate measures for each time point.*

When carrying out Aß-IDE kinetic study, this premise was not fulfilled: we were not able to achieve full degradation of Aß40 over time at different concentrations (Figure 1.8B). A possible explanation would be that unproteolysed Aß40 was in fact aggregated, thus the initial concentration was not reflecting the real monomeric Aß40 available for IDE to hydrolyse. This possibility was tested incubating with double the enzyme concentration (Figure 1.8B, light green). Surprisingly, we could achieve a higher consumption of substrate, meaning that either (i) unproteolysed Aß40 was indeed aggregated, but there was a complex equilibrium between monomer and oligomers that could be modulated upon enzyme addition, or that (ii) IDE was undergoing product inhibition or (iii) losing activity due to excessive turnovers. Overall, we could not kinetically parametrize this system. In fact, this

system should have been *a priori* considered as highly complex due to the substrate kinetics *per se*.

Subsequent Liquid Chromatography-High Resolution Mass Spectrometry (LC-HRMS) analysis of Aß degradation fragments was carried out by Dr. Marina Gay at the Mass Spectrometry Core Facility (IRB Barcelona).


***Figure 1.9.*** *IDE-mediated Aß40 cleavage sites and the corresponding generated peptide fragments. Each cleavage site has a colour associated, ranging from red to green. Mid-region peptides which include two cleavage sites are depicted with a colour gradient corresponding to the colours of both cleavage sites. Formerly reported cleavage sites[115,127] are depicted on top with a grey arrowhead, while the newly identified are shown in black arrowheads.*

This analysis revealed there were several short peptides corresponding to Aß mid-region only, meaning that they were the result of at least two IDE proteolytic steps (Figure 1.9). Since full-length Aß was still detected in this pool of fragments, this result suggested IDE could have even more affinity for Aß degradation fragments than for Aß itself. Hence, this result reinforced the former product inhibition hypothesis, since IDE could be "kidnapped" by these generated degradation fragments once formed. Moreover, this LC-HRMS analysis could also support the excessive turnovers hypothesis because IDE could lose activity due to simultaneous proteolysis of Aß and its degradation fragments. Further evidences to support either of these two hypotheses could have been gathered by monitoring Aß concentration upon re-addition of IDE at longer incubation times.

Importantly, our LC-HRMS analysis of IDE-mediated Aß fragments was consistent with the formerly reported cleavage sites (Figure 1.9, grey arrowheads).[115,127] Interestingly, we detected three additional sites (Figure 1.9, black arrowheads).

These results are in agreement with the unspecific substrate cleavage pattern, characteristic to IDE.[114]

Overall, we succeeded in expressing and purifying recombinant active IDE. We also showed that IDE cleaves monomeric Aß only, since the enzyme could not hydrolyse cross-linked dimers, trimers and tetramers. However, we did not fulfil the characterization of Aß-IDE kinetic system because Aß was not fully proteolysed when incubated with IDE at long times. Determination of IDE-mediated Aß fragments enabled the identification of three new cleavage sites, and it revealed that the enzyme also hydrolyses Aß fragments.

### 5. Molecular recycling within Aß fibrils in the presence of IDE

With effectively sonicated Aß fibrils and active IDE in hands, we could proceed to assess molecular recycling in the presence of the enzyme. The experimental design was identical to the one explained in section 1 (Figure 1.1B), the enzyme was simply added at the same time as fibrils were resuspended in $D_2O$ buffer. IDE was supplied at stoichiometric amounts (critical soluble Aß concentration is in the micromolar range[103]) in order to ensure there was enough IDE to proteolyse all the monomer in solution and that degradation fragments did not monopolise all the enzyme molecules. Moreover, IDE was added at three different concentrations to assess its dose-response effect.

First, we analysed molecular recycling under these new conditions in the absence of IDE. Contrary to our initial hypothesis and in spite of working with a homogeneous distribution of shorter fibrils, we did not detect an enhanced molecular recycling neither for Aß40 nor Aß42 fibrils (Figure 1.10B). In fact, in Aß40 fibrils at 4 days of exchange, $P_{fd}$ population only reached a relative fraction of 30%, compared to the roughly 60% measured in the former conditions (Figure 1.2A). Aß42 fibrils showed a similar behaviour in both experimental conditions, with a relative fraction of approximately 25% (Figures 1.10B and 1.1A).

Next, we compared the backbone amide protons exchanged in each isotopically labelled population in the two experiments (50 mM AA, 1 mm Tris, 0.01% $NaN_3$ pH 7.4 at RT vs 10 mM Tris pH 7.4 at 37ºC – Figure 1.2B vs Figure 1.10C). As expected, the lower mass peaks displayed an exchange pattern roughly corresponding to Aß molecules set in cross-ß sheet in amyloid fibrils.[119] Besides, the higher mass peaks also exhibited a full exchange of all backbone amide protons, indicating lack of structure through hydrogen-bonding.

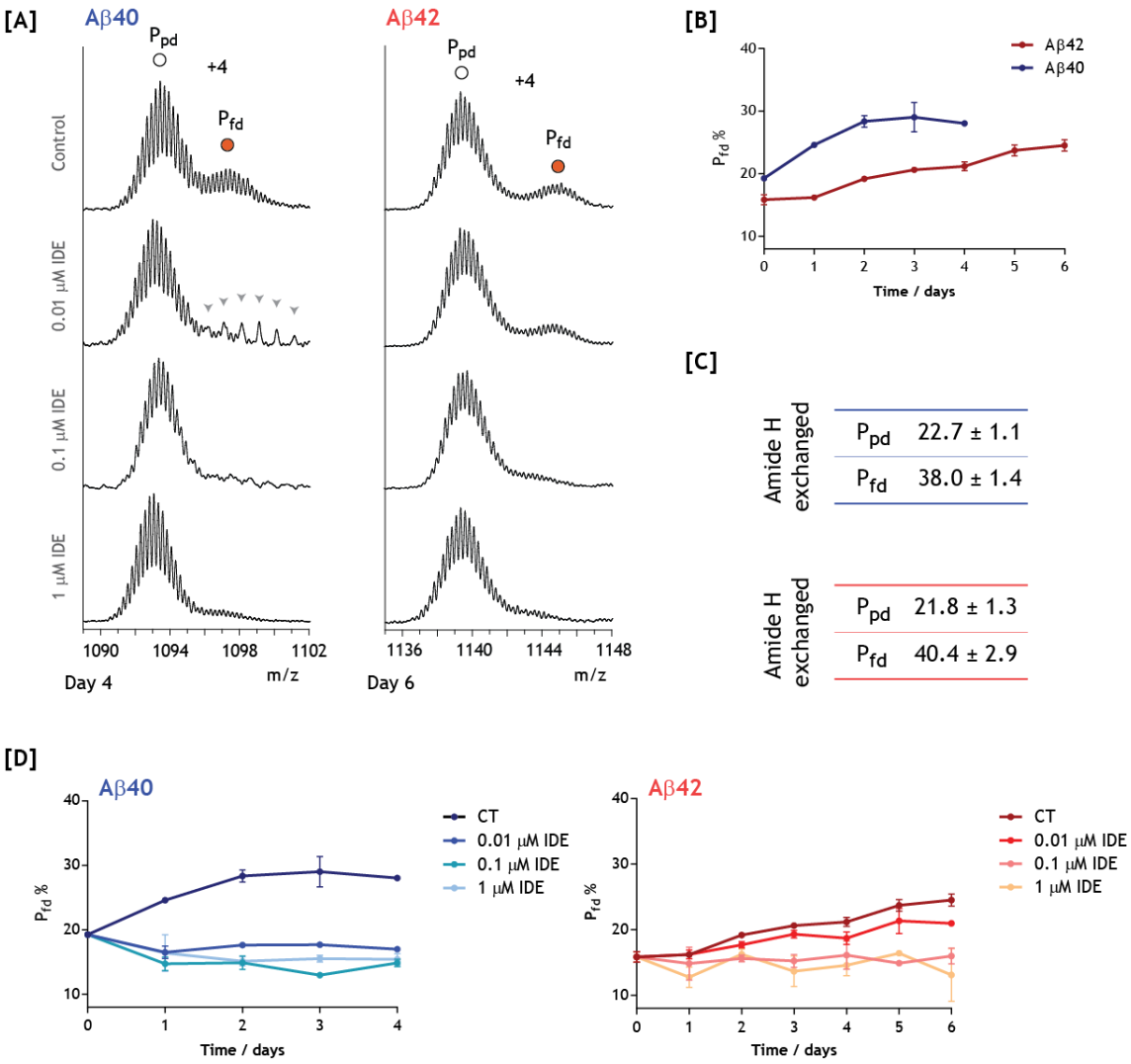


***Figure 1.10.*** *Molecular recycling within Aß amyloid fibrils in the presence of IDE.* **[A]** *Mass spectra (+4 charge state) showing the relative populations of $P_{pd}$ and $P_{fd}$ species of Aß40 (left, at day 4) and Aß42 fibrils (right, at day 6) incubated with 0/0.01/0.1/1 μM IDE (top to bottom).* **[B]** *Plot of the relative fraction of $P_{fd}$ as a function of time for Aß40 (blue) and Aß42 (red) fibrils without IDE.* **[C]** *Number of backbone amide protons exchanged in $P_{pd}$ and $P_{fd}$ populations. Aß40 and Aß42 depicted in blue and red, respectively.* **[D]** *Plot of the relative fraction of $P_{fd}$ as a function of time for Aß40 (blue) and Aß42 (red) fibrils with 0(CT)/0.01/0.1/1 μM IDE (darker to lighter colour), expressed as mean ± standard deviation.*

Upon incubation with IDE, the increase in the relative fraction of $P_{fd}$ species in Aß40 fibrils was halted in all three IDE-containing samples (Figure 1.10D in blue). This implied that IDE was able to cleave whatever was in solution and reincorporation of Aß molecules to the fibrils was not possible. Additionally, a +1 charge state weighting 1096 uma was detected in Aß40 0.01 μM IDE mass spectrum, overlaying with the $P_{fd}$ peak (Figure 1.10A, indicated with grey arrowheads). LC-HRMS studies of IDE-mediated Aß fragments allowed identification of this peptide as the fully deuterated

Aβ40 C-terminus fragment starting at Glycine-29, whose theoretical deuterated monoisotopic mass is 1096. The hydrophobic nature of this fragment could explain why this peptide had remained attached to the fibrils after the ultracentrifugation step.

With regard to Aβ42 fibrils, 0.01 μM IDE did not stop molecular recycling process to occur (Figure 1.10D in red). However, the presence of 0.1 and 1 μM IDE was sufficient to keep $P_{fd}$ relative fraction at basal levels. In other words, low IDE concentrations did not block Aβ molecules reincorporating to the fibrils whereas high IDE concentrations were able to disrupt molecular recycling. Rationalization of these data suggested that Aβ42 fibrils provided oligomers in complex equilibrium with monomers.

## Discussion

The mismatch between active IDE timespan and the timescale whereby molecular recycling was monitored led us to enhance molecular recycling through the generation of more fibril ends. Sonication was only effective if fibrils were prepared in carefully optimised experimental conditions, which ultimately yielded a similar or slower molecular recycling. Besides, we obtained active recombinant IDE, which proved to be selective for monomeric Aβ only, although no kinetic characterization of Aβ-IDE interaction was attained. Finally, Aβ40 fibrils showed to provide IDE-cleavable monomers, while Aβ42 fibrils released an undefined mixture of monomers and oligomers.

### 1. IDE characterization

IDE is a well-established Aβ-degrading enzyme, claimed to hydrolyse monomeric Aβ only. Up to date, there have not been direct evidences of the scope of such selectivity using properly characterised Aβ. Walsh *et al* showed that SDS-PAGE analysis of conditioned media of Aβ-expressing cells incubated with IDE exhibited low molecular weight SDS-stable oligomer bands and no traces of monomeric Aβ.[40] However, there was no further characterization of the nature of these SDS-stable Aβ oligomer bands. In fact, a recent paper has shown that these SDS-stable oligomer bands could also correspond to N-termini extended Aβ forms.[128] Mukherjee *et al* showed that pre-aggregated radiolabelled Aβ incubated with IDE did not release any radioactive soluble proteolytic product.[115] This result indicates that IDE is unable to proteolyse large undefined Aβ species, but no evidences on the precise extent of the selectivity are given. Indirect evidence of this scope was provided through IDE X-ray

crystal structure, which revealed a catalytic chamber that could only fit short peptides up to 50 amino acids long.[113] In this context, we have provided direct and faithful proof that IDE can only cleave monomeric Aß. In Chapter 2 we will show that cross-linked low molecular weight Aß40 oligomers analysed through SDS-PAGE provide *bona fide* oligomer stoichiometry and distribution, meaning that from our data we can conclude IDE indeed cleaves monomeric Aß but is unable to degrade oligomers starting from dimers (Figure 1.8A).

Kinetic characterization of Aß-IDE pair could have been considered *a priori* highly complex due to Aß (substrate) kinetics of aggregation. In fact, our kinetic study was not conclusive because Aß was not fully depleted after long incubation times (Figure 1.8B), which could be ascribed to Aß being partially aggregated. Therefore, even though we could monitor substrate consumption initial velocities, the established initial monomeric substrate concentration was most probably not correct. Conversely, Leissring *et al* reported kinetic parameters $K_m$ and $v_{max}$ for this enzyme-substrate pair through a newly designed experimental fluorescence-based approach, which allowed them to characterize IDE-mediated Aß consumption at 10-100 fold lower peptide concentration than in our study.[127] However, in spite of their successfully completed kinetic characterization, they did not provide evidence that the peptide was fully hydrolysed at each trace of Aß consumption over time. Importantly, all Michaelis-Menten premises, for instance complete substrate depletion, need to be fulfilled in order to validate the obtained kinetic parameters.

## 2. Molecular recycling within Aß amyloid fibrils

Despite striving to achieve an enhanced molecular recycling, sonicated fibrils obtained through carefully optimised conditions displayed a similar or even slower molecular recycling. The reason is that we focused our attention on obtaining more fibril ends, since Carulla *et al* had already reported that the more fibril ends, the larger $P_{fd}$ relative population at shorter periods of time.[104] Therefore, we focussed on optimizing fibril formation conditions to obtain mature fibrils that yielded homogenously shorter counterparts through sonication. Our optimised conditions implied a change in solvent composition, in terms of type and concentration of salt, and temperature: from 50 mM AA, 1 mM Tris, 0.01% $NaN_3$ pH 7.4 at RT to 10 mM Tris pH 7.4 at 37ºC. Under the new experimental conditions, we finally succeeded in obtaining shorter fibrils through mechanical disruption, but we did not consider that modification of Aß physicochemical environment could affect fibril stability. Certainly, there have been reports on the influence of changes in solvent

composition, pH or temperature on peptide aggregation kinetics,[129] and, in fact, we noticed that in the new conditions both Aß40 and Aß42 aggregated threefold faster (Figure 1.6A). Nevertheless, we could not foresee these physicochemical changes would additionally affect the thermodynamics of the system by stabilizing fibrils and ultimately slowing molecular recycling.

Although we did not obtain an enhanced molecular recycling, small amounts of Aß40 and Aß42 $P_{fd}$ species were detected all along the time course of the assay, even at initial times. More precisely, there was a basal $P_{fd}$ species at roughly 10% that could even be detected in the presence of high concentrations of IDE (Figure 1.10D). Sánchez *et al* considered it to result from non-specific binding of monomers to the fibrils.[103] If this were the case, monomers should be hydrolysed in the presence of the enzyme, implying they should progressively disappear from the mass spectra. In fact, we would expect that these monomers were released from the fibrils more easily compared to the recycling species, since the former are bound through non-specific interactions whilst the latter are through hydrogen-bonding. Based on a recent publication, an alternative explanation would be that molecules in the fibril ends undergo a two-state detachment from the fibrils, similarly to the sNMR reported interaction between monomers and protofibrils.[87] In this hypothesis, molecules comprising fibril ends would first break up all hydrogen-bonding, so that all backbone amide protons would fully exchange. Even if these molecules were not structured through cross-ß sheet anymore, other non-covalent interactions would keep them transiently attached to the fibrils ends. Subsequently, these molecules would detach from the fibril structure and would be released to the solvent. Therefore, the basal $P_{fd}$ species would correspond to transient fully exchanged species before being detached from the fibrils.

### 3. The nature of the recycling species

Under the optimised experimental conditions, Aß40 and Aß42 fibrils mass spectra showed the two expected well-defined peaks (Figure 1.10A). On the one hand, the lower mass peaks $P_{pd}$ displayed the exchange pattern of Aß molecules set in cross-ß sheet in amyloid fibrils. On the other hand, the higher mass peak $P_{fd}$ exhibited a full exchange of all backbone amide protons, indicating lack of structure through hydrogen-bonding. These results were consistent with those from the original description of molecular recycling within Aß amyloid fibrils.[103] The lack of hydrogen-bonding was also in agreement with $P_{fd}$ population being low structured either as monomers or low molecular weight oligomers. Importantly, these data support the

selection of IDE as the agent to discern the nature of the recycling species due to its exquisite selectivity for monomer versus its inability to hydrolyse the simplest Aß oligomer, i.e. the dimer.

Regarding the incubation of Aß40 fibrils with IDE, molecular recycling was blocked at the three different concentrations of enzyme used (Figure 1.10D in blue). These results together with the described exchange pattern were undoubtedly indicative of Aß40 $P_{fd}$ species, namely Aß40 recycling species, being monomers. Consistent to these results, a cTCCD study of Aß40 fibrils showed they provided mainly monomers and a very low population (1%) of mostly dimers to tetramers.[90]

In contrast, the picture in Aß42 fibrils incubated with IDE was far more complex. Even if 0.01 µM IDE didn't stop molecular recycling, 0.1 and 1 µM IDE showed to be sufficient to impede $P_{fd}$ relative fraction to increase over time (Figure 1.10D in red). Of note, all this reasoning has to be considered under the frame that the differences in Aß42 $P_{fd}$ relative fraction were little (from 15% to 25%) between control and IDE-containing samples. Taking into account that $P_{fd}$ had exchanged all amide protons, we could infer Aß42 fibrils release an undefined mixture of IDE-cleavable monomers and oligomers, which are not structured through hydrogen-bonding. Certainly, these monomers and oligomers establish a highly intricate equilibrium that IDE can only disturb at high concentrations.

An alternative explanation to the fact that Aß42 recycling species require a higher concentration of enzyme to disrupt molecular recycling is that IDE could possibly have different affinity for Aß40 and Aß42. Consistently, a computational study on Aß-IDE interaction reported that Aß42 interacted with IDE *in a manner significantly different* from that of Aß40.[130] However, this possibility is very unlikely since we were working with high concentrations of enzyme, meaning their slight different interaction could not be as determining as to display different molecular recycling patterns in the presence of high amounts of IDE.

Overall and in support of our data, measurement of Aß levels in brain ISF of living mice revealed there was a pool of soluble Aß38, Aß40 and Aß42 in aged transgenic mice displaying plaque deposition. Importantly, Aß38 and Aß40 pool decreased upon γ-secretase inhibition, whereas that of Aß42 remained stable only if plaques were present.[110] In agreement with our results, this data suggests that soluble Aß42 could had been supplied by amyloid fibrils and that murine IDE and other Aß degrading enzymes[112] expressed in the mice (i.e. Neprilysin) were unable to hydrolyse this Aß42 soluble pool.

Similarly to our change in the physicochemical properties of the media, the molecular recycling within Aß fibrils *in vivo* could be easily modulated by the physiological conditions and the presence of specific cofactors. In this context, it is tempting to speculate that what might differentiate AD patients and non-demented adults displaying AD-like amyloid deposition[26,27] are their specific physiological conditions that alter the thermodynamic stability of fibrils deposited in amyloid plaques. In other words, the physicochemical environment of brain amyloid plaques could determine a decreased or an enhanced molecular recycling within Aß fibrils, ultimately regulating the performance of amyloid plaques as potential reservoirs of oligomers. Furthermore, not only the thermodynamic stability of Aß fibrils determines their role in the disease, but also their chemical nature. Precisely, Aß42 fibrils recycle to a fewer extent compared to Aß40 fibrils, but the former provide oligomers that IDE, one of the most prominent Aß-degrading enzymes *in vivo*, cannot hydrolyse.

## Materials and methods

### Reagents

All reagents were purchased from Sigma-Aldrich unless otherwise specified.

### Fibril preparation

Aß peptides of 40 and 42 residues, Aß40 and Aß42, were synthesised and purified by Dr. James I. Elliott (New Haven). Aß was purified by SEC. First, it was dissolved at 8.5 mg/ml Aß concentration in 6.8 M guanidinium thiocyanate (GdnHSCN - Life Technologies), sonicated for 5 min, diluted to 4 M GdnHSCN at a 5 mg/ml Aß concentration, centrifuged at 10,000g for 5 min. The resulting solution was injected into a HiLoad Superdex 75 HR 16/60 column (GE Healthcare) previously equilibrated with 10 mM Tris, pH 7.4, and eluted at a flow rate of 1 ml/min. The system was kept at 4°C. The peak attributed to low molecular weight Aß was collected, and its peptide concentration was determined by Reverse Phase High Performance Liquid Chromatography (RP-HPLC-PDA). The Aß solutions were diluted to 30 µM and incubated at RT for fibril formation, which was monitored through ThT binding assay and TEM.

### RP-HPLC-PDA

RP-HPLC-PDA analysis was carried out using a Symmetry 300 C4 column (4.6 × 150 mm, 5 µm, 300 Å; Waters), a flow rate of 1 ml/min, and a linear gradient from 0 to 60% B in 15 min (A = 0.045% trifluoroacetic acid (TFA) in water, and B = 0.036% TFA in acetonitrile) at 60ºC. A calibration curve was generated based on Aβ40 and Aβ42 solutions that had previously been quantified by amino acid analysis.

### Amino Acid Analysis

An internal standard (2-aminobutanoic acid) was added to a given volume of Aß solution. The mixture was lyophilised and the peptide was subsequently hydrolysed (6 N hydrochloric acid (HCl), 110ºC, o/n). The amino acid content and the corresponding protein concentrations were determined using the Waters AccQ-Tag amino acid analysis method.

### ThT binding assay

ThT analysis was performed by mixing 50 µl of the Aß aggregating solutions withdrawn at specific times with 15 µl of 100 µM ThT and 35 µl of 142 mM Glycine at pH 8.3 in a Hard Shell® Thin Wall 96-well fluorescence plate (Bio-Rad). The ThT fluorescence of each sample was measured using a fluorescence plate reader (FluoDia T70, Photal, Photon Technology International) at excitation and emission wavelengths of 450 and 485 nm, respectively. The samples were analyzed in triplicate, and average fluorescence values and standard deviations were plotted.

### Electron microscopy

A 10 µl aliquot of the Aß amyloid fibril solution was applied to a Formvar-coated copper grid (400 mesh). After 1 min, the grid was washed with water and then negatively stained with 2% uranyl acetate (w/v). Samples were viewed in FEI Tecnai SPIRIT Company operating at 120 kV and the images acquired with an SIS Megaview III camera.

### Sonication of Aß fibrils

The fibrils were mechanically disrupted by ultrasonication immersing a 3 mm tapered microtip (Vibracell VCX 750) in the fibril solution, kept in ice to avoid sample heating upon sonication. The amplitude of the sonication pulse was set at 22% and it lasted for 1 min, in sequential on:off states at 5:1.

## Expression and purification of IDE

Human IDE was recombinantly expressed in-house, as detailed below. Only in specific cases, the enzyme was purchased to R&D Systems.

Human Met42-Leu1019 6-His tag IDE was successfully cloned in pOPINE[124] plasmid (work performed at the Protein Expression Unit – IRB Barcelona). B834 E. Coli cells were transformed with the plasmid and were grown at 25°C and 170 rpm in Luria Broth containing 0.1 mg/ml carbenicillin. When the $A_{600}$ of the culture reached 0.3–0.4 AU, the expression of recombinant IDE was induced by adding 50 mM IPTG. Cells were harvested 12 h after induction, centrifuged at 2700g for 30 min at 4ºC. All the following steps were carried out either on ice or at 4°C. Pelleted cells from 1 l culture were resuspended in 100 ml of buffer A (50 mM sodium phosphate, 500 mM sodium chloride, 1 mM tris(2-carboxyethyl)phosphine, 10 mM imidazole at pH 8.0) spiked with DNAse (Roche Diagnostics) and one pill of Complete EDTA-free (Roche Diagnostics). The resuspended cells were lysed in a Cell Disruptor (Constant Systems) and the obtained lysate was centrifuged at 30000g for 30 min. The soluble pool was filtered through a 0.45 µm filter (Millipore) and injected to a 5 ml HisTrap HP column (GE Healthcare) pre-equilibrated with 5 column volumes (CV) of Buffer A. We programmed a gradient whereby recombinant IDE eluted in the last step. The gradient mixed different percentages of buffer A and buffer B (buffer A with 200 mM imidazole and pH 7.4) as follows (the percentages are in terms of buffer B): 5 CV 0%, 15 CV 0-30%, 15 CV 30%, 10 CV 30-100% and 5 CV 100% buffer B. The fractions containing IDE were pooled, concentrated down to ~200 µl using 30 kDa-Vivaspin concentrator (Sartorius) and injected into a Superdex 200 10/300 (GE Healthcare) pre-equilibrated with the adequate buffer. Fractions containing monomeric IDE were pooled again and protein concentration was estimated using Nanodrop 2000 (ThermoFisher Scientific).

SDS-PAGE electrophoresis was run with aliquots from each purification step. The 7.5% acrylamide/bisacrylamide 1.5 mm-wide gel was prepared following the recipe detailed below.

| | Resolving | Stacking |
|---|---|---|
| Acrylamide/Bis 40% | 1.875 ml | 488 µl |
| $H_2O$ | 5.625 ml | 3.500 ml |
| Buffer | 2.600 ml | 1.250 ml |
| SDS 10% | 100 µl | 50 µl |
| APS 10% | 100 µl | 500 µl |
| TEMED | 10 µl | 5 µl |

Acrylamide/Biscarylamide solution (Amresco, Berlabo) was 37.1:1 at 40% (w/v). Resolving buffer was 1.5 M Tris·HCl pH 8.8, 0.4% SDS. Stacking buffer was 0.5 M Tris·HCl pH 6.5, 0.4% SDS. The gel was placed in a Tetrapack (Bio-Rad) cuvette and immersed in Running Buffer (1.92 M Glycine, 0.25 M Tris·HCl, 1% SDS). 10 µl-sample aliquots were mixed with 1.5 µl dithiotreitol (DTT) and 3 µl 5x Loading Buffer (312.5 mM Tris·HCl pH 6.8, 50% Glycerol, 10% SDS, 0.1% Bromophenol Blue). Next, they were boiled at 95ºC for 5 min and loaded into the gel. Gel was run at 80–100 V and stained with Commassie Blue.

## IDE specific activity

IDE specific activity was measured by its ability to cleave the fluorogenic peptide substrate Mca-RPPGFSAFK(Dnp)OH (R&D Systems) during the initial 1.5 min. IDE and the substrate were diluted in Assay Buffer (50 mM Tris·HCl, 1 M sodium chloride pH 7.5) at 0.2 µg/ml and 20 µM, respectively. Triplicates of 50 µl of diluted substrate were loaded into a plate (Costar 3635 UV-transparent) and the reaction was started upon addition of 50 µl diluted IDE. Fluorescence was measured every ~30 s, reading at excitation and emission wavelengths of 320 nm and 405 nm, respectively. Fluorescence background was also measured by addition of 50 µl of Assay Buffer instead of diluted IDE. A calibration curve was built with Mca-PL-OH (Bachem) to correlate fluorescence readout to proteolytic product formation. Specific activity was calculated as picomoles of product generated during the first 1.5 min per µg of enzyme, expressed as pmol/min/µg IDE.

## Preparation of cross-linked Aß40 oligomers

Aß was purified by SEC to obtain low molecular weight Aß, as described in fibril formation section. The column was equilibrated using 10 mM sodium phosphate pH 7.4 and eluted at 4ºC at a flow rate of 1 ml/min. The peak attributed to low molecular weight Aß was collected and its protein concentration determined. The peptide solution was then diluted to 150 µM, frozen, and kept at -20 ºC until used.

PICUP reaction was used to prepare cross-linked Aß40 oligomers. PICUP experimental set-up consisted of a camera body and a 150-W slide projector. A PCR tube containing the reaction mixture to be cross-linked was placed inside the camera body for irradiation. The sample was irradiated via the slide projector for a short time, precisely controlled by the camera shutter. PICUP reactions were done using an Aß/$Ru(bpy)_3^{2+}$/APS ratio of 1:2:5, optimised conditions which will be further described in Chapter 2. To this end, 4 µl of 3 mM $Ru(bpy)_3^{2+}$ and 4 µl of 7.5 mM APS

were added to 40 µl of 150 µM Aß solution described above. The mixture was irradiated for 1 s at a distance of 10 cm and immediately quenched by adding 6.5 µl of 4 M DTT. After the PICUP reaction, the reagents were removed using Bio-Spin P30 columns (Bio-Rad) equilibrated in 10 mM AA at pH 8.5.

### Incubation of cross-linked Aß oligomers with 0.1 µM IDE

Freshly prepared Aß40 PICUP samples were incubated for 30, 60, 120 and 180 min with 0.1 µM freshly purified IDE. At each time point, triplicates of 20 µl were taken from the pool and rapidly frozen with liquid nitrogen. Triplicate controls for initial and final time points of Aß40 PICUP samples were also kept.

10 µl of 3x sample buffer (150 µl 10% SDS, 75 µl 4 M DTT, 400 µl $H_2O$, 375 µl 8x sample buffer – 8 ml 1 M Tris pH 6.8, 9.3 ml 87% Glycerol, 5 mg Coomassie Brilliant Blue G, 2.8 ml $H_2O$) was added to 20 µl-aliquot sample to be analysed by SDS-PAGE. The samples were boiled at 95ºC for 5 min and a 20-µl aliquot of each sample was electrophoresed in 0.75 mm-thick SDS-PAGE gels containing 15% acrylamide (detailed in Materials and methods in Chapter 2). Gels were run with Cathode buffer (0.1 M Tris·base, 0.1 M Tricine, 1 g/l SDS) in the inner cavity and Anode buffer (0.2 M Tris·HCl pH 8.9) in the outer cavity. Electrophoresis was performed at 80–100 V and the gel was subsequently silver-stained.

### Kinetic study of Aß-IDE interaction

Low molecular weight Aß40 was purified by SEC in 50 mM ammonium carbonate and lyophilised into appropriate aliquots. Next, the peptide was resuspended in 50 mM AA, 1 mM Tris, 0.01% $NaN_3$ pH 7.4. IDE (R&D Systems) was immediately added at 30 or 60 nM concentration. At each indicated time point, 100 µl triplicates were sampled and 12 µl of 4.6% TFA were added to stop the enzymatic reaction. Samples were then kept at -20ºC and injected in RP-HPLC-PDA (see conditions in corresponding section). The average and standard deviations were plotted in GraphPad and one phase exponential curve adjusted to the whole data set.

### IDE-mediated Aß fragmentation identification

Low molecular weight Aß40 was purified by SEC in 50 mM ammonium carbonate and lyophilised into appropriate aliquots. Next, the peptide was resuspended in 50 mM AA, 1 mM Tris, 0.01% $NaN_3$ pH 7.4. IDE (R&D Systems) was immediately added at 30 nM. Three hours later, 100 µl triplicates were sampled and 12 µl of 4.6% TFA were

added to quench the enzymatic reaction. Salts were removed using a C18 ZipTip (Waters) and the fragments were identified by LC-HRMS, as detailed below (work performed at the Mass Spectrometry Core Facility – IRB Barcelona).

Independent triplicates of 50 pmol of sample were analysed using BioBasic C18 analytical column (5 µm, 150 × 2.1 mm; Thermo) at a flow rate of 100 µl/min comprising a linear gradient running from 5 to 50% B in 40 min (A= 0.1% formic acid (FA) in water, B= 0.1% FA in acetonitrile). The column outlet was directly connected to an Advion TriVersa NanoMate, which was used as a splitter and as the nanospray source of an LTQ-FT Ultra mass spectrometer (Thermo Scientific). Positive polarity was used with a spray voltage in the NanoMate source set to 1.7 kV. The capillary voltage, capillary temperature, and tube lens on the LTQ-FT were tuned to 40 V, 200ºC, and 100 V, respectively. LTQ-FT Ultra is powered by Xcalibur software (vs. 2.0SR2). Spectra deconvolution was performed with Xtract algorithm. Database searches were performed in Protein Discover 1.3 with Aß40 and IDE Uniprot database. The reported Aß fragments were selected only if they appeared in the peptide list of the three independent replicates. Moreover, each cleavage site was proposed only if the two resulting peptides were detected.

### H/D exchange of Aß fibrils

Amyloid fibrils prepared in 10 mM Tris pH 7.4 were ultracentrifuged using an Optima TLX ultracentrifuge (Beckman) with an MLA 130 rotor (Beckman) at 100000g for 30 min at 4ºC. These conditions have been reported to enable separation of monomer and oligomers from mature fibrils[116,117] and were chosen to obtain homogeneous preparations of Aß amyloid fibrils. The supernatant was removed from the pellet, and it was subsequently diluted in the corresponding deuterated buffer (pH* 7.0), using the same volume that had been lost upon removal of the supernatant. These were mixed using a pipette tip, and then incubated at RT with agitation (500 rpm) (Vortemp 50, Labnet). Aliquots of 100 µl were taken at various time points from 0 to 4-6 days for ESI-MS analysis. Each aliquot was then ultracentrifuged using a TLA 120.1 rotor (Beckman) at 353000g for 1 h at 4ºC. The supernatant was immediately removed, and the pellet was freeze-dried and stored at -20 ºC until analysis. These prolonged, high-speed ultracentrifugation conditions were employed in order to sediment all the fibrils.

## H/D exchange analyzed by ESI-MS

Amyloid fibril samples exposed to H/D exchange and processed as described above, were next dissolved in 100 µl of 95% DMSO-$d_6$/5% $D_2O$ at pH* 4.0 (adjusted with dichloroacetic-$d_3$ acid), which breaks the fibrils down into monomers while preserving the deuterium content of the protein molecules.[103,118] After dissolution, the deuterium content of the samples was analysed by ESI-MS on an LCT Premier XETM TOF system (Waters) equipped with the standard ESI source and a modified nano-ESI probe. The cone gas tubing was detached, left loose inside the source and set to the maximum value of 300 l/h to provide an inert atmosphere during sample ionization within the ESI source. Samples were electrosprayed from gold-coated glass capillaries (ThermoFisher Scientific) with an applied capillary voltage of 2 to 2.8 kV and a cone voltage of 140 V. The same dead time (3 min) was used for sample preparation and parameter adjustment for all measurements. Over time, the peak corresponding to the $P_{pd}$ species gradually converted into the peak corresponding to the $P_{fd}$ species, confirming that $P_{pd}$ and $P_{fd}$ correspond to two isotopically distinct populations of Aß molecules within the Aß fibrils. The spectra were analysed using MassLynx V4.1 (Waters). All mass spectra presented are averages of ten seconds acquisition. Aß peaks (including +3, +4, and +5 charge states) were observed and the most abundant +4 charge state was selected for analysis. To calculate the area of $P_{pd}$ and of $P_{fd}$ at different times of exchange, the spectra were fitted to the sum of two Gaussian peaks using the GraphPad program.

## Preservation of H/D exchange information: controls for forward and back exchange

To determine the number of exposed backbone amides in the $P_{pd}$ and the $P_{fd}$ populations, we employed controls for forward exchange (FE) and back exchange (BE). In the conditions we used to analyse the samples, FE refers to the additional incorporation of deuterium atoms due to exchange with the solubilizing solvent (95% DMSO-$d_6$/5% $D_2O$ at pH* 4), whereas BE refers to the loss of incorporated deuterium due to exchange with hydrogens of atmospheric water as a result of the hygroscopic nature of DMSO and/or during ionization itself. To account for FE and BE, we used the following correction method adapted from a previously reported one.[131]

$$\text{Number of exposed amides} = m - MW - S + BE - FE \qquad \text{(Equation 2)}$$

$$FE = m_{0\%} - MW - S \qquad \text{(Equation 3)}$$

$$BE = MW + S + N - m_{100\%} \quad \text{(Equation 4)}$$

whereby m is the measured average mass of H/D exchanged fibrils corresponding to either $P_{pd}$ or $P_{fd}$; MW is the measured average molecular weight of Aß42 in $H_2O$ (MW = 4514.1 Da); $m_{0\%}$ is the measured mass of fully protonated Aß42 amyloid fibrils prepared by incubating Aß42 in $H_2O$ at pH 2.0 for 4 days and processed as with the H/D exchanged fibrils ($m_{0\%}$ = 4543.4 Da); and $m_{100\%}$ is the measured mass of fully deuterated Aß42 amyloid fibrils prepared by incubating Aß42 in $D_2O$ at pH* 1.6 for 4 days and processed as with the H/D exchanged fibrils ($m_{100\%}$ = 4566.8 Da). The theoretical number of exchangeable hydrogens in Aß42 monomer was calculated by considering all the labile hydrogens in the side chains and in the main chain. These hydrogens are those that are covalently bound to nitrogen, oxygen or sulfur atoms but not to carbon atoms. The Aß42 monomer contains 41 labile hydrogens from the main chain amide groups (N = 41 in equation 4) and 27 labile hydrogens from the side chains and the hydrogens at the chain termini (S = 27 in equations 3 and 4). This gives a total of 68 exchangeable hydrogens. Equation 3 gives a value of 2.3, meaning that roughly two backbone amide protons had undergone FE. Application of equation 4 gives a value of 15.2, meaning that approximately fifteen deuterons (out of sixty eight) had undergone BE.

# Chapter 2.

# Insights into early stage Aß aggregation

## Context

As thoroughly described in the Introduction, Aß aggregation involves different species that exist in complex equilibrium and evolve as a function of time, starting from low molecular weight (LMW) aggregates to amyloid fibrils. This complex equilibrium is portrayed by heterogeneous mixture of transient Aß oligomers of a broad range of sizes, which are in fast and dynamic equilibrium between them.[35,36] Biophysicists and structural biologists have devoted huge efforts to develop techniques to overcome these dynamics and heterogeneity.

One of these developed techniques is the PICUP reaction, which was first designed by Kodadek *et al* back in the 90's[78] and next implemented to study Aß aggregation by the Teplow group.[46,79,80] PICUP is a photochemical reaction able to cross-link pre-existing non-covalent oligomers by oxidative coupling providing a snapshot of the different species present in a mixture (see Box 2). It is a highly suitable method because (i) there is no need to pre-modify the native peptide sequence to introduce chemically reactive moieties, (ii) the short reaction times allow the characterization of dynamic ensembles, (iii) the use of photo-activable reagents enables accurate control of the reaction by light, and (iv) it is applicable at a wide range of temperatures and pH.[78] However, it is necessary to mention that since each additional peptide unit needs the formation of at least one covalent bond, the higher the oligomer order, the lower the cross-linking efficiency. Thus, the PICUP reaction is better suited for the study of LMW oligomer species.

The focus of Aß research has shifted in the last decades from the fibrillar insoluble forms to the soluble oligomers, the initial and intermediate species in Aß aggregation process.[17] In this context, submission of LMW Aß to PICUP reaction and successive analysis through SDS-PAGE has received particular recognition in the field. This analysis led to the conclusion that Aß40 aggregate through monomers up to tetramers, and that pentamers and hexamers constitute the basic building blocks for Aß42 aggregation.[46,79]

### Box 2. PICUP mechanism

PICUP proceeds first by the photo-oxidation of tris(2,2'-bipiridil)-dichlororuthenium(II) hexahydrate cation ($Ru(bpy)_3^{2+}$ - Ru(II)) by visible light in the presence of an electron acceptor, usually persulfate

introduced in the form of ammonium persulfate (APS).[78] Briefly, irradiation of $Ru(bpy)_3^{2+}$ at 452 nm allows a metal-to-ligand transition such that $Ru(bpy)_3^{2+}$ achieves an excited state ($Ru(bpy)_3^{2+}$*), whose potential of reduction is lower than that of the ground state ruthenium cation. Consequently, APS withdraws an electron from $Ru(bpy)_3^{2+}$* generating a sulfate radical and $Ru(bpy)_3^{3+}$ (Ru(III)). Ru(III) is a highly oxidant species able to capture an electron from a nearby protein molecule, such that Ru(III) is recycled to Ru(II) on its ground state and a radical is formed in the protein. This radical is unstable and extremely reactive so it rapidly disappears though intra- and intermolecular reactions, meaning it is able to react with an adjacent protein forming a covalent bond (Figure 2.1C). Theoretically, such radical could be formed anywhere in the protein. However, backbone atoms are not expected to undergo this redox reaction due to steric hindrance. The most labile residue side chains are the ones able to transiently stabilize the unpaired electron by resonance, hyper-conjugation or neighbouring group effect, or combination of the three; this mainly includes tryptophan, tyrosine and histidine.[80,132] Finally, the radical is transformed to a covalent link through coupling to a nearby nucleophilic side chain – such as cysteine, serine, phenylalanine, tryptophan or tyrosine –, and subsequent removal of a hydrogen atom by the initially generated sulphate radical.[78] Of note, although APS reduction potential is very high, this compound is unable to perform the equivalent PICUP oxidative coupling due to kinetic issues.[133]

In this frame of reference, we aimed at isolating these cross-linked species to submit them to a thorough structural analysis. The combined use of ESI-IM-MS, molecular dynamic (MD) simulations and circular dichroism (CD) would ultimately provide structural models for these early Aß aggregates.

The results presented in this chapter follow previous work performed by Dr. Rosa Pujol-Pina during her doctoral thesis. Some of the work presented here has been performed with the invaluable help of Roberta Mazzucato, who carried out a Leonardo da Vinci research stage in the lab during the development of the project. Dr. Marta Vilaseca, head of the Mass Spectrometry Core Facility (IRB Barcelona), has been extremely helpful to produce and analyse all the MS data presented in this chapter. In collaboration with the laboratory of Prof. Modesto Orozco, Dr. Annalisa

Arcella generated and optimised through MD simulations the presented molecular models for these early Aß oligomers.

## Results

### 1. Aß40 and Aß42 apparently oligomerise through distinct pathways

We obtained Aß40 and Aß42 peptides in their lowest aggregation state by SEC following previously described protocols.[45,80] We designated the samples obtained as LMW Aß40 and Aß42 since they contained monomer in rapid equilibrium with low order oligomers (Figure 2.1A). Many reports have already shown that SEC-isolated aggregate-free preparations of Aß consist reproducibly of monomers in dynamic equilibrium with LMW species instead of singly monomeric species.[134,135]

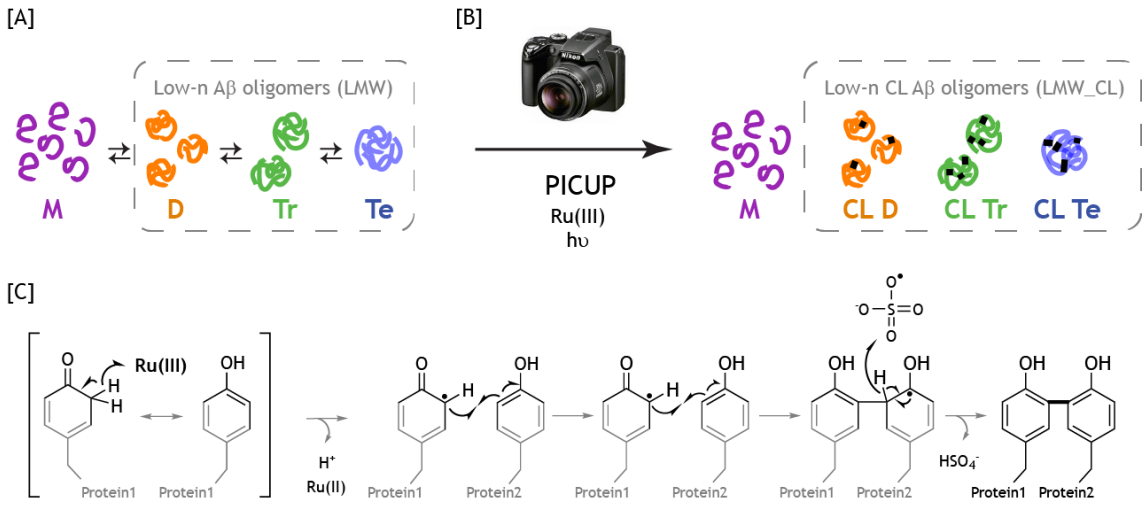


***Figure 2.1.*** **[A]** *LMW Aß samples contain monomers in equilibrium with low order Aß oligomers.* **[B]** *LMW_CL Aß samples are obtained by subjecting their LMW counterparts to PICUP.* **[C]** *The most plausible PICUP mechanism adapted from Fancy* et al[78]

To study LMW species, we froze their dynamic equilibrium by submitting LMW Aß samples to PICUP such that we obtained the corresponding cross-linked (CL) species (Figure 2.1B), from now on referred to as LMW CL (LMW_CL) Aß40 and Aß42. PICUP was performed following previously described conditions,[46,79,80] this is Aß:$Ru(bpy)_3^{2+}$:APS ratio of 1:2:40. Analysis of LMW and LMW_CL samples by silver stained SDS-PAGE showed that we succeeded in reproducing previously reported results (Figure 2.2, lanes 1, 3, 4 and 6).[46] First, LMW Aß40 ran as the expected monomeric band, whereas LMW Aß42 showed three bands corresponding to monomer (M), trimer (Tr) and tetramer (Te). Next, LMW_CL Aß40 electrophoresed as four bands with decreasing intensity from M to Te and an additional faint band of pentamer (Pt). Finally, LMW_CL Aß42 showed an oligomeric distribution going from M

to Tr, with decreasing intensity with higher oligomer order, and from Te up to octamer (O), displaying a Gaussian-like distribution intensity.

In all, these results apparently support the withstanding hypothesis that Aβ40 and Aβ42 oligomerise through distinct pathways. This is, Aβ40 through M up to Te, while Aβ42 does so mainly through Pt and hexamers (Hx).

## 2. Chemically well-defined cross-linked oligomers

### – PICUP reagents ratio

First, we aimed at assessing the chemical homogeneity of LMW_CL samples, a key aspect to characterize Aβ oligomerization which is overlooked in SDS-PAGE analysis. Sample homogeneity was addressed first by means of RP-HPLC-PDA. Since chromatograms were recorded at 220 nm where the peptide bond absorbs, we could obtain a first glance of peptide sample homogeneity. Analysis of LMW_CL Aβ40 samples that underwent PICUP at Aβ:$Ru(bpy)_3^{2+}$:APS 1:2:40 reagent ratio showed more (Figure 2.3A) than the expected four/five peaks that could be detected in SDS-PAGE (Figure 2.2, lane 3). Dr. Marta Vilaseca performed further analysis of the sample by LC-HRMS. This analysis revealed that there where many oxidised by-products, as there were incorporation of 16 u and multiples thereof to monomeric and cross-linked oligomeric Aβ40 molecular weights.

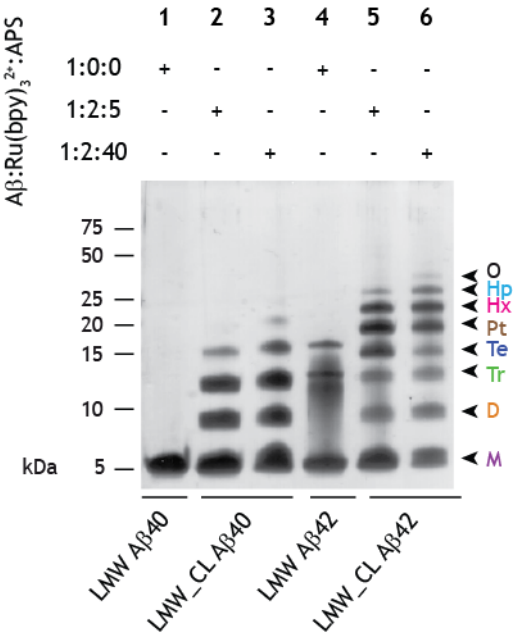


***Figure 2.2.*** *Characterization of LMW and LMW_CL Aβ40 and Aβ42 oligomer distribution by SDS-PAGE. LMW_CL Aβ40 and Aβ42 samples were prepared using two different Aβ:$Ru(bpy)_3^{2+}$:APS ratios, namely 1:2:5 and 1:2:40. M = monomer, D = dimer, Tr = trimer, Te = tetramer, Pt = pentamer, Hx = hexamer, Hp = heptamer, O = octamer*

To minimise peptide oxidation, Dr. Rosa Pujol-Pina, Roberta Mazzucato and I worked together to optimise PICUP conditions starting by the reagent ratio. An 8-fold reduction of APS concentration, this is a reagent ratio of Aβ:$Ru(bpy)_3^{2+}$:APS 1:2:5, yielded a much nicer RP-HPLC-PDA chromatogram in which we could

single out four well-defined peaks (Figure 2.3B). LC-HRMS analysis of the three most abundant peaks identified unequivocally Aβ40 M, CL Aβ40 dimer (D) and CL Aβ40 Tr. The two latter exhibited the expected loss of two hydrogens upon formation of each bond (Figure 2.1C) – this is CL Aβ40 D and Tr had lost 2 and 6 hydrogens, respectively. This was consistent with CL Aβ40 D forming a sole covalent bond and CL Aβ40 Tr creating three covalent bonds (Figure 2.3C). Although the abundance of CL Aβ40 Te was low, we detected a +10 charge state consistent with the formation of four covalent bonds within them ($MW_{theor}$ = 17308.5936; $M_{exp}$ = 17300.5311; ΔHs = -8).

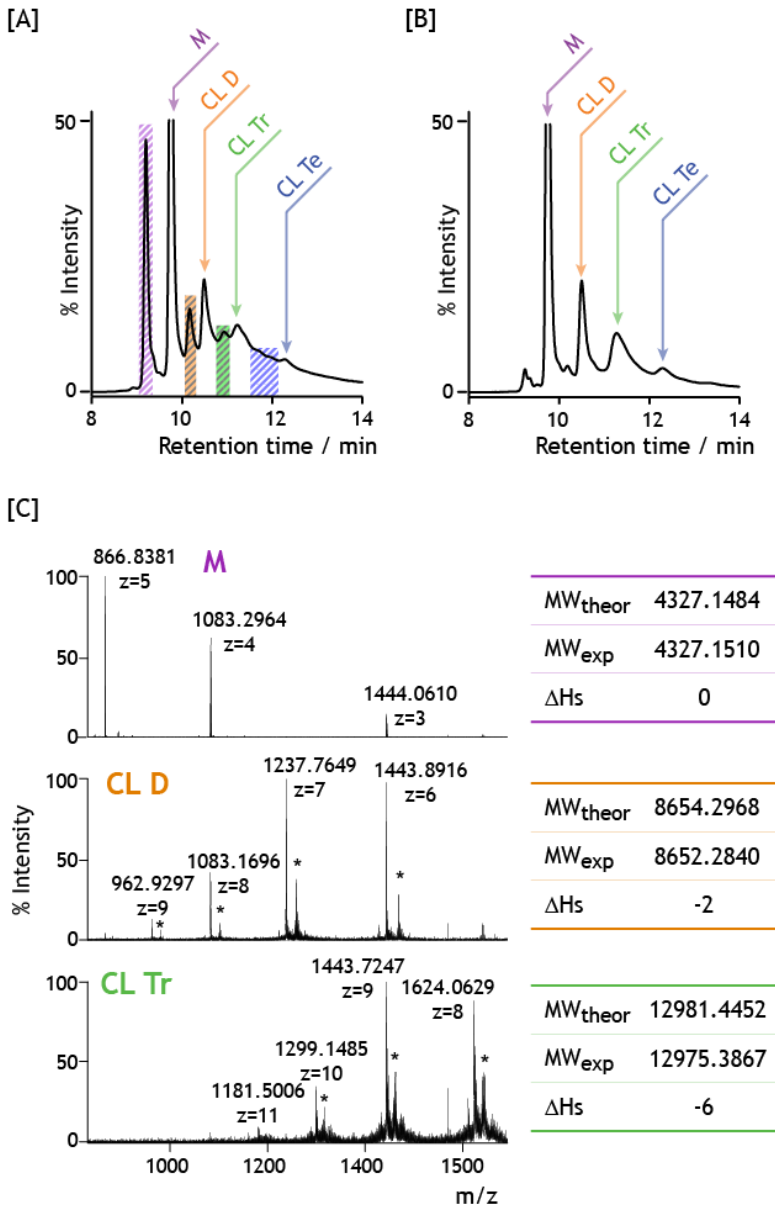


| | |
|---|---|
| $MW_{theor}$ | 4327.1484 |
| $MW_{exp}$ | 4327.1510 |
| ΔHs | 0 |

| | |
|---|---|
| $MW_{theor}$ | 8654.2968 |
| $MW_{exp}$ | 8652.2840 |
| ΔHs | -2 |

| | |
|---|---|
| $MW_{theor}$ | 12981.4452 |
| $MW_{exp}$ | 12975.3867 |
| ΔHs | -6 |

***Figure 2.3.*** *RP-HPLC-PDA characterization of LMW_CL Aβ40, using an Aβ:Ru(bpy)$_3^{2+}$:APS ratio of* **[A]** *1:2:40 and* **[B]** *1:2:5. LC-HRMS of LMW_CL Aβ40 prepared at 1:2:40 ratio revealed different degrees of oxidised by-products indicated as dashed bars in panel* **[A]**. **[C]** *LC-HRMS of LMW_CL Aβ40 prepared at 1:2:5 ratio. Theoretical monoisotopic mass ($MW_{theor}$) considering the intact mass of the oligomer without any cross-links, experimental monoisotopic mass ($MW_{exp}$), and the resulting loss of hydrogen atoms upon cross-linking (ΔHs). The peaks labelled with an * correspond to DTT adducts.*

SDS-PAGE of LMW_CL Aβ40 and Aβ42 obtained under these new PICUP conditions (Figure 2.2, lanes 2 and 5) showed a slight loss of CL species in favour of M abundance. We could not detect Pt for LMW_CL Aβ40 or O for LMW_CL Aβ42. Altogether, although by performing PICUP at Aβ:Ru(bpy)$_3^{2+}$:APS 1:2:5 ratio we

observed a modest reduction in the global CL yield, we achieved a highly homogeneous sample of chemically well-defined CL oligomers.

### – Chemical reduction of methionine-35 sulfoxide

Even if we had minimised the formation of oxidised by-products by fine tuning PICUP conditions, we still observed a small percentage of these oxidised species. One of the most oxidation-prone sites in Aß sequence is the thioether of methionine-35 ($^{35}$Met), which can easily generate the corresponding sulfoxide in the presence of oxidising agents such as APS, one of the reagents in the PICUP reaction. Therefore, the acquisition of 16 u could most probably have happened at $^{35}$Met. One of the objectives of Roberta Mazzucato's Leonardo da Vinci project was to actively eliminate the oxidised by-products through the reduction of methionine sulfoxide. This chemical reduction was achieved using ammonium iodine ($NH_4I$) in TFA, in the presence of dimethyl sulphide ($Me_2S$) as a scavenger.[136] Briefly, protonation of sulfoxide in strong acidic media such as TFA allows the nucleophilic attack by iodide, which yields the reduced methionine thioether and iodine. RP-HPLC-PDA chromatogram of CL Aß40 D that had underwent chemical reduction showed a large decrease of the oxidised species (Figure 2.4 indicated in arrows).

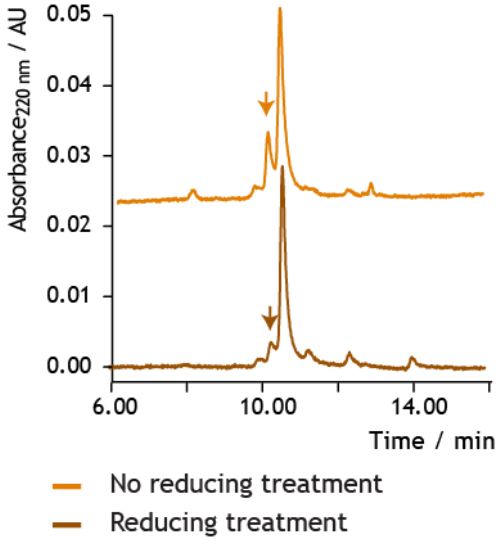


***Figure 2.4.*** *RP-HPLC-PDA chromatograms of Aß40 CL D after optimised PICUP reaction (top, orange) and subsequent chemical reduction of $^{35}$Met (bottom, brown).*

To summarize, optimization of PICUP conditions and chemical reduction of $^{35}$Met sulfoxide ensured chemically well-defined CL Aß40 and Aß42 oligomers, which is imperative to accurately characterize early Aß oligomerization.

## 3. Isolation of cross-linked oligomers

With chemically well-defined CL oligomers in hands, we proceeded to isolate them by SEC. Direct injection of Aß40 and Aß42 PICUP crudes yielded chromatograms displaying a plethora of peaks, although two intense peaks clearly stood out. These two peaks corresponded to large Aß multimers eluting in the void volume (Figure

2.5A, indicated with arrowheads) and to the LMW Aß peak (M in purple, Figure 2.5A). Certainly, Aß42 aggregated faster than Aß40 since the void volume peak was more intense in LMW_CL Aß42 chromatogram compared to LMW_CL Aß40. It is necessary to point, though, that the void volume peak was an overrepresentation of the amount of large oligomeric states found in solution. According to the exclusion limit of the gel filtration columns used, the void volume peak represented oligomers larger than octadecamers, whose absorbance is at least 18 times larger than a single monomeric molecule.

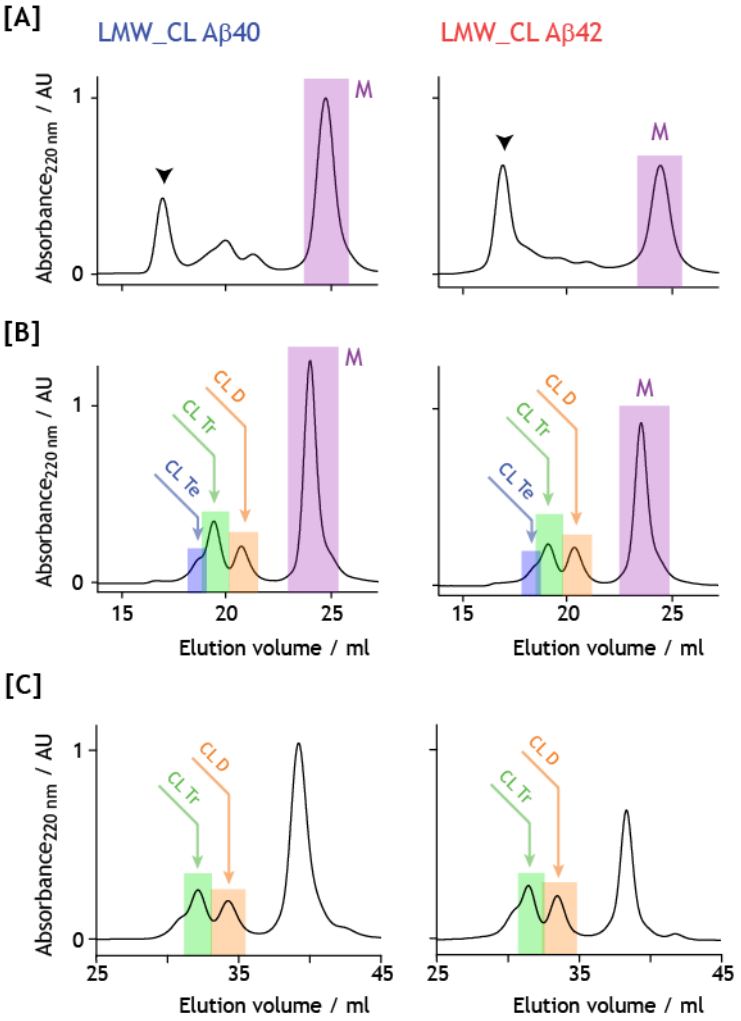


***Figure 2.5.*** *Isolation of CL LMW oligomers by SEC.* **[A]** *Direct injection of PICUP crude of Aß40 (left) and Aß42 (right) in two Superdex 75 (S75) in tandem. LMW peak is indicated with M and the purple bar, while the multimers eluting at the void volume with the arrowheads.* **[B]** *Identical PICUP crudes pretreated with GdnHSCN and injected in tandem S75. Peaks corresponding to CL D, CL Tr and CL Te are indicated in orange, green and blue, respectively.* **[C]** *PICUP crude injected in optimized column configuration of two S75 and one S200 connected one after the other.*

Consequently, pure CL oligomers could not be isolated through this procedure because they were slightly aggregated. Therefore, Roberta Mazzucato and I implemented a new strategy based on the same principles as SDS-PAGE, this is denaturation/disaggregation followed by size fractionation. Denaturation/disaggregation stood for lyophilisation and subsequent resuspension in 6.8 M GdnHSCN, while size fractionation was again performed by SEC. GdnHSCN is a strong chaotropic salt which is able to disaggregate the highly dense and insoluble amyloid plaque cores.[137] Essentially, GdnHSCN was used to disrupt all non-covalent Aß-Aß

interactions, preserving only the covalent ones formed during the PICUP reaction. We referred to this strategy as GdnHSCN-SEC analysis.

GdnHSCN-SEC analysis of LMW_CL Aß40 and Aß42 samples produced chromatograms with four peaks (Figure 2.5B). Roughly, LMW_CL Aß40 oligomer distribution was in agreement with SDS-PAGE results (Figure 2.2, lane 2) and RP-HPLC-PDA chromatogram (Figure 2.3B). Conversely, LMW_CL Aß42 oligomer distribution in SDS-PAGE was not limited to four bands as in GdnHSCN-SEC analysis, but up to seven (Figure 2.2, lane 5). Therefore, subsequent characterization of SEC peaks was required and actually performed by ESI-MS.

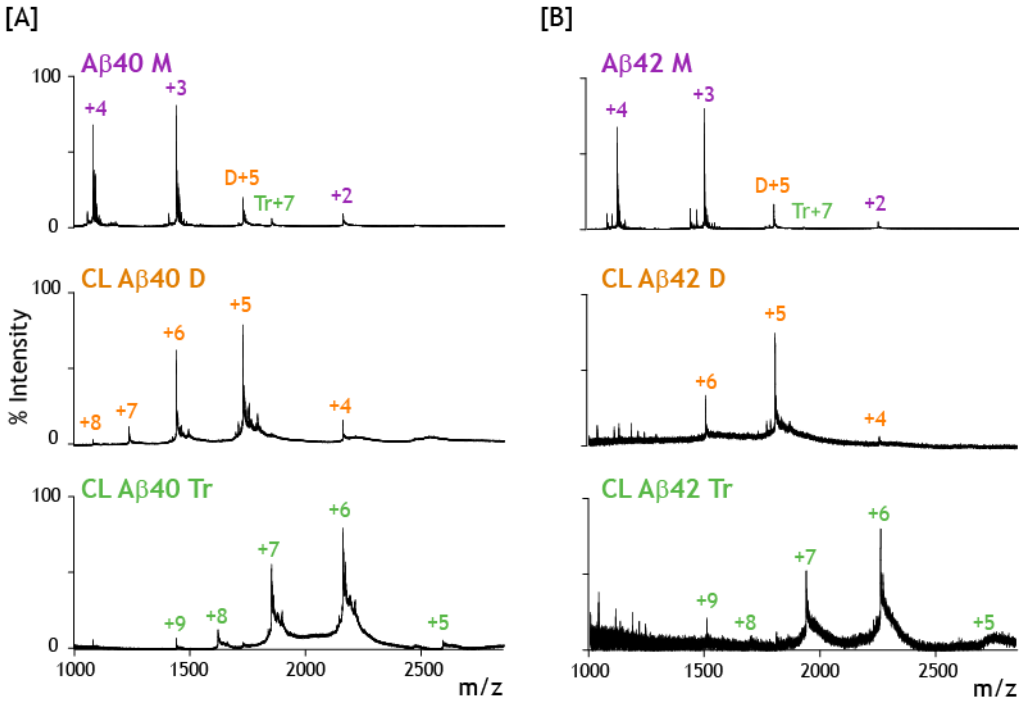


***Figure 2.6.*** *ESI-MS spectra corresponding to peaks detected after GdnHSCN-SEC analysis of* **[A]** *LMW_CL Aß40 and* **[B]** *LMW_CL Aß42 samples. From top to bottom, monomer in purple, CL D in orange and CL Tr in green.*

ESI-MS analysis performed by Dr. Marta Vilaseca showed that the peaks eluting at 24.0, 20.7, and 19.4 ml in LMW_CL Aß40 and at 23.5, 20.3, and 19.1 ml in LMW_CL Aß42 samples corresponded to M, CL D, and CL Tr of Aß40 (Figure 2.6A) and Aß42 (Figure 2.6B), respectively. Although peaks eluting at 18.7 ml in LMW_CL Aß40 and at 18.4 ml in LMW_CL Aß42 (Figure 2.5B) samples were low in abundance, ESI-MS analysis revealed the presence of +8 and +7 charge states corresponding to CL Te. Interestingly, Aß40 M and Aß42 M mass spectra showed peaks corresponding to D +5 and Tr +7 (Figure 2.6). These results converge with the aforementioned description

of the nature of monomeric Aß preparations, namely a mixture of M and LMW oligomers in rapid equilibrium between them (Figure 2.1A).[134]

Additionally, several column configurations with different exclusion limits were tested to achieve the highest peak resolution at the lowest peak broadening. The best performance was achieved by connecting two Superdex 75 10/300 and one Superdex 200 10/300 one after the other (Figure 2.5C).

In conclusion, we attained effective separation of LMW_CL oligomers, which were unequivocally identified. LMW_CL Aß40 oligomer order and distribution was consistent with SDS-PAGE and RP-HPLC-PDA data. However, LMW_CL Aß42 distribution by GdnHSCN-SEC was limited up to Te, while SDS-PAGE analysis displayed up to heptamer (Hp).

## 4. SDS-PAGE revisited

The different Aß42 CL oligomer distribution obtained through SDS-PAGE and GdnHSCN-SEC suggested that SDS could have stabilised or induced Aß42 aggregation. Along the same lines, various groups have expressed their concerns on Aß SDS-PAGE analysis, especially that of Aß42.[46,83,84] This is supported by evidences such as submicellar (sub-CMC) and higher than critical micellar concentration (supra-CMC) of SDS inducing fast oligomerization of Aß42,[46] or Aß42 forming SDS-stable oligomers, i.e. globulomers.[102,138] This is not surprising taking into account that Aß is an amphipathic protein, born out of the cell membrane.

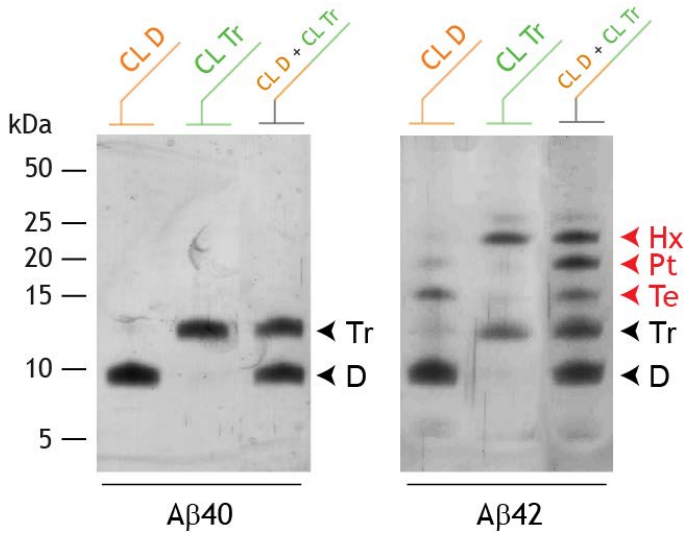


***Figure 2.7.*** *SDS-PAGE analysis of isolated CL D and Tr, as well as mixtures of them for Aß40 and Aß42 obtained after GdnHSCN-SEC fractionation. The red arrows indicate oligomers formed artefactually in the presence of SDS*

The effective isolation of pure LMW_CL oligomers offered a unique opportunity to study the effect of SDS on Aß oligomerization. We analysed Aß40 and Aß42 CL dimers, CL trimers and their mixture by SDS-PAGE (Figure 2.7). All Aß40 samples electrophoresed with the expected molecular weight. Strikingly, CL Aß42 D run also as Te, CL Aß42 Tr also as Hx and their mixture also as Te, Pt and Hx. Since thorough characterization had already been undertaken to characterize CL Aß42 D and Tr, there was no doubt Te, Pt and Hx were artefacts of SDS-PAGE.

Importantly, we have provided clear evidence that SDS affects Aß42 oligomerisation. Consequently, SDS-PAGE is not a reliable technique to assess Aß oligomer stoichiometry and distribution, especially that of Aß42. Moreover, the similar Aß40 and Aß42 CL oligomer distribution gathered through GdnHSCN-SEC analysis indicates that both Aß alloforms aggregate through the same initial intermediates. Overall, these results challenge established conclusions drawn from Aß SDS-PAGE analysis such as the withstanding hypothesis that Pt and Hx are the basic building blocks of Aß42 oligomerization.[46]

## 5. Structural models for LMW oligomers

Having isolated LMW Aß samples, we proceeded to gather structural information of these CL early Aß species. ESI-IM-MS allows individual characterization of coexisting transient species, either covalent or non-covalent. IM resolves species with identical m/z according to their collisional cross-section (Ω) (Figure 2.8).[43,47,73] Ω is informative of the overall shape and molecular size, delivering structural insights into the analysed molecules. Compared to other techniques providing measures of molecular size such as dynamic light scattering, ESI-IM-MS additionally brings at lower concentrations of sample the precise molecular weight, indicative of the chemical nature in terms of stoichiometry and chemical modifications.

Dr. Marta Vilaseca analysed the isolated pure Aß40 and Aß42 CL D and Tr to ESI-IM-MS analysis in order to obtain their molecular size. The generated two-dimensional ESI-IM-MS spectra were projected on the drift time axis. More precisely, we projected the traces at m/z 1732 (D +5) and m/z 1856 (Tr +7) for Aß40 species, and m/z 1806 (D +5) and m/z 1932 (Tr +7) for Aß42 oligomers; these charge states were either the most abundant ones or distinctive to each CL oligomer species (Figure 2.6). Each trace displayed the expected single peaks, although Aß42 CL oligomers exhibited minor shoulders at shorter drift times corresponding to the formation of larger species. In fact, this was consistent with the aforementioned higher tendency of Aß42 to aggregate (Figure 2.9A).

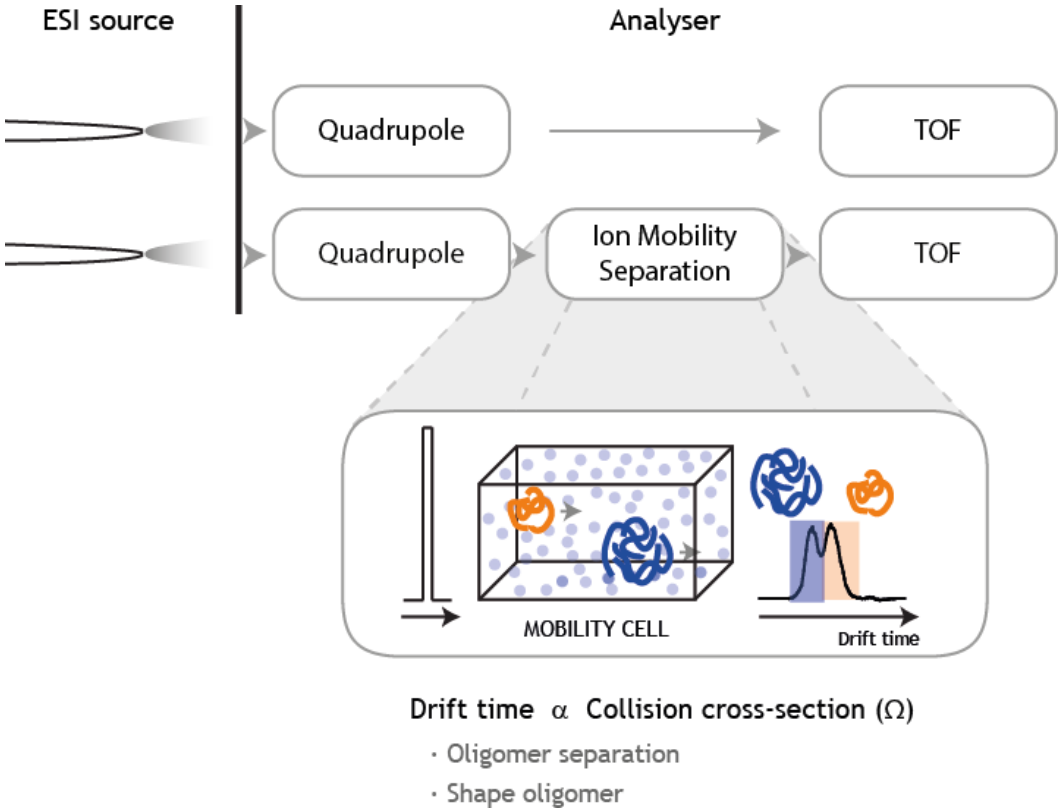


***Figure 2.8.*** *Traditional ESI-MS (top) spectrometer vs ESI-IM-MS (bottom). ESI-IM-MS possesses an ion mobility separation chamber, namely mobility cell, where the separation of different conformers and/or multimers with identical m/z takes place. Separation is performed according to their collisional cross-section. Gas atoms inside the mobility cell are depicted as blue spheres.*

Correlation between drift time and Ω (Figure 2.8) had been previously obtained by Dr. Rosa Pujol through proper calibration of the instrument.[139] Interestingly, the interpolated Ω values for CL dimers were extremely similar to the Ω of non-covalent dimers, also obtained by Dr. Rosa Pujol during her doctoral thesis (Figure 2.9B, Dimer vs CL dimer bars).[139] These results indicated CL oligomers were indeed good mimics of their non-covalent counterparts. Hence, we validated the extrapolation of early Aß oligomers structural analysis from the study of their covalently linked surrogates.

To rationalise the experimentally obtained Ω values, Dr. Annalisa Arcella constructed three structural models of Aß40 D and Aß42 D (Figure 2.9B). These models were built and named nuclear,[140] fibrillar,[141] or compact,[142,143] on the basis of various structural restraints reported for Aß aggregates. All their predicted Ω values were markedly larger than the experimental ones (Figure 2.9B), which indicated that none of the proposed models fitted the experimental data. Thus, to build more realistic structural models and achieve better sampling, Dr. Annalisa Arcella ran atomistic MD simulations using the replica exchange method and simulation

conditions similar to those in a ESI-MS experiment.[144] All the models, irrespective of their original conformation, collapsed to adopt globular structures without defined secondary structure (Figure 2.9B). Importantly, the average Ω value of this ensemble was very similar to the experimental values obtained for the non-covalent and CL dimers (Figure 2.9B).

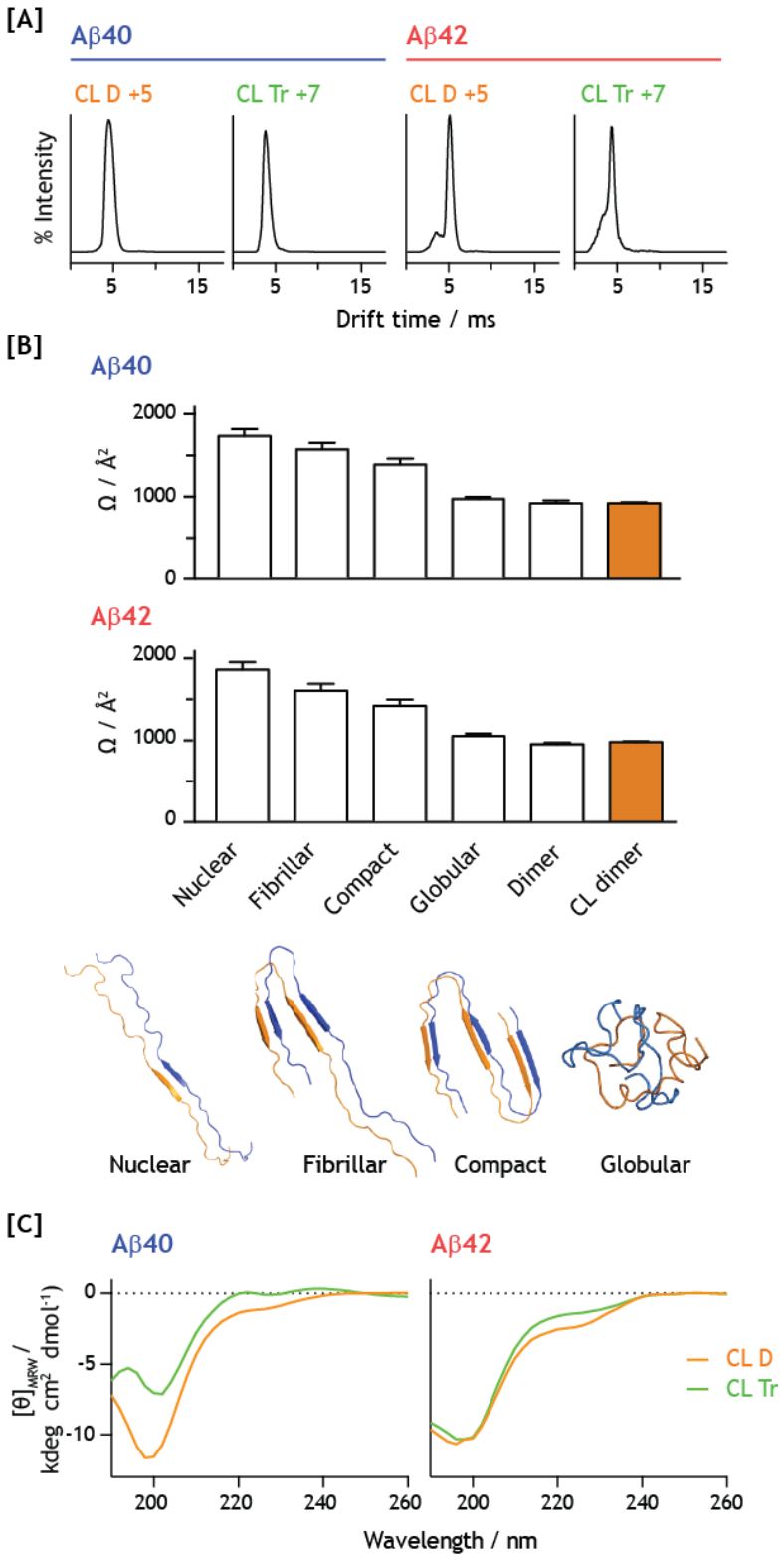


***Figure 2.9.*** *Structural analysis of CL dimers and trimers.* **[A]** *Projections of the ESI-IM-MS spectra on the drift time axis for m/z 1732 (D +5) and m/z 1856 (Tr +7) for Aβ40 CL D and CL Tr (left) and m/z 1806 (D +5) and m/z 1932 (Tr +7) for Aβ42 CL D and CL Tr (right)* **[B]** *Comparison of Ω values obtained from previously described Aβ40 D theoretical models, MD optimized globular model and non-covalent and CL Aβ40 dimers experimental measures (top). Equivalent analysis for Aβ42 (middle). Theoretical dimer models and globular dimer obtained from MD simulations (bottom).* **[C]** *CD spectra of pure CL D (orange) and CL Tr (green) for Aβ40 (left) and Aβ42 (right).*

To validate our molecular models and having access to the pure LMW_CL oligomers, Roberta Mazzucato and I analysed CL Aβ40 and Aβ42 D and Tr by CD spectroscopy (Figure 2.9C). All the samples featured the same large minimum centred at 200 nm, distinctive of random coil secondary structure. Importantly, this experimental data is consistent with the globular models obtained, thereby indicating that LMW_CL oligomers indeed display a globular shape devoid of secondary structure elements.

## Discussion

Optimization of PICUP conditions and chemical reduction of residual $^{35}$Met sulfoxide has delivered chemically well-defined CL Aβ40 and Aβ42 oligomers. GdnHSCN-SEC procedure has afforded effective separation of LMW_CL oligomers. Moreover, GdnHSCN-SEC analysis has shown that the LMW oligomer distribution captured by the PICUP reaction is very similar for both Aβ40 and Aβ42. Importantly, our results evidence that SDS-PAGE is not a reliable technique to assess Aβ oligomer stoichiometry and distribution. Moreover, our findings indicate unequivocally that Pt and Hx are artefacts of LMW_CL Aβ42 SDS-PAGE analysis. Further ESI-IM-MS analysis of CL species has shown that they are good mimics of the non-covalent counterparts, implying their structural analysis can be extrapolated to the early Aβ oligomers. Structural restraints obtained through ESI-IM-MS analysis have been rationalised by means of MD simulations, which have resulted in molecular models displaying globular shape without secondary structure. This lack of secondary structure has been validated by analysis of the isolated CL oligomers by means of CD spectroscopy. Importantly, we have shown Aβ40 and Aβ42 D and Tr, which adopt a globular structure lacking defined secondary structure, are the earliest oligomers formed during aggregation for both Aβ40 and Aβ42.

1. SDS-PAGE: why Aβ42?

The different Aβ42 CL oligomer distributions gathered through SDS-PAGE and GdnHSCN-SEC analysis indicated that SDS could be stabilizing or inducing Aβ42 aggregation. SDS is a surfactant committed to disaggregate and denature protein samples, yet in some cases it might be able to stabilize pre-existing species and/or induce aggregation, such as for amphipathic and/or aggregating-prone peptides and proteins.[82] As a matter of fact, analogous artefactual aggregation by SDS had already been observed back in the 80's for Hepatitis B surface antigen polypeptides.[145] Our SDS-PAGE analysis of well-defined pure Aβ42 CL oligomers has provided conclusive evidence that indeed SDS affects Aβ42 aggregation and that SDS-PAGE is affording a

misrepresentation of the real assembly state of the peptide (Figure 2.7). Consistently, SDS-PAGE-isolated CL Aβ42 oligomers had been reported to be unstable upon re-electrophoreses.[81] This result reinforces our findings that Aβ42 Pt and Hx are not *bona fide* CL oligomers; instead they are compounds of CL D and Tr in the presence of SDS.

Overall, these results show that SDS-PAGE is not suitable to analyse LMW_CL Aβ42. By contrast, SDS-PAGE analysis of LMW_CL Aβ40 does not pose such reticence. This suggests that LMW_CL Aβ42 abnormal behaviour in SDS-PAGE is due to a specific interaction between Aβ42 and SDS. A quick survey of data published on this interaction reveals the particular relationship of this peptide with SDS. First, SDS is able to form and stabilize definite Aβ42 oligomers, i.e. pre-globulomers and globulomers.[102,138] Second, elution of LMW Aβ42 in SEC with mobile phase including sub-CMC and supra-CMC concentrations of SDS showed an increased Aβ42 oligomerisation compared to eluting the peptide with no SDS in the mobile phase.[82] Third, sub-CMC SDS enhanced Aβ42 aggregation tracked by ThT assay.[83] Fourth, NMR studies undertaken in our group have recently shown that SDS does not fully deplete and/or actually stabilizes Aβ42-Aβ42 interactions at supra-CMC concentrations.[146]

Some reports shed light into the essence of this behavior by performing chemical modifications in the Aβ sequence. On the one hand, oxidation of $^{35}$Met to the corresponding sulfoxide ($^{35}$MetO), which increases Aβ42 polarity at the C-terminus, determines that LMW_CL $^{35}$MetO-Aβ42 sample exhibits an oligomer distribution similar to that of LMW_CL Aβ40.[147] In this work, the authors state that the original Aβ42 aggregation pattern, including mainly pentamers and hexamers, is *blocked* by $^{35}$MetO. However, there is not such consensus in the field since reports using other techniques observe accelerated,[148] similar[149] or reduced[150] fibrillization in the presence of $^{35}$MetO compared to wild-type Aβ42. Moreover, we have already shown that Aβ42 Pt and Hx are artefacts from SDS-PAGE analysis. Therefore, we can ascribe this LMW_CL $^{35}$MetO-Aβ42 SDS-PAGE oligomer distribution to the recovery of classical protein-detergent interaction between Aβ42 and SDS; this is the removal of Aβ42-Aβ42 interactions by SDS. On the other hand, a decrease in polarity in $^{35}$Met position by replacement for norleucine, homoleucine[147] and valine[151] keeps LMW_CL Aβ42 abnormal performance in SDS-PAGE. Furthermore, analyses of LMW_CL Aβ41 and Aβ43 also display oligomer distribution comparable to that of LMW_CL Aβ42.[79] These results suggest there is a highly stable C-termini interaction that SDS cannot disrupt, which has been reported for SDS-stable dimeric pre-globulomers through NMR and HDX-NMR.[102] Overall, the structural elements – studied so far – fundamental for

hypothetical SDS-stabilized interaction are the length of the Aß C-terminus itself and the polarity of $^{35}$Met position. This C-termini hypothesis is further supported by the aforementioned NMR study from our research group, in which the reported stabilized Aß42-Aß42 interaction is derived from chemical shifts at $^{35}$Met position.[146] Consequently, such interaction should take place over $^{35}$Met position, or at least close-by.

## 2. Insights into early stage Aß oligomerization

The development of a fractionation protocol with a previous disaggregating treatment granted us access to pure isolated LMW_CL oligomers of defined order. We characterised these species by CD spectroscopy (Figure 2.9C). Combination of CD data with structural information derived from ESI-IM-MS Ω values, and atomistic MD simulations (Figure 2.9), showed that D and Tr have a globular fold lacking defined secondary structure. This observation contrasts with previous publications where SDS-PAGE purified CL Aß40 D, Tr and Te were suggested to adopt a ß-sheet structure.[81] In the aforementioned work, the authors used PICUP conditions that, in our hands, afforded a heterogeneous mixture of oxidised products when analysed by RP-HPLC-PDA and LC-HRMS (Figure 2.3). Moreover, the authors fractionated the oligomers using SDS-PAGE, and although several purification steps were applied, there is the possibility that SDS contaminated the samples, thus affecting the structure of the purified oligomers.

Our findings challenge the longstanding conclusion that Pt and Hx are Aß42 aggregation building blocks. Such conclusion was built upon the use of SDS-PAGE to characterize Aß oligomers samples, and we have shown that Pt and Hx form artefactually from D and Tr in the presence of SDS.[46] GdnHSCN-SEC analysis of LMW_CL oligomers evidences that Aß40 and Aß42 oligomerise through the same intermediates, although we cannot exclude that PICUP has not been able to capture larger species found in solution. It is remarkable, though, that there are not prominent differences between their oligomer distributions, meaning there is not a LMW oligomer of specific stoichiometry and/or abundance that differentiates their initial aggregation patterns. With regards to the higher tendency of Aß42 to aggregate compared to Aß40, it is noticeable that there are no elements of secondary structure or the formation of specific oligomers (different than most abundant dimers and trimers) that can account for it. Alternatively, the higher aggregation propensity of Aß42 peptide could be ascribed to the higher surface

hydrophobicity of the oligomers formed, as previously pointed in other reports using HypF-N as a model amyloid protein.[152]

Finally, ESI-IM-MS analysis of Aβ40 and Aβ42 CL D and Tr shows they adopt a globular shape without defined secondary structure. These results can be extrapolated to the earliest oligomers formed during Aβ aggregation because CL oligomers are good mimics of the non-covalent counterparts. Since structural models for other higher order Aβ oligomers have been reported to adopt a ß-sheet structure,[142,143,153] our findings that Aβ D and Tr are globular and lack defined secondary structure is critical for the development of diagnostic and therapeutic strategies that specifically target Aβ oligomerisation.

## Materials and methods

### Preparation of LMW Aβ40 and Aβ42

LMW Aβ40 and Aβ42 preparations were obtained using SEC. First, Aβ was dissolved at 8.5 mg/ml Aβ concentration in 6.8 M GdnHSCN, sonicated for 5 min, diluted to 4 M GdnHSCN at a 5 mg/ml Aβ concentration, centrifuged at 10,000g for 5 min. The resulting solution was injected into a HiLoad Superdex 75 HR 16/60 column (GE Healthcare) previously equilibrated with 10 mM sodium phosphate, pH 7.4, and eluted at a flow rate of 1 ml/min. The system was kept at 4°C. The peak attributed to low molecular weight Aβ was collected, and its peptide concentration was determined by RP-HPLC-PDA. The peptide solution was then diluted to 150 μM, frozen, and kept at -20ºC until used.

### RP-HPLC-PDA analysis

RP-HPLC-PDA analysis (Waters Alliance 2695 equipped with 2998 photodiode array detector) was carried out using a Symmetry 300 C4 column (4.6 × 150 mm, 5 μm, 300 Å; Waters), a flow rate of 1 ml/min, and a linear gradient from 0 to 60% B in 15 min (A = 0.045% TFA in water, and B = 0.036% TFA in acetonitrile) at 60ºC. A calibration curve was generated based on Aβ40 and Aβ42 solutions that had previously been quantified by amino acid analysis.

### PICUP reaction

The PICUP reaction was initially run following descriptions in the literature.[80] The experimental set-up consisted of a camera body and a 150-W slide projector. A PCR tube containing the reaction mixture to be cross-linked was placed inside the camera

body for irradiation. The sample was irradiated via the slide projector for a short time, precisely controlled by the camera shutter. PICUP reactions were done using an Aß/$Ru(bpy)_3^{2+}$/APS ratio of 1:2:40. To this end, 4 µl of 3 mM $Ru(bpy)_3^{2+}$ and 4 µl of 60 mM APS were added to 40 µl of 150 µM LMW Aß in 10 mM sodium phosphate buffer. The mixture was irradiated for 1 s at a distance of 10 cm and immediately quenched by adding 6.5 µl of 4 M DTT. Later on, reaction conditions were optimised to prevent Aß oxidation. The best conditions were found when using a lower proportion of APS, Aß:$Ru(bpy)_3^{2+}$:APS 1:2:5, a distance of 10 cm, and an irradiation time of 1 s. Unless otherwise stated, an Aß/$Ru(bpy)_3^{2+}$/APS ratio of 1:2:5 was used to prevent formation of oxidised byproducts and to obtain chemically well-defined cross-linked oligomers. After the PICUP reaction, the reagents, which are incompatible with ESI-IM-MS and RP-HPLC-PDA analysis, were removed using Bio-Spin P30 columns (Bio-Rad) equilibrated in 10 mM AA pH 8.5. For comparative purposes, PICUP samples were also passed through Bio-Spin P30 columns when analysed by SDS-PAGE.

**SDS-PAGE**

10 µl of 3x sample buffer (150 µl 10% SDS, 75 µl 4 M DTT, 400 µl $H_2O$, 375 µl 8x sample buffer – 8 ml 1 M Tris pH 6.8, 9.3 ml 87% Glycerol, 5 mg Coomassie Brilliant Blue G, 2.8 ml $H_2O$) were added to 20 µl-aliquot sample to be analysed by SDS-PAGE. The samples were boiled at 95ºC for 5 min and a 20-µl aliquot of each sample was electrophoresed in 0.75 mm-thick SDS-PAGE gels containing 15% acrylamide, as described below.

| | Resolving | Stacking |
|---|---|---|
| Acrylamide/Bis 40% | 4.000 ml | 1.000 ml |
| $H_2O$ | 1.300 ml | 2.000 ml |
| 99% Glycerol | 1.200 ml | - |
| 3 M Tris pH 8.5 | 3.350 ml | 1.050 ml |
| SDS 20% | 50 µl | 16 µl |
| APS 10% | 150 µl | 50 µl |
| TEMED | 6 µl | 6 µl |

Gels were run with Cathode buffer (0.1 M Tris·base, 0.1 M Tricine, 1 g/L SDS) in the inner cavity and Anode buffer (0.2 M Tris·HCl pH 8.9) in the outer cavity. Electrophoresis was performed at 80–100 V and the gel was subsequently silver-stained.

**LC-HRMS**

180 pmols of LMW_CL Aß40 was analysed using a BioSuite pPhenyl 1000 analytical column (10 µm, 2 × 75 mm; Waters) at a flow rate of 100 µl/min comprising a linear

gradient running from 5 to 80% B in 60 min (A= 0.1% FA in water, B= 0.1% FA in acetonitrile). The column outlet was directly connected to an Advion TriVersa NanoMate, which was used as a splitter and as the nanospray source of an LTQ-FT Ultra mass spectrometer (Thermo Scientific). Positive polarity was used with a spray voltage in the NanoMate source set to 1.7 kV. The capillary voltage, capillary temperature, and tube lens on the LTQ-FT were tuned to 40 V, 200ºC, and 100 V, respectively.

### Reduction of $^{35}$Met

To completely reduce all oxidised methionine residues, 500 µl of the quenched PICUP reaction was lyophilised and resuspended in TFA containing 30 equivalents of $Me_2S$-$NH_4I$ and left for 2 h at 4ºC on a rotating wheel. Afterwards, TFA was evaporated under a stream of nitrogen and 500 µl of $H_2O$ were added to the sample. The mixture was then lyophilised.

### GdnHSCN-SEC

The lyophilised sample was resuspended in 6.8 M GdnHSCN at an Aß concentration of 8.5 mg/ml, and subsequently diluted with $H_2O$ to 5 mg/ml of peptide and 4 M GdnHSCN. The resulting Aß solution was injected into two or three columns in series: either Superdex 75 HR 10/300-Superdex 200 HR10/300 or Superdex 75 HR 10/300-Superdex 75 HR 10/300-Superdex 200 HR10/300. The columns were equilibrated in 10 mM AA pH 8.5, and the samples eluted at 4ºC at a flow rate of 0.5 ml/min.

### ESI-IM-MS

IM-MS experiments were performed on a Synapt HDMS (Waters) quadrupole-traveling wave IMS-oaTOF mass spectrometer, equipped with an Advion TriVersa NanoMate (Advion Biosciences). Positive ESI was used with a capillary voltage of 1.7 kV. A sampling cone voltage of 40 V and a backing pressure of 5.7 mbar were set for the observation of LMW Aß oligomers. Data were acquired over the m/z range of 500 to 5000 for 2 min. The ion accelerating voltage in the trap T-wave device was 6 V unless otherwise stated; the ion accelerating voltage in the transfer T-wave device was kept constant at 4 V. The IM gas flow was kept at 23 ml/min. IM-MS data were obtained at three wave heights: 7, 7.5 and 8. The drift time Ω function had been calibrated using the proteins ubiquitin, myoglobin and cytochrome C.[139] Drift times had been corrected for both mass-dependent and mass-independent times. The raw

data were processed using Mass Lynx v4.1 software (Waters). The reported data are the average of three independent experiments.

## Far-UV CD Spectroscopy

CD spectra were recorded on a Jasco 815 spectrometer from 190 to 250 nm with a data pitch of 0.2 nm, a bandwidth of 2 nm, and a scan speed of 50 nm/min with a 4 s time response. A 1-cm cell was used. After GdnHSCN-SEC fractionation using three columns in series equilibrated in 10 mM sodium phosphate at pH 8.5, spectra for CL Aβ40 and Aβ42 dimers, and trimers were acquired at 4°C. CD data were analysed using the SpectraManager program.

# Appendix A.

# The neurotoxicity of cross-linked Aß dimers

## Context

Genetic studies showed AD-linked mutations were only located in APP and in the presenilins,[3] and they all entailed an enhanced Aß aggregation. That is the reason why few years ago the focus of AD research was devoted to the visible insoluble amyloid plaques.[20] Nowadays, this focus has shifted to the soluble Aß species because this pool has been shown to correlate much better to the severity of cognitive decline in patients, than the deposition of amyloid plaques.[21,22] However, these soluble species are ill-defined species because of a prevailing poor structural characterization and the absence of sample preparation standardization in the field.[69,70] Moreover, as thoroughly described in the Introduction, Aß aggregation is an extremely dynamic process in which there are not singly defined species but instead an heterogeneous mixture of multimers composed of several alloforms of Aß, ranging from 37 to 43 amino acids long, which might even be phosphorylated, oxidised or nitrosilated.[14] In spite of all these hurdles, many presumable neurotoxic oligomers have been described over the years.

The structure-activity studies (SAR) of the neurotoxic Aß oligomers described to date can be classified into 3 major groups: *in vivo*, *ex vivo* and *in vitro*. The criterion applied is based on the procedure to isolate the oligomers and on how the biological activity is assessed. *In vivo* studies lean on transgenic (Tg) mouse models by which biological activity is addressed either through behavioural tests or post-mortem histological assessment. This approach isn't strictly a SAR since it doesn't yield clues on the Aß neurotoxic structure, but brings out potentially useful biomarkers and diagnostic tools, as well as mechanistic insights. However, lack of Tg mice reproducing completely all AD phenotypes is still a matter of debate.[18] After the breakthrough of the pluripotent stem cell technology, promising studies with patients' neural cells are underway.[154] In contrast, *ex vivo* and *in vitro* SAR are based on the exogenous delivery of isolated Aß species to animals and/or cell cultures, with the conspicuous concern on the uncontrolled evolution of these Aß preparations in the tissues or cultures.[155] *Ex vivo* approaches isolate Aß neurotoxins from AD patients' brain homogenates. However, the isolation procedure does not exclude the formation of artefactual Aß species. *In vitro* studies rely on formation of neurotoxic Aß oligomers from recombinant or SPPS sources, and by chemical (salts, pH, detergents, lipids…), physical (temperature) and/or mechanical (shaking) means. The concern is whether the obtained species correspond to real oligomers functionally meaningful in AD pathology.

Three main presumable toxic mechanisms have emerged over the last 20 years. First, some reports[156] claim a membrane-mediated mechanism by formation of Aß pores/channels in the cellular membrane[157] and/or by direct membrane permeation through perturbation of membrane lipids. This includes the hypothetical peroxidation of membrane lipids by reactive oxygen species (ROS) originated from Aß-copper (II) ($Cu^{2+}$) redox interaction.[158] The second mechanism has been attributed to Aß-mediated functional disruption of synapse receptors such as N-methyl D-aspartate receptor,[159,160] Insulin Receptor,[161] $PrP^{c}$,[94,162] or leukocyte immunoglobulin-like receptor B2,[163] among others.[164] Third, evidences of tau protein-dependence on the exerted neurotoxicity has motivated the study of an alternative toxic pathway in which Aß triggers tau dysfunction, and subsequent cell death.[11,165,166] Overall, these huge amount of data and hypotheses might simply reveal that not a single mechanism is driving Aß neurotoxicity.[155]

Faithful SAR have been assessed by means of a huge plethora of biological assays.[69] The first to be implemented were the ones evaluating cytotoxicity in general terms, without any mechanistic insight. These included assays monitoring cellular metabolism, activation of apoptotic pathways[167-170] or direct cellular death by live/dead cell staining.[37,39,171] The star in the assays tracking cellular metabolism was 3-(4,5-dimethylthiazol-2-yl)-2,5-diphenyltetrazolium bromide (MTT) reduction assay.[38,56,172] MTT assay is based on the reduction of soluble MTT to purple insoluble MTT formazan by the action of mitochondrial respiratory chain enzymes; this assay is routinely used in many fields to measure cell viability.[173] However, some reports claimed that either Aß enhanced MTT formazan exocytosis[174] or that MTT formazan formed needle-shaped crystals in the presence of Aß that disrupted the cell membrane.[171] In the end, this implied an overestimation of cellular death. Nowadays, many groups in the Aß research field still work with formazan salts, but those yielding soluble products such as 2,3-Bis-(2-Methoxy-4-Nitro-5-Sulfophenyl)-2H-Tetrazolium-5-Carboxanilide (XTT) or AlamarBlue®.[171] Finally, another assay whose readout is cell viability is lactate dehydrogenase (LDH) release, extensively used to assess Aß biological activity too.[81,167,171,173] This assay quantifies the release of LDH, a cytoplasmatic enzyme, due to cell membrane disruption, implying a membrane-mediated toxic mechanism.

Even though cytotoxicity assays have been broadly used so far, many groups realised some time ago that overt neuronal death only appears at the very end stage of AD. Subsequently, in intermediate phases of the disease, when cognitive decline is progressively increasing, more subtle and transient toxic events are more likely to be

happening. That's why many efforts were then devoted to examine synaptotoxicity. The biological assays designed to address this synaptotoxicity were (i) the assessment of synaptic morphology[42,167,171,175] in terms of spine density and synapse distortion/loss and (ii) electrophysiological measurements at the synapses such as long-term potentiation (LTP), long-term depression (LTD),[160] patch-clamp and measurement of *firing rates* in neuronal networks.[169] LTP assessment has received particular attention[37,40,176] since it reflects synaptic plasticity and it has long been recognised as an *in vitro* correlate of learning and memory. Moreover, its measurement coupled to the addition of specific receptor inhibitors[42,160] sheds light into the mechanism of LTP alteration. In parallel, behavioural tests in rodents have also been used to address neurotoxicity. Briefly, icv injection of Aß preparations in mice/rats is followed by passive avoidance,[42] contextual fear conditioning,[169] or alternating lever cyclic ratio tests.[41,177]

Besides, other groups have focused on an intracellular toxic marker; this is calcium ($Ca^{2+}$) influx. $Ca^{2+}$ plays fundamental roles in neurons such as the control of membrane excitability, mitochondrial metabolism and the release of neurotransmitters. $Ca^{2+}$ also mediates activity-dependent changes in gene expression, and drives neuronal growth, differentiation and transition to apoptosis.[178] Moreover, $Ca^{2+}$ regulates serine/threonine phosphatase calcineurin, a protein tightly involved in neuronal physiology.[179] Therefore, disturbance of $Ca^{2+}$ homeostasis might lead to apoptosis, excessive phoshorilation of key neuronal proteins and/or alteration of membrane potential, leading ultimately to death. Interestingly, Aß oligomers have been reported to interfere in exogenous $Ca^{2+}$ influx primarily in axons, inhibiting mitochondrial transport.[165] Such influx has been claimed to be mediated by either synaptic receptors or membrane leakage.[156,157]

Finally, this last paragraph is devoted to the third hypothetical mechanism of toxicity which involves tau protein. First, tau phosphorylation and accumulation in NFTs have been proved to be downstream of Aß aggregation, since Aß icv injection in tau Tg mice exacerbates both tau phenotypes.[180] Next, APP/tau Tg mice which develop plaque deposition and tau hyperphosphorylation – but not NFT formation – suffer from memory deficits and shorter lifespan. Knocking-out tau gene, lethality and memory impairment are rescued.[12] In this framework, Zempel *et al* performed a thorough descriptive analysis of Aß-tau mediated neurotoxicity.[165] An Aß oligomer preparation named ADDLs[37] was shown to induce tau phosphorylation and its missorting from axons to somatodendrites, such that wherever tau was missorted, spine density was reduced and there was a decrease in microtubules and

mitochondria, as well as a local $Ca^{2+}$ increase. Further studies showed that Aß dimers induced cytoskeletal disruption and neurite degeneration, phenotypes that were rescued upon tau gene knock-down.[11] Additionally, tau was proved to be required for Aß induced LTP alteration.[166]

## Results

In the context of this overview on Aß-mediated neurotoxicity in AD, the work by Shankar *et al*[42] on neurotoxic dimers isolated from AD brain samples inspired us to address whether our CL Aß dimers were toxic to primary neuronal cultures. In fact, this was imperative to us taking into account that our species might be relevant in the disease, since PICUP mechanism proceeds through a similar mechanism as ROS could presumably form CL Aß species *in vivo*[181] (Figure A1). Interestingly, similar hypothesis arose from studies on transglutaminase-catalysed Aß cross-linking, which yields biologic active moieties that inhibit LTP in mice brain slices.[176]

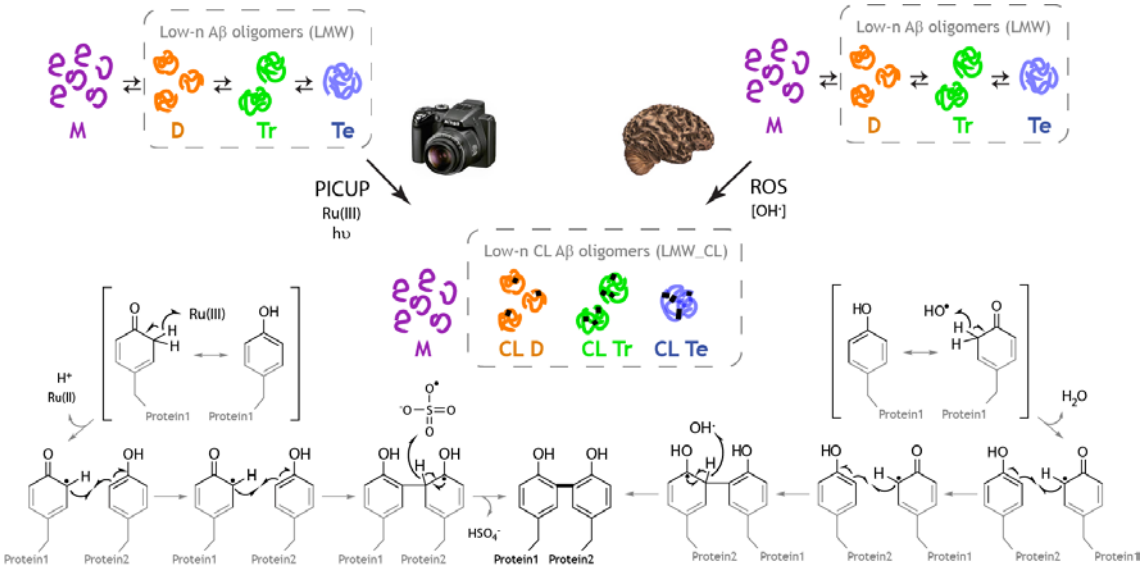


***Figure A1.*** *Comparison between PICUP and ROS mechanisms on their ability to form intra- or intermolecular covalent bonds between nearby susceptible residues.*

### 1. MTT assay: starting point to address CL dimer neurotoxicity

We selected MTT assay as our starting point to assess CL Aß40 dimer neurotoxicity. The reason is that we had previous successful experience in MTT implementation in rat primary hippocampal neuronal cultures.[56] This was possible thanks to the longstanding collaboration with the group of Prof. Eduardo Soriano (Universitat de Barcelona), precisely with the help of Dr. Lluís Pujadas and Dr. Daniela Rossi on the primary neuronal cultures and the use of MTT assays. Further XTT assays were

performed with the invaluable help of postdoctoral fellow Dr. Aurelio Vázquez de la Torre.

MTT assay addresses cell viability in terms of cellular metabolic activity. MTT is a tetrazolium soluble salt that upon the action of the mitochondrial respiratory chain enzymes is reduced to insoluble purple formazan crystals. Such crystals are then dissolved and the generated formazan is quantified spectrophotometrically, thus its absorbance correlates with the amount of living cells. This assay is extensively applied in many fields because of its simplicity and the use of inexpensive instrumentation.[173]

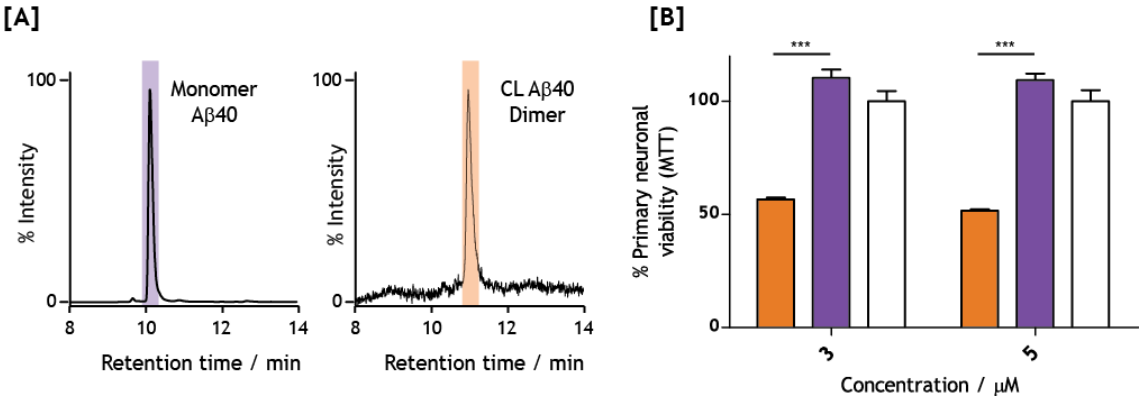


***Figure A2.*** *MTT assays of CL Aβ40 dimer.* **[A]** *RP-HPLC-PDA chromatograms of Aβ40 monomer and CL dimer.* **[B]** *MTT results of one of the three independent primary neuronal cultures that were incubated with 3 and 5 μM nominal concentrations of CL Aβ40 dimer (orange bar) and Aβ40 monomer (purple bar) as control; also the vehicle (white bar) was used as negative control. Each column represents quadruplicate measures in terms of mean ± standard deviation. Significant differences indicated by asterisks (p-value < 0.001 is ***).*

First, we obtained CL Aß40 dimer by submitting LMW Aß40 to the PICUP reaction, followed by subsequent analytical RP-HPLC-PDA purification performed manually (Figure A2-A). Conversely to what has been described in Chapter 2, at this point of the project dimer purification wasn't still optimised to be performed by GdnHSCN-SEC analysis. Excitingly, three independent MTT assays in quadruplicate measures showed that CL Aß40 dimer was toxic to neuronal cells at 3 and 5 μM nominal concentrations up to only 50% cell viability in a slight dose-dependent fashion (Figure A2-B). Incubation of Aß40 monomer or the vehicle, following identical sample preparation as CL Aß40 dimer, did not induce any toxic effect. These results were in agreement with previous studies reporting toxicity for Aß dimers: LTP was inhibited by SDS-stable dimers from AD brains,[42] and CL Aß40 dimers (obtained also through

PICUP reaction and successive isolation from SDS-PAGE gel) were shown to be toxic to PC12 cells (cell line from rats) as measured by MTT assay.[81]

## 2. Overcoming MTT: XTT assay

In spite of these positive MTT results, we realised there were few concerns in the application of this methodology to address Aß neurotoxicity. It was reported that either Aß enhanced MTT formazan exocytosis[174] or that Aß induced formation of MTT formazan needle-shaped crystals able to disrupt the cell membrane.[171] In the end, this implied an overestimation of cellular death. This is why we decided to repeat identical exposure of hippocampal neuronal cells to CL Aß40 dimer, this time monitored by XTT cell viability assay. The principle of XTT assay is alike MTT with the exception that XTT formazan is soluble, excluding the possibility of membrane disturbance by formazan crystals.[171] Importantly, this time CL Aß40 dimer was obtained following GdnHSCN-SEC procedure instead of RP-HPLC-PDA manual purification (Figure A3-A). Because of the purification procedure, CL dimer was incubated at 0.16 and 0.27 µM nominal concentrations, this is around 20-fold lower than in MTT assays. Surprisingly, incubation of CL Aß40 dimer monitored by XTT assay didn't yield at all the extent of cellular death recorded in the MTT assays (Figure A3-B).

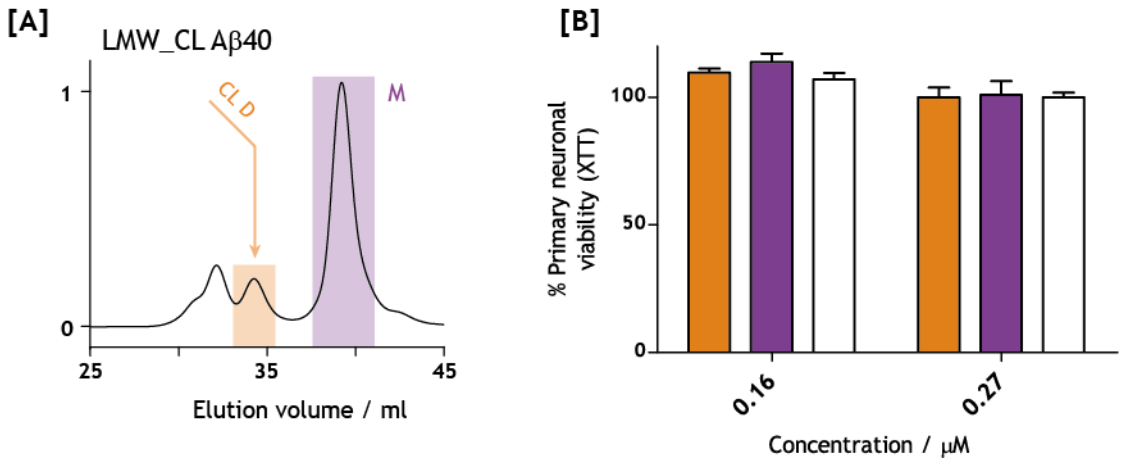


***Figure A3.*** *XTT assays of CL Aß40 dimer.* **[A]** *GdnHSCN-SEC chromatogram of LMW_CL Aß40, CL dimer depicted in light orange.* **[B]** *XTT results of primary neuronal cultures incubated with 0.16 and 0.27 µM nominal concentrations of CL Aß40 dimer (orange bar) and Aß40 monomer (purple bar) as control; also the vehicle (white bar) was used as negative control. Each column represents quadruplicate measures in terms of mean ± standard deviation.*

This result could be explained by three distinct and complementary hypotheses. First, the reduction in CL Aß40 dimer nominal concentration could be sufficient to

decline its neurotoxic activity in the time scale of the experiment (24 hours), meaning that maybe more subtle toxic events are occurring that do not end in neuronal death over this time range. Second, MTT assay toxicity could be indeed a readout of an enhanced MTT formazan exocytosis[174] or else of membrane disruption by MTT formazan crystals as described in Wogulis *et al*.[171] In fact, in this article they show similar differences on the performance of identical Aß samples in MTT and XTT assays. Third, the purification protocol could be crucial to understand the divergence in the output of both assays: in MTT assays CL Aß40 dimer was purified by means of RP-HPLC-PDA, whilst in XTT assay by GdnHSCN-SEC procedure. The toxicity displayed in the MTT assays could be explained by the mere presence of TFA salts, which eluted with the peptide (because of TFA acid present in RP-HPLC-PDA mobile phases) and that might not had volatilized during sample lyophilisation. In pharmaceutical drug discovery programs, TFA salts have been described as undesirable counterions associated to RP-HPLC-PDA purification. The reasons are that these salts could lead to potential toxic effects, and that they have been shown to induce reduced pharmacokinetic properties.[182] Overall, the second and third hypotheses imply CL Aß40 dimer is not toxic to hippocampal neuronal cells. Nonetheless, the first hypothesis could also be plausible in that more subtle undetectable toxic events could be taking place.

### 3. From bulk measurements to single cell resolution: SICM

During my research stage in Prof. Klenerman's group at the University of Cambridge, I had the opportunity to assess dimer neurotoxicity at extremely high resolution and focusing on more subtle toxic events such as $Ca^{2+}$ intracellular influx. All the work presented in this section has been performed with the invaluable help of Dr. Nadia Shivji (neuroglial cultures preparation) and Dr. Anna Drews (expertise in SICM instrumentation and $Ca^{2+}$ influx experiments).

The Klenerman's group had previous experience in assessing Aß neurotoxicity in hippocampal neuroglial cultures. They focused their attention to $Ca^{2+}$ influx as an intracellular toxic marker, which was measured by means of the fluorescent intracellular $Ca^{2+}$-sensitive dye Fura-2.[183] In this work, they observed that very low Aß concentrations (500-0.2 nM, comparable to XTT assay concentrations) induced $Ca^{2+}$ influx in astrocytes, but not in neurons. They attributed cell-type specific response to the different cellular membrane composition. Moreover, they claimed the mechanism of such toxicity was through the formation of pores in the membrane,

instead of specific binding to membrane receptors due to the low Aß concentration applied, similarly to what was concluded by other groups.[157]

When I joined the group, they were pushing this approach a step forward: they were able to deliver Aß and to assess the subsequent induced $Ca^{2+}$ influx at individual cells, by means of Ion Scanning Conductance Microscopy (SICM).

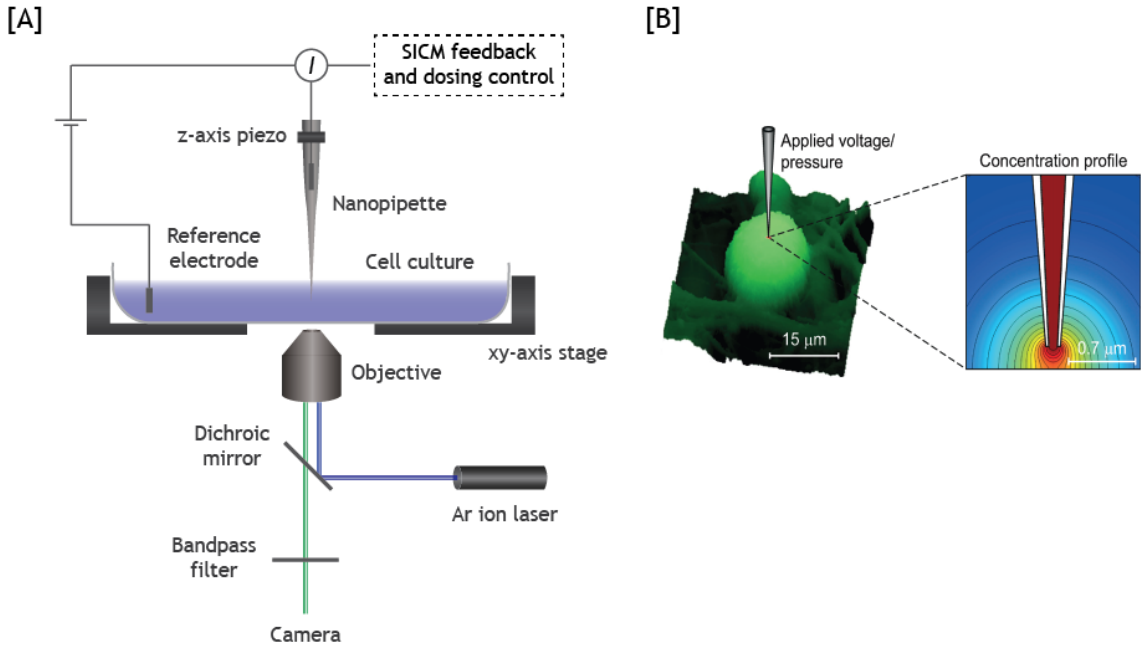


***Figure A4.*** *Scanning Ion Conductance Microscopy (SICM).* **[A]** *Scheme of SICM setup.* **[B]** *Illustration of nanopipette delivery over a living cell and the concentration profile from the tip of the nanopipette. Image reproduced from Piper* et al[184].

SICM was born as scanning probe microscopy technique based on nanopipettes.[184] In SICM, the nanopipette is filled with an electrolyte solution and immersed in an electrolytic bath; one electrode is placed in the pipette, while the electrode of reference is submerged in the bath. The ion current flowing between the two electrodes depends on the tip-cell separation, meaning that the feedback signal of this current is used to precisely control the distance between the nanopipette and the cell (Figure A4-A). Therefore, this technique is highly suitable to perform non-contact imaging of live cells. SICM is now also implemented as a tool to deliver (bio)molecules to the surface of living cells with nanometric precision.[185,186] This allows the study of induced biological processes at single cell resolution, which allows differentiating distinct behaviours in co-cultured cells. Such delivery is performed by introducing the molecule of interest in the electrolytic solution of the nanopipette and the release is prompted by application of voltage or pressure. The controlled application of the molecule is regulated by the nanopipette-cell distance,

because as the nanopipette gets closer, the concentration profile shifts from a broad profile to progressively more localized delivery (Figure A4-B).

In our studies, CL Aß42 dimer was exquisitely delivered over each cell through its introduction in the nanopipette and subsequent application of pressure. Intracellular calcium influx was taken as the toxic marker and it was measured by labelling cells with $Ca^{2+}$-sensitive dye Fluo4. CL Aß42 dimer was previously obtained by PICUP reaction and successive purification by GdnHSCN-SEC procedure in 10 mM AA pH 8.5, a buffer that slows down Aß aggregation. We selected CL Aß42 dimer instead of CL Aß40 dimer to try to get positive results in the shortest period of time, since Aß42 has largely been recognized to be more neurotoxic than Aß40. Few minutes before sample application, CL Aß42 dimer was dissolved in phosphate buffered saline buffer (PBS) down to 500 nM nominal concentration – comparable to that in XTT assay – and cells were labelled with fluorescent intracellular $Ca^{2+}$-sensitive dye Fluo-4.

The application of CL Aß42 dimer to neurons and astrocytes yielded oscillating or increasing $Ca^{2+}$ influx over time, reflected in transient or progressive – respectively – increases in intracellular fluorescence (Figure A5). Interestingly, Aß42 monomer didn't exhibit such biological activity. On the one hand, neuronal $Ca^{2+}$ influx (Figure A5-A) was assessed in four independent sets of measures (global n = 17), and only two of them displayed a maximum of $Ca^{2+}$ intake significantly different compared to negative control (Blank – 10 mM AA pH 8.5 diluted to the same ratio in PBS). On the other hand, astrocytic $Ca^{2+}$ influx (Figure A5-B) was monitored in three independent sets (global n = 13), and only one of them showed a peak of intracellular $Ca^{2+}$ concentration significantly different to negative control. These results demonstrate a huge inter-set variability (differences in average normalised maximum fluorescence between sets), meaning neuroglial cultures are extremely sensitive to their preparation and age. Besides, intra-set variability (standard deviations in normalised maximum fluorescence) arises from differences in cell to cell response to CL Aß42 dimer injury, in contrast to the congruent absence of $Ca^{2+}$ influx for all Aß42 monomer or blank measures (very low standard deviations). This could be explained by differences in individual cell membrane composition, which might modulate cell susceptibility to CL Aß42 dimer damage. Finally, the maximum $Ca^{2+}$ intake for neurons is roughly higher than for astrocytes, which contrasts to the previous results obtained in the Klenerman's group.[183] The main difference in both studies lies on the type of Aß oligomer sample, each of whom might have different affinities for neuronal and astrocytic cell membrane compositions.

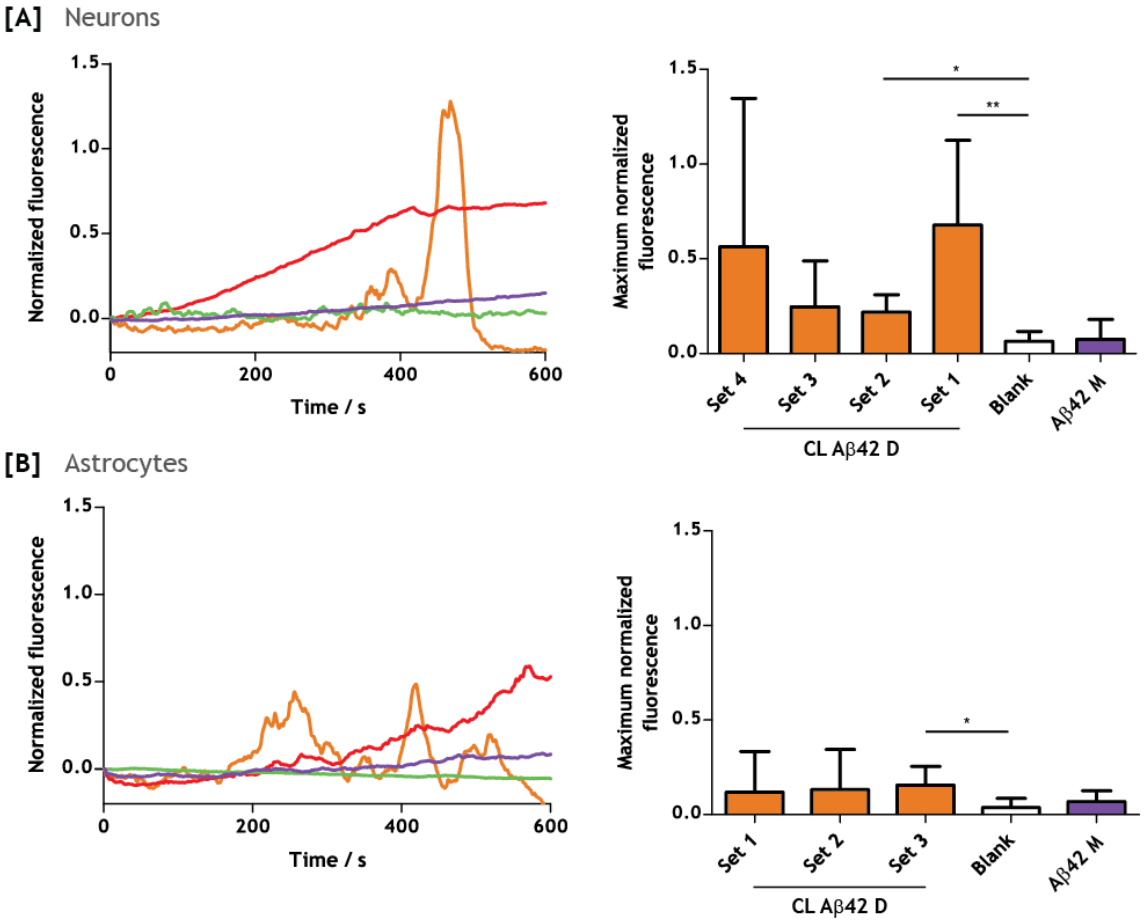


***Figure A5.*** *SICM assays of CL Aβ42 dimer on neuroglial culture.* **[A]** *Representative fluorescence traces of $Ca^{2+}$ influx induced by the delivery to* ***neurons*** *of blank (green - vehicle diluted in PBS), Aβ42 monomer (purple) and CL Aβ42 dimer (orange and red). The trace in orange represents an oscillating $Ca^{2+}$ influx, while the red corresponds to a progressive increase of intracellular calcium. Columns represent the mean ± standard deviation maximum normalized fluorescence achieved for each independent set of cells. Set 1 to 4 (orange bars) correspond to the administration of CL Aβ42 dimer, the blank (white bar) and Aβ42 monomer (purple bar).* **[B]** *Representative fluorescence traces of $Ca^{2+}$ influx induced by the delivery to* ***astrocytes*** *of blank (green), Aβ42 monomer (purple) and CL Aβ42 dimer (orange – oscillating, red – progressive increase). Columns represent the mean ± standard deviation maximum normalized fluorescence achieved for each independent set of cells. Set 1 to 3 (orange bars) correspond to CL Aβ42 dimer. Significant differences indicated by asterisks (p-value < 0.1 is *, p-value < 0.01 is **).*

Of note, we cannot guarantee that the recorded $Ca^{2+}$ influxes are strictly due to CL Aβ42 dimer. We cannot discard covalent dimers evolve to bigger aggregates when diluted in PBS. In fact, O'Nuallain *et al*[187] reported that their engineered Aβ40 disulphide cross-linked dimer ($(AβS26C)_2$, 26-serine was substituted by a cysteine) aggregated much faster than wild-type Aβ40, and even much faster if the sample was

agitated. In general, agitation is known to induce faster aggregation in amyloid proteins, similarly as the ionic strength of the media does.[129] The dilution of our CL Aβ42 dimer in PBS implies its exposure to higher ionic strength, meaning it might undergo similar enhanced aggregation as $(AβS26C)_2$ does by itself and when submitted to agitation.

Overall, we have shown MTT assay is not suited to address Aβ oligomer toxicity. XTT assay has revealed that physiological concentrations of CL Aβ40 dimers do not cause neuronal death. Instead, more subtle toxic events such as intracellular $Ca^{2+}$ influx were caused by CL Aβ42 dimers in both neurons and astrocytes.

## Materials and methods

### Aβ40/Aβ42 sample preparation

Procedures are all described in Materials and methods in Chapter 2, except RP-HPLC-PDA purification. CL Aβ40 samples were prepared using PICUP conditions involving an Aβ:$Ru(bpy)_3^{2+}$:APS ratio of 1:2:5. Next, the reagents incompatible with RP-HPLC-PDA purification were removed using Bio-Spin P30 columns (Bio-Rad) pre-equilibrated with 10 mM AA pH 8.5. CL Aβ40 dimer was purified using a Symmetry 300 C4 column (4.6 × 150 mm, 5 µm, 300 Å, Waters) at a flow rate of 1 mL/min and a linear gradient from 0 to 25% B in 2 min, and from 25 to 40% B in 15 min (A = 0.045% TFA in water, and B = 0.036% TFA in acetonitrile) at 60ºC. Fractions corresponding to CL Aβ40 dimer were combined, quantified by amino acid analysis, freeze-dried and kept at -20ºC until used.

### Amino Acid Analysis

An internal standard (2-aminobutanoic acid) was added to a given volume of Aβ solution. The mixture was lyophilized and the peptide was subsequently hydrolysed (6 N HCl, 110ºC, o/n). The amino acid content and the corresponding protein concentrations were determined using the Waters AccQ-Tag amino acid analysis method.

### Primary Neuronal Cultures for MTT and XTT assays

Hippocampal neurons were obtained from E16 OF1 mouse embryos (Charles River Laboratories). Briefly, brains were dissected in PBS containing 3% glucose, and hippocampi were dissected out. After trypsin (Gibco) and DNAse (Roche Diagnostics) treatments, tissue pieces were dissociated by gentle sweeping. Cells were then

counted and seeded onto poly-D-lysine-coated dishes in Neurobasal medium containing B27 supplement (Gibco). All experiments involving animals were performed in accordance with the European Community Council directive for the care and use of laboratory animals and were approved by the local ethical committee.

### Neuronal Viability Measurements – MTT and XTT

Primary hippocampal neurons were seeded at 30,000 cells/well in 96-well plates (Costar), maintained for 72–96 h, and then treated with thawed Aß samples or the corresponding volumes of vehicle (10 mM AA pH 8.5) as a control. After 24 h at 37°C, neuronal viability was determined using the MTT assay (Cell Proliferation Kit I) or XTT assay (Cell Proliferation Kit II) from Roche. Neuronal viability was expressed as percent of MTT/XTT absorbance in treated cells as compared to cognate vehicle treated cells, which was taken as 100%. The assay was quantified at 595 nm, using the 690 nm absorbance as reference, on an absorbance plate reader.

### Primary Neuroglial Cultures for SICM measurements

Mixed cultures of neurons and glial cells were prepared from Sprague–Dawley rat pups 2–4 days postpartum (UCL breeding colony). Experimental procedures were performed in full compliance with the United Kingdom Animal (Scientific Procedures) Act of 1986. The hippocampus and cortex were removed and placed in ice-cold PBS ($Ca^{2+}$ and $Mg^{2+}$-free, Invitrogen). The tissue was then minced and trypsinized (0.25% for 5 min at 37°C), triturated, and plated on poly-D-lysine-coated coverslips, and cultured in Neurobasal A medium (Invitrogen) supplemented with B-27 (Invitrogen) and 2 mM L-glutamine. Cultures were maintained at 37°C in a humidified atmosphere of 5% $CO_2$ and 95% air, and the medium was in each case replaced twice a week and maintained for 12–15 days before experimental use to ensure the expression of glutamate and other receptors. Neurons were easily distinguishable from glia using microscopy: they appeared phase bright, had smooth rounded somata and distinct processes, and lay just above the focal plane of the glial layer.

### Cell labelling to measure $Ca^{2+}$ influx

Neuroglial cultures were loaded for 15 min at 37°C with the calcium indicator dye Fluo4-AM (Life Technologies) at 4 µM final concentration in Leibovitz's L-15 Medium (Life Technologies). When measuring $Ca^{2+}$ influx in astrocytes, 300 µM of 2-Methyl-6-(phenylethynyl)-pyridine (MPEP) were added to L15 media. MPEP is a potent,

selective and systemically active mGlu5 receptor antagonist which is added to avoid unspecific $Ca^{2+}$ transients in astrocytes.

## Nanopipettes and SICM setup

Nanopipettes were pulled with a laser-based pipette puller (Model P-2000; Sutter Instruments) from borosilicate capillaries (outer diameter 1 mm, inner diameter 0.58 mm) from Intracel, U.K., resulting in an inner half-cone angle of $\theta = 3^{\circ}$ and an inner tip radius of approximately r = 50 nm. A silver chloride pellet was used as reference electrode for ion conductance measurements.

In the SICM setup, a dual channel Axon MultiClamp 700B patch-clamp amplifier (Molecular Devices) was used to measure the ion current and the electrochemical Faraday current. A gain of 1 mV/pA and a 5 kHz low pass filter was used for the ion conductance measurements. The electrochemical signal was recorded with a low-pass filter of 40 Hz. Application of pressure over the pipette was done using a home-built pressure application setup and adjusted manually while monitoring the pressure with a pressure sensor (Pressure Monitor 100D, World Precision Instruments). A mercury lamp provided with a blue light filter (460–480 nm) was used to illuminate the selected neuron or astrocyte, and the fluorescence from the entire cell body was then collected with a photomultiplier (D-104-814, Photon Technology International) and a green light filter (500– 550 nm). The light was turned off between applications to reduce photobleaching and cell photodamage. Imaging was made with an inverted Nikon TE200 microscope (Nikon Corporation). Videos were recorded for 10 min and then processed with ImageJ software (NIH). Normalized fluorescence is calculated as the fluorescence at the given time with respect to the fluorescence at time 0.

## Summary of Statistical Analysis

GraphPad Prism was used for all statistical analyses. The data are presented as mean ± standard deviation except when stated otherwise. The Student-t test was used to calculate significant differences, presented in terms of p-value.

# Appendix B.

# Cross-linked species modulate Aß aggregation

## Context

Prion diseases and other neurodegenerative disorders share several pathologic similarities such as neuronal loss, gliosis or accumulation of aggregated protein(s). That is the reason why recent cutting edge research has been focused in the links between them, notably on the connection between prion diseases and AD.[188]

Prion diseases can be genetic, idiopathic or infectious in origin, in contrast to AD, which has been proved to be triggered by the two first causes only. Interestingly, it is the infectivity of prions that inspired the quest to prove that protein corruptive templating is the underlying mechanism for amyloid deposition in AD.[188-192] In the seminal work of Meyer-Luehmann *et al*, young healthy Tg mice were icv injected with brain extracts of AD patients and of aged Tg mice displaying amyloidosis.[19] This injection advanced their onset of plaque deposition in a time- and concentration-dependent fashion. Selective removal of Aß from these extracts or injection of brain extracts of human age-matched controls did not enhance amyloidosis, implying that Aß is necessary for such effect. Consistently, active or passive immunization of mice against Aß also abrogated premature plaque deposition. Moreover, Aß needed to be aggregated, since extracts from young Tg mice were not able to induce faster deposition. Enlarging the parallelism to prions, Aß seeds were resistant to formic acid denaturation, but not to formaldehyde,[193] and their spreading pattern over the brain was through axonally coupled regions to the injection site. Furthermore, synthetic Aß was able to incite plaque deposition, although it was not as potent as brain-derived Aß.[194] Crucially, Aß seeds also displayed a strain-like functional diversity, trait distinctive to prions by which their structural conformation determines the behavioural and pathological phenotypes.[195] Seemingly, Aß plaques in the injected mice reproduced the features of those of the original host, either from Tg mice[19] or AD patients[196] brain extracts. Besides, evidences for Aß strains have also emerged from *in vitro* and *ex vivo* studies. The most striking *in vitro* study revealed that two distinct Aß fibril morphologies possessed different neurotoxicity.[52] The most significant *ex vivo* study showed that fibrils extracted from two AD patients with distinct clinical histories had different morphologies and structures.[197] Finally, additional proof of prions and Aß protein similarities is that Aß seed competent entities are both soluble proteinase-K (PK)-sensitive species and insoluble aggregated PK-resistant structures.[198] Overall, Aß protein has been shown to perform corruptive protein templating that enhances strain-dependent plaque deposition *in vivo*.

Nevertheless, there are several concerns to the application of the prion paradigm to Aß protein and AD. First, the inclusion of Aß under the category of prion with the inherent connotation of infectivity has been shown to be misleading. Oral, intravenous, intraocular and intranasal administration of Aß seeds failed to enhance plaque deposition.[199] Moreover, such connotation would have enormous implications in the healthcare systems and in the working procedure in many research laboratories,[69] which luckily doesn't seem to be the case. To reconcile the prion paradigm and Aß, Walker and Jucker proposed in a recent review[188] to define prions as "proteinaceous nucleating particles" instead of "proteinaceous infectious particles", unifying amyloids and prions in terms of their molecular mechanism of action.

Second, Aß has been shown to seed plaque deposition, but none of the discussed papers have addressed the remaining AD phenotypes such as intracellular NFT accumulation nor cognitive decline.[69] Furthermore, according to the current view of amyloid neurotoxicity, the enhancement of plaque deposition would improve mice cognitive performance[69] by clearing out neurotoxic soluble Aß oligomers. Besides, studies in large cohorts have demonstrated that up to 40% of non-demented older adults have AD-like amyloid deposition without compromised cognitive function.[26,27]

## Results

Within this context, we hypothesised that our CL Aß40 species might act as seeds able to enhance Aß aggregation. Importantly, these cross-linked species might also be present *in vivo*, since PICUP mechanism proceeds through similar reaction intermediates as ROS could presumably form CL Aß species in vivo[181] (Appendix A, Figure A1). Promising work with synthetic Aß seeding *in vivo* had already been undertaken by Stöhr *et al*, in which they observed enhanced plaque deposition with concomitant gliosis using wild type (WT) Aß40 and cross-linked $(Aß40S26C)_2$ dimer (see Appendix A).[194] Fritschi *et al* detected an enhanced *in vitro* fibrillization when incubating recombinant Aß40 with aged Tg mice and AD patients' brain extracts.[193] ThT (Figure B1-B) fluorescence was used as a surrogate marker for fibril formation, since this molecule fluoresces when it binds to cross-ß sheet structures such as Aß amyloid fibrils.[36,58] Besides, Ono *et al* isolated CL Aß40 species, through PICUP reaction and subsequent purification from SDS-PAGE bands, and incubated them with WT Aß40.[81] Consistent to these previous reports, CL species stimulated Aß fibrillisation, according to ThT binding assay data.

In our studies, we obtained Aß40 M and CL Aß40 D and Tr by means of PICUP reaction and successive purification by GdnHSCN-SEC procedure (Figure B1-C). Next, we added each species at a low molar ratio to independent Aß40 monomeric solutions readily purified by SEC. The selected buffer was 10 mM Tris pH 7.4, which prompted fibril formation in a reasonable time scale (see Chapter 1, Figure 1.6). Addition of Aß40 M that had also undergone PICUP reaction and GdnHSCN-SEC purification was taken as the reference curve for negative control (Figure B1-A, purple curve). Fibrillisation was monitored through ThT fluorescence, measured at specific time points.

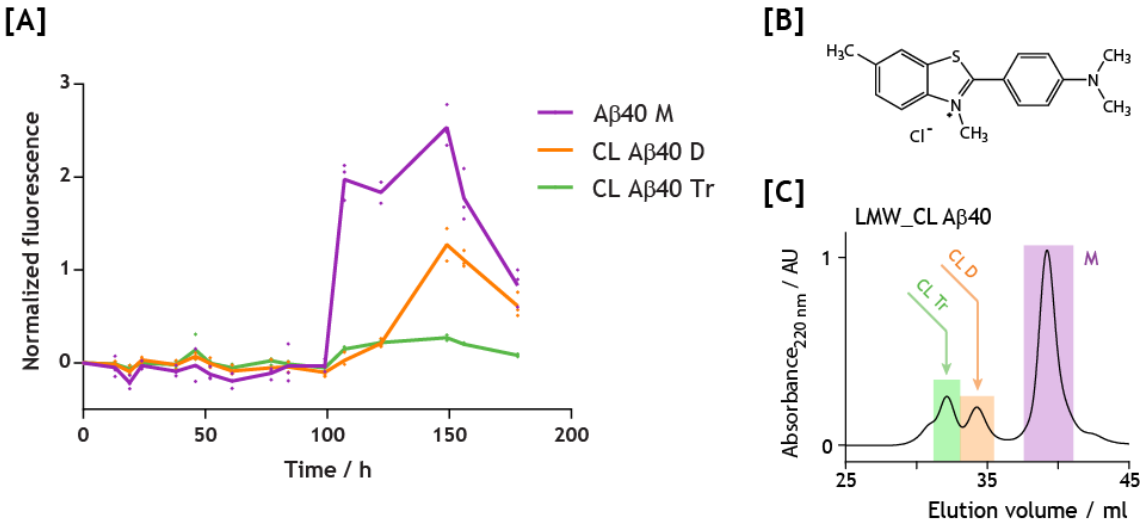


***Figure B1.*** *ThT fluorescence assay.* **[A]** *ThT fluorescence traces over time of fresh monomeric Aß40 incubated in the presence of CL Aß40 dimers (D, orange) and trimers (Tr, green). Aß40 monomer (M, purple) obtained through the same procedure as CL D and CL Tr was added at identical molar ratio and used as negative control. Triplicate measures for each time point are depicted as individual spots and the line unites the mean values for each time point.* **[B]** *Molecular structure of ThT.* **[C]** *Obtention of Aß40 monomer and CL Aß40 dimers and trimers by PICUP reaction and successive GdnHSCN-SEC purification.*

Addition of sub-stoichiometric amounts of CL Aß40 D surprisingly led to a delay in the fluorescence increase, this is an extended lag phase and a delayed fibrillization (Figure B1-A). The presence of CL Aß40 Tr directly inhibited fibril formation. Besides, it is noticeable that fluorescence intensity decays after the sigmoidal increase in the control and CL Aß40 D samples. This is due to the collapse of the formed fibrils, such that less ThT molecules can bind and fluoresce. Overall, it is important to point that these data represent a single experiment, thus repetition of the assay is required to confirm these results. However, ThT binding assays have always been associated to low reproducibility. Recently, Sara Linse's group overcame such misconception

through optimised Aß purification procedures.[66] Therefore, we would repeat these seeding assays following their robust and verified protocols yielding reproducible kinetic data.

Nonetheless, our results illustrate a modulation of Aß aggregation by small amounts of CL Aß species. CL Aß 40 D promoted a delay in fibril formation, implying a possible stabilisation of intermediate species. Interestingly, previous work in the laboratory demonstrated that the most neurotoxic species are the ones populating prefibrillar stages of aggregation.[56] Meanwhile, the presence of CL Aß40 Tr fully prevented fibrillisation. Even if ThT assay was informative of the lack of fibrillar species, other techniques, such as HDX coupled to MS[56] or TEM, would shed more light on the nature of the species present in solution over time. Finally, our results are in conflict with the aforementioned reports on synthetic Aß seeding experiments. We need to perform further experiments to confirm them, and to address this divergence.

## Materials and methods

### Aß40/Aß42 sample preparation

Procedures to obtain CL species are described in Materials and methods in Chapter 2. GdnHSCN-SEC purification was performed with 10 mM Tris pH 7.4 as elution buffer.

To obtain monomeric Aß, we used SEC: Aß was dissolved in 6.8 M GdnHSCN, sonicated for 5 min, diluted to 4 M GdnHSCN at a 5 mg/ml Aß concentration, centrifuged at 10,000g for 5 min. The resulting solution was injected into a HiLoad Superdex 75 HR 16/60 column (GE Healthcare) previously equilibrated with 10 mM Tris, pH 7.4, and eluted at a flow rate of 1 ml/min. The system was kept at 4°C. The peak attributed to monomeric Aß was collected, and its peptide concentration was determined by RP-HPLC-PDA. The Aß solutions were diluted to 30 µM, then the cross-linked species were added at 1:60 molar ratio (CL species to monomeric Aß40) and left to aggregate at 37ºC.

### ThT binding assay

ThT analysis was performed by mixing 50 µl of the Aß aggregating solutions withdrawn at specific times with 15 µl of 100 µM ThT and 35 µl of 142 mM Glycine at pH 8.3 in a Hard Shell® Thin Wall 96-well fluorescence plate (Bio-Rad). The ThT fluorescence of each sample was measured using a fluorescence plate reader (FluoDia T70, Photal, Photon Technology International) at excitation and emission

wavelengths of 450 and 485 nm, respectively. The samples were analyzed in triplicate, and average fluorescence values were joined by a curve.

# Conclusions

The conclusions related to the first objective of the thesis are the following:

1. Molecular recycling within Aß fibrils has been shown to be highly dependent on the physicochemical properties of the fibrils.
2. We have successfully expressed and purified active recombinant insulin degrading enzyme (IDE). We have shown that IDE specifically proteolyses monomeric Aß. We have also determined that Aß-IDE kinetic system is highly complex and it cannot be addressed through the classical Michaelis-Menten model. Moreover, we have detected three additional Aß cleavage sites in addition to the ones already reported.
3. Under the optimized experimental conditions, Aß40 fibrils have shown to provide IDE-cleavable monomers, whilst Aß42 fibrils release an undefined mixture of monomers and oligomers in complex equilibrium.

The conclusions answering the second objective of the thesis are detailed below:

4. We have successfully optimized the PICUP reaction and the chemical reduction of methionine-35 to obtain chemically well-defined cross-linked low molecular weight Aß oligomers.
5. We have isolated cross-linked Aß dimers and trimers by means of a disaggregating treatment coupled to size exclusion chromatography.
6. We have found clear evidences that SDS-PAGE is not a reliable technique to assess Aß oligomer stoichiometry, specifically that of Aß42.
7. Ion mobility coupled to electrospray ionization mass spectrometry (ESI-IM-MS) study of cross-linked dimers has shown that cross-linked oligomers are good mimics of their non-covalent counterparts.
8. Combined study of cross-linked dimers and trimers through ESI-IM-MS, circular dichroism, and molecular dynamics simulations, has revealed that dimers and trimers possess a globular shape without defined secondary structure.
9. Altogether, although Aß42 shows a higher tendency to aggregate than Aß40, both Aß40 and Aß42 undergo aggregation through the same early oligomers.
10. MTT toxicity assay has been shown to be inappropriate to address Aß oligomer toxicity. Cross-linked Aß42 dimers induce calcium influx, an intracellular marker for neurotoxicity, in both neurons and astrocytes.

11. Cross-linked Aβ40 dimers and trimers effectively modulate Aβ40 aggregation process.

# Resum en català

## Introducció

Les malalties amiloidogèniques agrupen un total de 50 desordres caracteritzats per l'agregació de determinades proteïnes acumulades en òrgans o teixits específics en forma de dipòsits amiloides. Alguns d'aquests desordres són neurodegeneratius com ara la malaltia de Parkinson, les malalties priòniques o la malaltia d'Alzheimer (MA).

MA és una malaltia crònica i progressiva d'origen neurològic que representa el 60% de les demències diagnosticades. Els primers símptomes són la falta de retenció de la memòria recent i l'evolució de la malaltia procedeix cap a la pèrdua gradual de les capacitats cognitives més bàsiques. La seva prevalença es dobla cada 5 anys a partir dels 65 anys, essent l'edat el major factor de risc. L'any 2011, es va comptabilitzar que 35 milions de persones estaven afectades per MA i es calcula que el nombre d'afectats es pot triplicar de cara l'any 2050. Amb aquests números i el seu elevadíssim cost social i econòmic, MA s'ha convertit en una de les grans prioritats biomèdiques a nivell mundial.

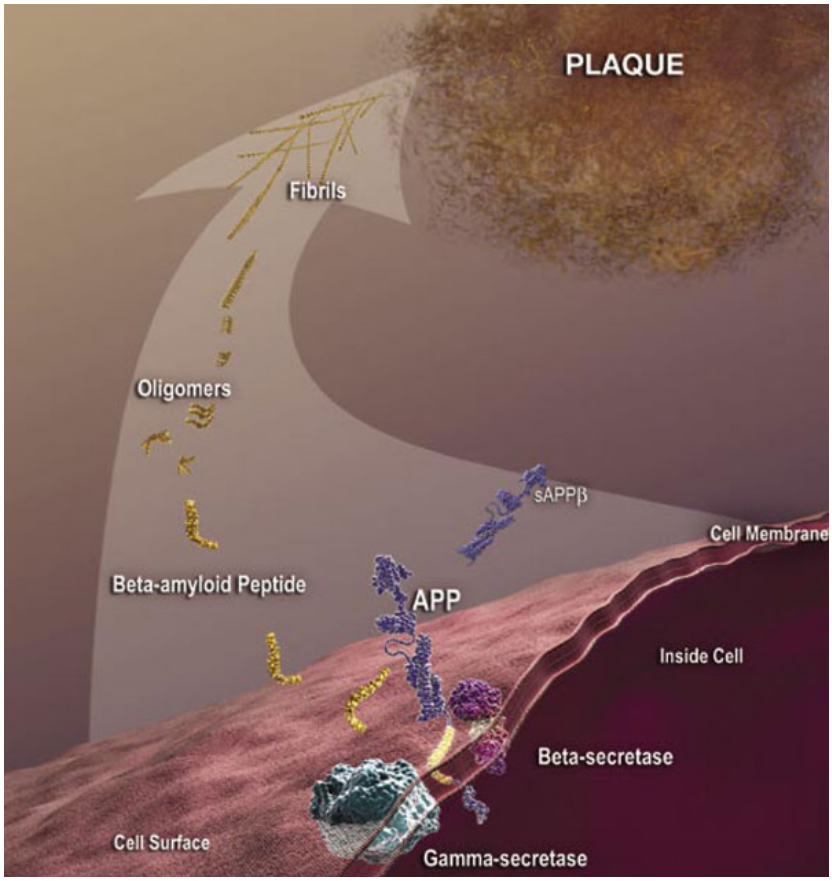


***Figura RC1.*** *Representació de la formació d'Aß mitjançant l'acció seqüencial de la ß- i la γ-secretases. El processament aberrant d'Aß en determina la seva acumulació i agregació fins a la formació de fibres, principal component de les plaques amiloides. Aquesta imatge és copyright de The National Institute of Health (NIH).*

La MA es diagnostica a través de 3 marcadors histopatològics: la mort neuronal, l'acumulació intracel·lular de cabdells neurofibrillars formats per proteïna tau híperfosforilada i la presència de dipòsits extracel·lulars – altrament coneguts com a

plaques amiloides – composats fonamentalment per la proteïna beta-amiloide (de les sigles en anglès Aß). Evidències histològiques, genètiques, bioquímiques i models de ratolins transgènics atribueixen a Aß un paper central en la malaltia. Per contra, encara no es coneix la seva connexió amb la neurotoxicitat observada en la MA, per bé que s'ha provat que el fenotip patològic de la proteïna tau es induït per Aß.

Aß és el producte metabòlic de l'acció seqüencial de la ß- i γ-secretasa sobre la proteïna de membrana coneguda com a proteïna precursora amiloide (Figura RC1). L'escissió que duu a terme la γ-secretasa no és específica, de manera que es generen varies isoformes d'Aß: Aß40 està formada per 40 aminoàcids i és la isoforma que es produeix més abundantment; Aß42 posseeix dos aminoàcids més a l'extrem C-terminal, és la isoforma més estretament associada a la MA i es caracteritza per tenir una major tendència a agregar.

Tot i el seu rol central en la malaltia, Aß es produeix de forma regular en humans sans. És el processament aberrant de la proteïna que en determina la seva acumulació i agregació, primer en intermedis oligomèrics transitoris que evolucionen cap a les estructures fibril·lars disposades en forma de làmina-ß i que composen les plaques amiloides (Figura RC1).

Fa un parell de dècades, aquestes plaques eren considerades els agents neurotòxics de la MA. Posteriors estudis van observar que l'abundància d'aquestes plaques correlacionava lleument amb els dèficits cognitius dels pacients. En canvi, aquests dèficits eren directament proporcionals a la quantitat d'Aß soluble present en el cervell dels malalts. De totes maneres, aquesta Aß soluble representa un conjunt d'espècies oligomèriques indefinit i heterogeni. La comunitat científica està dedicant esforços en identificar l'estructura d'aquestes espècies i el seu nexe amb la neurotoxicitat de la MA per a dissenyar estratègies terapèutiques efectives. Aquest repte és molt exigent ja que el procés d'agregació d'Aß és extremadament heterogeni i dinàmic.

## Capítol 1. La naturalesa de les espècies reciclants en les fibres amiloides d'Aß

La falta de correlació entre l'abundància de les plaques amiloides i els dèficits cognitius dels pacients va relegar les fibres amiloides a ser considerades el simple producte final inert de l'agregació d'Aß. No obstant, posteriors evidències histològiques i d'assajos *in vitro* van donar suport a la descripció d'aquestes fibres com a potencials reservoris d'oligòmers neurotòxics. Un d'aquests estudis *in vitro* va

demostrar que una població homogènia de fibres estava en equilibri amb una determinada proporció d'Aß soluble. Aquesta Aß soluble provenia de les molècules que composaven els extrems de les fibres, tal que aquestes es dissociaven de la fibra, es trobaven en solució durant un determinat període de temps i es reincorporaven als extrems de les fibres. Aquest fenomen va ser descrit com a reciclatge molecular. Donada la rellevància patològica de les espècies solubles d'Aß i el paper de les fibres com a potencials reservoris d'oligòmers neurotòxics, l'objectiu del present capítol era determinar la naturalesa de les espècies *reciclants* de les fibres d'Aß.

## 1. Resultats

El reciclatge molecular es va descriure a través de la tècnica de bescanvi protó/deuteri (de les sigles en anglès HDX) monitoritzat per espectrometria de masses. HDX avalua la disponibilitat dels protons amida a ser bescanviats pels deuteris del medi. En condicions estàndard els protons amida es bescanvien ràpidament. Per contra, la seva velocitat de bescanvi es redueix dràsticament si aquests estan formant ponts d'hidrogen o es troben inaccessibles al dissolvent per la seva incorporació en elements estables d'estructura.

En el cas de l'estudi de la dinàmica de les fibres d'Aß, en primer lloc es van preparar les fibres en un dissolvent aquós. A continuació, es va seleccionar una població homogènia de fibres per ultracentrifugació i se les va exposar a una solució d'òxid de deuteri. A diferents temps de marcatge isotòpic, les fibres mostrejades es liofilitzaven i posteriorment es dissolien en una solució de dimetilsulfòxid (de les sigles en anglès DMSO). Aquesta solució de DMSO trencava les fibres en els seus components monomèrics conservant la seva informació de bescanvi. La injecció d'aquesta solució de monòmers a l'espectròmetre de masses proporcionava uns espectres de masses que mostraven dos pics definits. El pic de baix pes molecular representava espècies amb un patró de bescanvi corresponent a molècules d'Aß disposades en estructura ß-creuada, característic de les fibres amiloides. Per contra, el pic d'alt pes molecular corresponia a molècules d'Aß amb tots els protons amida bescanviats. Donat que la intensitat d'aquest últim pic augmentava amb el temps de marcatge, el model de la dinàmica de les fibres s'explicava tal que les molècules dels extrems de les fibres es dissociaven, bescanviaven tots els protons amida i es tornaven a reincorporar a la població de fibres.

L'estratègia per esbrinar la identitat de les espècies *reciclants* es va dissenyar en base a la selectivitat de l'enzim insulin-degrading enzyme (IDE), capaç de degradar

únicament monòmers d'Aß. D'aquesta manera, si l'espècie *reciclant* era monomèrica, a l'espectre de masses només apareixeria el pic de baix pes molecular. En canvi, si l'espècie *reciclant* era oligomèrica, el procés de reciclatge molecular no es veuria alterat.

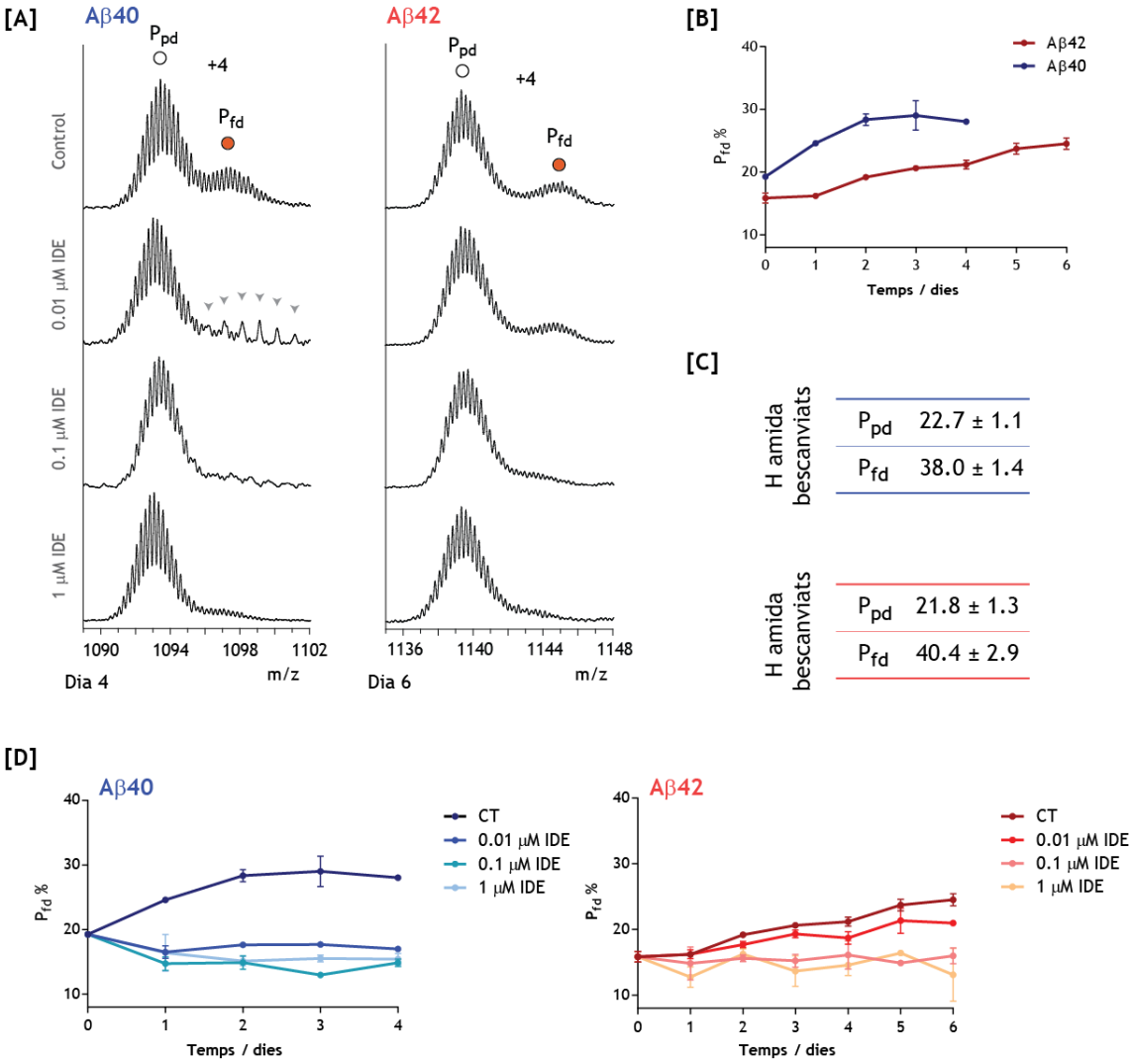


***Figura RC2.*** *Reciclatge molecular en les fibres d'Aß en presència d'IDE.* **[A]** *Espectre de masses mostrant les poblacions relatives de les poblacions $P_{pd}$ i $P_{fd}$ per Aß40 (esquerra, dia 4) i Aß42 (dreta, dia 6) incubades amb 0/0.01/0.1/1 μM IDE.* **[B]** *Gràfica de la fracció relativa de $P_{fd}$ en funció del temps per les fibres d'Aß40 (blau) i les d'Aß42 (vermell).* **[C]** *Número de protons amida bescanviats en les poblacions $P_{pd}$ i $P_{fd}$. Aß40 i Aß42 representats en blau i vermell, respectivament.* **[D]** *Gràfiques de la fracció relativa de la població $P_{fd}$ en funció del temps per les fibres d'Aß40 (blau) i Aß42 (vermell) amb 0(CT)/0.01/0.1/1 μM IDE (major a menor intensitat de color).*

D'entrada, donat que l'activitat de l'enzim no era estable més enllà d'una setmana i que el procés de reciclatge molecular s'avaluava durant un mes sencer, vam decidir estimular el procés de reciclatge per tal d'encaixar les escales de temps dels dos

processos. Per tal d'estimular-ho, vam centrar els esforços en obtenir més extrems de fibres on aquest reciclatge molecular es podia produir. L'obtenció de més extrems es va assolir a través de l'optimització de la formació de fibres, per tal que aquestes fibres en proporcionessin de més curtes un cop sotmeses a un procés de sonicació.

L'altra peça del puzle era la obtenció d'IDE recombinant activa. Vàrem optimitzar la seva expressió i purificació, assolint una activitat específica lleugerament més elevada que la de l'IDE comercial. A continuació, vam demostrar que la selectivitat de l'IDE raïa en que era capaç de degradar Aß monomèrica, mentre que no aconseguia hidrolitzar el dímer covalent. Aquest resultat es trobava en concordança amb les conclusions extretes mitjançant la determinació de la seva estructura cristal·logràfica, en què el centre catalític només encabia pèptids de menys de 50 aminoàcids. Finalment, no vam aconseguir caracteritzar cinèticament el parell Aß-IDE com a substrat-enzim. La raó és que les gràfiques consum de substrat front el temps no assolien una degradació total de la proteïna a llargs temps. Això excloïa la seva parametrització cinètica en el marc de la teoria clàssica de Michaelis-Menten.

Un cop vam obtenir les fibres homogèniament sonicades i l'IDE pura i activa, vam procedir a l'estudi del procés de reciclatge molecular en presència de l'enzim. Abans però, vam estudiar el reciclatge molecular en absència de l'IDE en les condicions experimentals optimitzades. D'una banda, els dos pics en els espectres de masses (Figura RC2-A) i el seu patró de bescanvi (Figura RC2-C) es reproduïen com en les condicions anteriors. D'altra banda, vam constatar que el reciclatge molecular en aquestes noves condicions era similar o bé que s'havia reduït (Figura RC2-B).

Un cop incubades amb IDE, els espectres de masses de les fibres d'Aß40 mostraven que les espècies reciclants d'Aß40 eren ràpidament hidrolitzades per l'enzim ja que no es detectava la seva reincorporació a les fibres (Figura RC2-D en blau). En canvi, les fibres Aß42 requerien altes concentracions d'IDE per veure alteracions en el seu reciclatge molecular (Figura RC2-D en vermell). Per tant, els resultats indicaven que les fibres d'Aß40 estaven en equilibri amb monòmers, mentre que les fibres d'Aß42 proporcionaven una mescla indefinida i complexa de monòmers i oligòmers poc estructurats.

## 2. Discussió

Per a la determinació de la naturalesa de les espècies reciclants de les fibres d'Aß40 i Aß42 es va plantejar d'entrada ajustar les escales de temps del l'activitat enzimàtica i el procés de reciclatge molecular. Per tal d'estimular el reciclatge molecular vam optimitzar les condicions de formació de fibres de tal manera que les

fibres madures proporcionessin fibres més curtes un cop sotmeses a sonicació. Encara que aquestes fibres disposaven de més extrems, el canvi de les condicions experimentals va determinar que el procés de reciclatge s'alentís. D'altra banda, vam obtenir IDE activa que mostrava selectivitat per Aß monomèrica front a dímers covalents. Malauradament, no vam ser capaços de caracteritzar Aß-IDE com a sistema cinètic donat que Aß no es degradava per complet a llargs temps d'incubació amb IDE. La incubació de les fibres sonicades amb IDE activa va demostrar que les fibres d'Aß40 proporcionaven monòmers, mentre que les fibres d'Aß42 alliberaven una mescla indefinida de monòmers i oligòmers poc estructurats.

La selectivitat de l'IDE pel monòmer d'Aß ja s'havia descrit amb anterioritat, per bé que les evidències que es proporcionaven eren poc sòlides, no mostraven l'abast de la selectivitat o eren mesures indirectes. La caracterització que vam dur a terme va evidenciar que l'enzim era únicament capaç de degradar monòmer i deixava intactes els oligòmers més petits corresponents al dímers, trímers i tetràmers covalents. D'altra banda, no vam aconseguir caracteritzar cinèticament el parell Aß-IDE ja que Aß no es degradava per complet a llargs temps d'incubació amb l'IDE. Un report anterior que sí detallava els corresponents paràmetres cinètics, no donava proves de que s'assolís aquesta degradació completa.

La optimització de la formació de fibres i la seva posterior sonicació estaven dirigides a obtenir un major reciclatge molecular tant el les fibres d'Aß40 com en les d'Aß42. Per contra, va resultar que les fibres en aquestes noves condicions agregaven més ràpid i un cop formades eren més estables. Altres estudis ja indicaven que canvis en el medi fisicoquímic d'Aß determinava canvis en la seva cinètica d'agregació. El que no esperàvem és que aquests canvis determinessin un canvi en la termodinàmica del sistema, és a dir en l'estabilitat de les fibres.

La incubació de les fibres d'Aß amb IDE va proporcionar informació sobre la naturalesa de les espècies reciclants. En el cas de les fibres d'Aß40, l'increment de l'espècie totalment deuterada en funció del temps es va bloquejar en presència de les tres concentracions d'IDE. Donat que era una espècie totalment deuterada i que l'enzim era capaç d'hidrolitzar-la en qualsevol de les tres concentracions, no hi ha dubtes en afirmar que l'espècie reciclant en les fibres d'Aß40 és monomèrica.

La situació en el cas de les fibres d'Aß42 és més complexa. Concentracions baixes d'enzim no alteraven el reciclatge molecular, mentre que concentracions altres impedien la reincorporació de les espècies reciclants a les fibres. Amb aquests resultats es pot inferir que les fibres d'Aß42 alliberen una mescla indefinida de

monòmers i oligòmers. D'una banda, aquests monòmers són fàcilment hidrolitzables per l'IDE. Per l'altra, les dades de masses indiquen que aquests oligòmers no es troben estructurats mitjançant ponts d'hidrogen. Així doncs, aquests monòmers i oligòmers estableixen un equilibri complex que només és pertorbat amb altes concentracions d'IDE.

Una explicació alternativa al fet que les fibres d'Aβ42 necessitessin una concentració més elevada d'enzim per què el seu reciclatge es veiés alterat és que l'IDE podria tenir una diferent afinitat per Aβ40 i Aβ42. En favor d'aquest argument, un estudi computacional sobre la interacció Aβ-IDE indicava que Aβ42 interaccionava amb l'IDE d'una manera significativament diferent de com ho feia Aβ40.

En consonància amb els nostres resultats, la mesura dels nivells d'Aβ en el fluid intersticial del cervell de ratolins vius va indicar que la inhibició de la γ-secretasa no determinava la reducció dels nivells d'Aβ42 soluble en ratolins amb plaques amiloides. Per contra, la inhibició de la secretasa sí determinava la disminució dels nivells d'Aβ40. Aquests resultats semblaven indicar que l'Aβ42 soluble era alliberada de les plaques amiloides i que l'IDE present en el fluid intersticial no era capaç d'hidrolitzar-la.

En conclusió, l'estabilitat de les fibres és un factor determinant en la rellevància de les fibres d'Aβ en la MA. En funció de les condicions fisiològiques i de la presència de determinats cofactors aquestes poden veure afectades les seves propietats de reciclatge. D'altra banda, no només és important la seva estabilitat sinó el tipus d'espècies que proporcionen a través d'aquest procés. Les fibres d'Aβ42 proporcionen poques espècies reciclants, però aquestes consisteixen en oligòmers de baix pes molecular que l'IDE no és capaç d'hidrolitzar.

## Capítol 2. Estadiatges inicials de l'agregació d'Aβ

La caracterització dels estadiatges inicials de l'agregació d'Aβ ha centrat l'atenció de molts estudis en el camp de la MA. Això s'explica per la rellevància patològica dels oligòmers solubles d'Aβ i les evidències recents de l'estreta correlació entre la MA i la presència de dímers resistents a dodecil sulfat de sodi (de les sigles en anglès SDS) en extractes de cervell. L'objectiu d'aquest capítol era caracteritzar aquests estadiatges inicials d'agregació d'Aβ en termes d'estequiometria i estructura.

## 1. Resultats

Anteriors estudis sobre els estadiatges inicials d'agregació d'Aß utilitzaven la reacció de PICUP per la seva capacitat de congelar la ràpida dinàmica existent entre els oligòmers de baix pes molecular. PICUP és una reacció fotoquímica que crea enllaços covalents entre residus de proteïnes que interaccionen de forma no covalent, sense necessitat de pre-modificar la seqüència de les proteïnes involucrades. D'aquesta manera, el conjunt d'oligòmers covalents obtinguts a través d'aquesta reacció representava els estats d'agregació d'Aß en aquell precís instant. Posteriorment, aquest conjunt era analitzat mitjançant electroforesi en gel amb SDS (de les sigles en anglès SDS-PAGE). Aquest anàlisi va determinar que Aß40 oligomeritzava a través de monòmer, dímer, trímer i tetràmer. Per contra, Aß42 ho feia majoritàriament a través de pentàmer i hexàmer.

Seguint aquests anteriors treballs, vam abordar l'estudi de l'estructura dels oligòmers d'Aß de baix pes molecular a partir de la reacció de PICUP. D'aquesta manera congelàvem la seva dinàmica i fèiem possible el seu aïllament i posterior caracterització de forma individual. En primer lloc, vam analitzar les mostres de PICUP per cromatografia líquida per fase reversa (de les sigles en anglès RP-HPLC-PDA) i espectrometria de masses d'alta resolució (de les sigles en anglès LC-HRMS) per avaluar la seva homogeneïtat química, ja que l'anàlisi per SDS-PAGE no podia proporcionar aquesta informació. Els cromatogrames i espectres obtinguts posaven de manifest que les mostres posseïen un alt grau d'oxidació, fet probablement derivat de les condicions altament oxidants de la reacció de PICUP. Per tant, vam procedir a optimitzar les condicions de la reacció per tal de minimitzar aquesta oxidació col·lateral del pèptid. Addicionalment, donat que la posició més sensible d'Aß a condicions oxidants és el tioèter de la metionina-35, vam implementar la reducció química del sulfòxid al corresponent tioèter. És així com vam obtenir químicament ben definits els oligòmers covalents corresponents als estadiatges inicials de l'agregació d'Aß.

A continuació, vam intentar aïllar aquests oligòmers covalents mitjançant cromatografia per exclusió molecular (de les sigles en anglès SEC) per tal d'obtenir una major quantitat que a través de l'extracció de les bandes de SDS-PAGE. Inesperadament, vàrem obtenir molts més pics que els reportats en l'anàlisi per SDS-PAGE, entre els que destacaven el pic del monòmer i el del volum mort – corresponent a espècies d'alt pes molecular. Això succeïa tant per Aß40 com per

Aß42, tot i que el cromatograma d'Aß42 reflectia la seva major tendència a agregar que Aß40.

Per tal de determinar quines d'aquestes espècies estaven efectivament unides per enllaços covalents, vàrem plantejar reproduir les condicions experimentals de SDS-PAGE introduint un agent desnaturalitzant previ a la separació per exclusió molecular, en aquest cas tiocianat de guanidini (de les sigles en anglès GdnHSCN). Els pics obtinguts van ser posteriorment identificats per espectrometria de masses (de les sigles en anglès ESI-MS). Sorprenentment, els cromatogrames obtinguts mostraven una distribució de monòmer a tetràmer tant per Aß40 com per Aß42. Per esbrinar per què l'anàlisi per SDS-PAGE indicava que les distribucions d'ambdós pèptids eren diferents front a la seva similitud per GdnHSCN-SEC, vam analitzar els dímers i trímers purs d'Aß40 i Aß42 per SDS-PAGE. Els oligòmers covalents d'Aß40 van proporcionar les bandes esperades, mentre que els dímers i trímers d'Aß42 també es detectaven com a tetràmers i hexàmers, respectivament (Figura RC3). És així com vàrem determinar que SDS-PAGE proporcionava artefactes en l'anàlisi d'Aß42, tal i com ja s'apuntava en altres estudis.

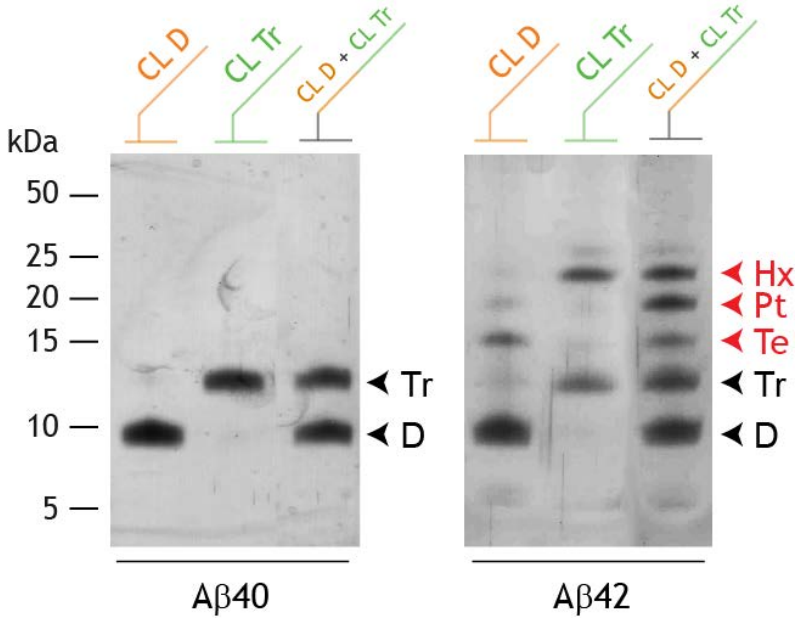


***Figura RC3.*** *Anàlisi per SDS-PAGE dels dímers (CL D, en taronja) i trímers (CL Tr, en verd) covalents purs d'Aß40 i Aß42, així com la mescla d'ambdós (CL D + CL Tr, en taronja i verd). Els caps de fletxa en vermell indiquen els oligòmers formats artefactualment en presència de SDS. D = dímer covalent, Tr = trímer covalent, Te = tetràmer artefactual, P = pentàmer artefactual, Hx = hexàmer artefactual.*

Un cop aïllats per SEC, l'anàlisi de la topologia d'aquests oligòmers covalents es va dur a terme mitjançant mobilitat iònica acoblada a espectrometria de masses (de les

sigles en anglès ESI-IM-MS) (Figura RC4A). Prèviament calibrat, aquest instrument ens va proporcionar la secció col·lisional de cada un dels oligòmers. Aquesta restricció estructural i posteriors simulacions per dinàmica molecular (MD) van permetre construir els models moleculars que millor explicaven aquestes dades (Figura RC4B). Aquests models indicaven que tant dímers com trímers d'Aβ40 i Aβ42 mostraven una forma globular sense estructura secundària definida, tal com vam confirmar analitzant els dímers i trímers purs per dicroisme circular (CD) (Figura RC4C).

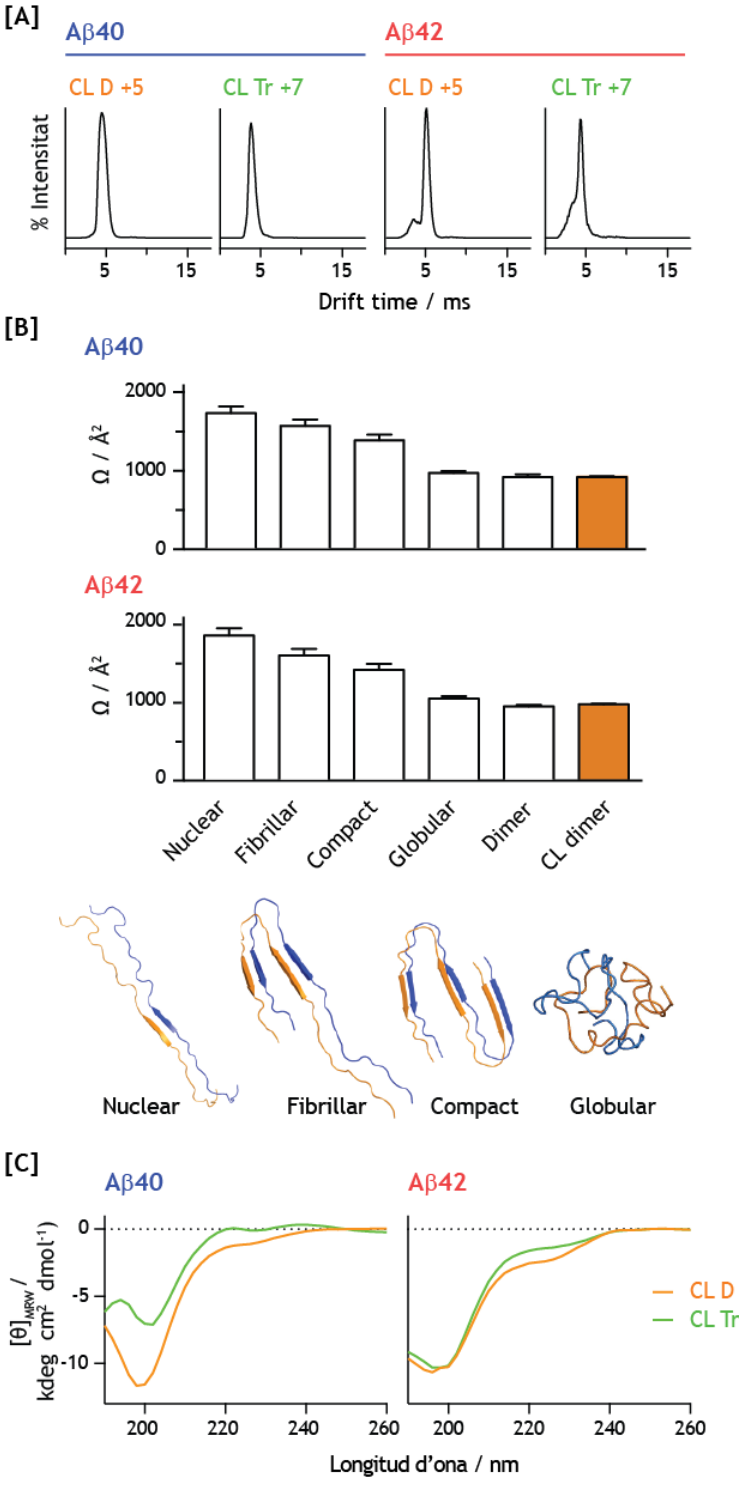


***Figura RC4.*** *Anàlisi estructural dels dímers i trímers covalents.* **[A]** *Projecció dels espectres d'ESI-IM-MS en el eix del drift time per m/z 1732 (D +5 Aβ40) i m/z 1856 (Tr +7 Aβ40), m/z 1806 (D +5 Aβ42) i m/z 1932 (Tr +7 Aβ42)* **[B]** *Gràfica comparativa dels valors de Ω obtinguts pels models teòrics prèviament descrits, pel model globular de les simulacions per dinàmica molecular i els valors experimentals dels dímers no covalents i covalents d'Aβ40 (superior) i d'Aβ42 (inferior). Representació de cada model (inferior).* **[C]** *Anàlisi de l'estructura secundària dels dímers (taronja) i trímers covalents (verd).*

En conjunt, hem determinat que Aβ40 i Aβ42 oligomeritzen inicialment a través de dímers i trímers globulars sense estructura secundària definida, per bé que Aβ42 té una major tendència a agregar.

## 2. Discussió

Per tal d'estudiar els oligòmers de baix pes molecular que es formen en els estadiatges inicials de l'agregació d'Aβ, hem optimizat la reacció de PICUP i hem implementat una reacció dirigida a reduir l'oxidació col·lateral de la metionina-35. Un cop hem obtingut els oligòmers covalents ben definits químicament, hem procedit a aïllar-los mitjançant cromatografia d'exclusió molecular obtenint uns cromatogrames en els que s'observa que Aβ42 té una major tendència a agregar que Aβ40. Simulant les condicions de SDS-PAGE, hem aplicat un tractament desnaturalitzant previ a la SEC que indica que les mostres d'Aβ40 i Aβ42 sotmeses a la reacció de PICUP estan composades per una mateixa distribució de monòmers a tetràmers. Un cop aïllats, l'anàlisi dels dímers i trímers purs per SDS-PAGE demostra que aquesta tècnica proporciona artefactes en l'anàlisi d'Aβ42. D'altra banda, l'anàlisi d'aquests mateixos dímers i trímers purs per ESI-IM-MS, MD i CD mostra que aquests oligòmers de baix pes molecular tenen una forma globular sense estructura secundària definida.

Alguns estudis ja han deixat constància de la particular relació entre Aβ42 i SDS. En aquests estudis es reporta com SDS és capaç de fomentar l'agregació d'Aβ42, així com també la seva capacitat per induir la formació d'oligòmers d'Aβ42 d'estructura definida. En el cas de l'estudi d'Aβ42 mitjançant SDS-PAGE, canvis en la polaritat o la llargada de l'extrem C-terminal d'Aβ42 semblen interrompre aquesta tendència a generar artefactes. Per tant, aquestes evidències indiquen que SDS podria induir o estabilitzar una interacció Aβ42-Aβ42 a través dels seus extrems C-terminals.

Ambdós Aβ40 i Aβ42 oligomeritzen a través de dímers i trímers globulars sense estructura secundària definida, per bé que Aβ42 té una major tendència a agregar que Aβ40. Aquest patró d'agregació ja estava descrit per Aβ40, en canvi l'anàlisi per SDS-PAGE d'Aβ42 indicava que oligomeritzava a través de pentàmers i hexàmers. Després de deixar patent que pentàmers i hexàmers són artefactes generats per SDS-PAGE, es pot assumir que Aβ40 i Aβ42 oligomeritzen a través dels mateixos intermedis. Per contra, no es pot excloure que PICUP no hagi sigut capaç de capturar espècies de major pes molecular. De totes maneres, la manca de diferències en la distribució d'oligòmers per SEC entre Aβ40 i Aβ42 no deixa dubte que no hi ha un oligòmer d'estequiometria o abundància particular que diferenciï els seus patrons

d'agregació. De fet, no hi ha cap element d'estructura secundària ni es detecta l'aparició d'algun tipus d'oligòmer diferent dels dímers i trímers que expliqui la major tendència d'agregació que mostra Aβ42 en front Aβ40.

## Apèndix A. La neurotoxicitat dels dímers covalents d'Aβ

En els últims 20 anys, la neurotoxicitat d'Aβ s'ha associat de manera independent a tres possibles mecanismes. Alguns estudis indiquen que Aβ exerceix la seva toxicitat pertorbant la membrana cel·lular, a través de la formació de porus o bé directament permeabilitzant-la. Un segon mecanisme s'ha focalitzat en la interacció específica d'Aβ amb receptors de les sinapsis neuronals. El tercer mecanisme s'ha centrat en Aβ com el desencadenant de la disfunció de tau i la seva posterior acumulació en la seva variant híperfosforilada, que en última instància determina la mort cel·lular. En termes generals, el fet que s'hagin identificat i validat mecanismes de neurotoxicitat independents podria indicar que Aβ exerceix la seva toxicitat a través de múltiples mecanismes de manera simultània. Per tal d'avaluar aquesta neurotoxicitat s'han proposat i emprat una gran varietat d'assajos, des dels que avaluen la citotoxicitat en termes generals, fins als que determinen l'efecte neurotòxic a nivell de sinapsi neuronal.

Recentment, Shankar *et al* van reportar la neurotoxicitat de dímers obtinguts d'extractes de cervell de malalts de la MA, que mostraven resistència a la desnaturalització per SDS. D'altra banda, el mecanisme de PICUP procedeix a través dels mateixos intermedis que el mecanisme mitjançant el que les espècies reactives d'oxigen podrien generar oligòmers covalents d'Aβ *in vivo*. La rellevància dels nostres oligòmers covalents en el context de la MA seria notòria si es confirmés la seva presència en el cervell de malalts de la MA i si aquests mostressin neurotoxicitat.

La neurotoxicitat dels nostres dímers covalents d'Aβ es va avaluar en cultius neuronals o neuroglials primaris mitjançant tres assajos diferents. Cada un dels assajos es va dur a terme (i) avaluant la toxicitat amb diferents marcadors, (ii) introduint diferents concentracions de dímer i (iii) determinant l'efecte tòxic en el conjunt del cultiu o bé individualment, cèl·lula a cèl·lula.

El primer assaig es va dur a terme a concentracions de dímer covalent d'Aβ40 de l'ordre de micromolar i la toxicitat es va determinar a partir del assaig clàssic de MTT. Tres assajos independents van mostrar que els dímers eren tòxics per les neurones a aquestes concentracions. De totes maneres, no vam poder excloure que

el resultat fos un artefacte de la interacció de les molècules de MTT amb Aß, tal i com s'ha reportat anteriorment a la literatura, o bé que la toxicitat fos causada per les impureses introduïdes amb els dímers com a resultat del seu procés de purificació.

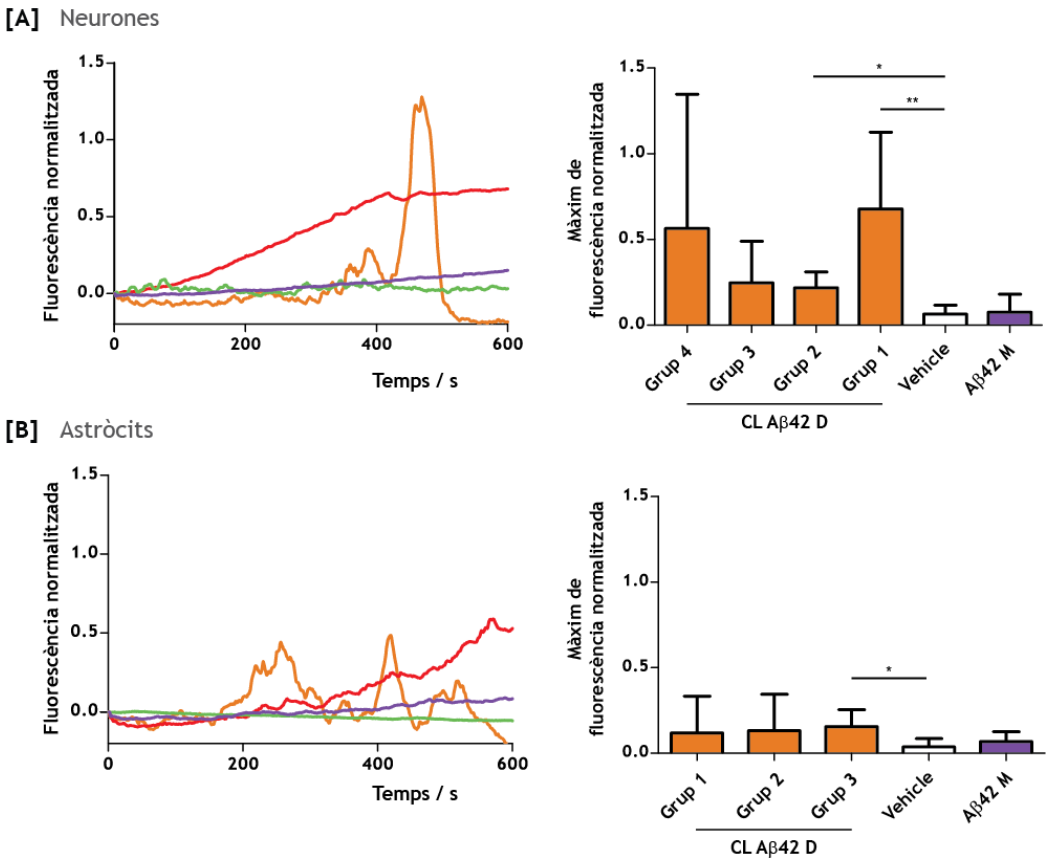


***Figura RC5.*** *Assajos de toxicitat del dímer covalent d'Aß42 en cultius neuroglials. El dímer s'administra mitjançant SICM i el marcador de toxicitat és l'influx intracel·lular de calci, mesurat a partir del fluoròfor Fluo4 sensible a calci que han internalitzat les cèl·lules.* **[A]** *Traces de fluorescència representatives de l'influx de calci en* ***neurones*** *induït pel vehicle (verd), el monòmer d'Aß42 (violeta) i el dímer covalent d'Aß42 (taronja i vermell). La traça en taronja representa un influx de calci oscil·lant, la traça en vermell correspon a un increment de calci intracel·lular gradual. Les columnes representen la mitjana ± desviació estàndard de la màxima fluorescència assolida per cada grup independent de cèl·lules. Grups 1-4 (taronja) corresponen a l'administració de dímer covalent Aß42, vehicle (blanc) i monòmer Aß42 (violeta).* **[B]** *Traces de fluorescència representatives de l'influx de calci en* ***astròcits*** *induït pel vehicle (verd), el monòmer d'Aß42 (violeta) i el dímer covalent d'Aß42 (taronja-oscil·lant i vermell-increment). Les columnes representen la mitjana ± desviació estàndard de la màxima fluorescència assolida per cada grup independent de cèl·lules. Grups 1-3 (taronja) corresponen a l'administració de dímer covalent Aß42, vehicle (blanc) i monòmer Aß42 (violeta). Les diferències significatives estan indicades amb asteriscs (p-value < 0.1 és *, p-value < 0.01 és **).*

El segon assaig va consistir en la introducció del dímer covalent d'Aß40 a concentracions de l'ordre de nanomolar i la toxicitat es va estudiar mitjançant l'assaig de XTT, alternativa al MTT que no s'ha reportat que interaccioni amb Aß generant artefactes. En aquest cas, els dímers no van ser tòxics per a les neurones.

El tercer assaig va avaluar la toxicitat dels dímers covalents d'Aß42 a concentracions de l'ordre de nanomolar. Aquests dímers van ser subministrats individualment, cèl·lula a cèl·lula, mitjançant la tècnica Scanning Ion Conductance Microscopy (de les sigles en anglès SICM) i el marcador de toxicitat va ser la inducció d'influx de calci a nivell intracel·lular (Figura RC5). Els dímers van resultar ser tòxics a aquestes concentracions tant en neurones com en astròcits, tot i que hi va haver una gran variabilitat en termes de màxima concentració de calci intracel·lular per a cada una de les cèl·lules estudiades.

## Apèndix B. La modulació de l'agregació d'Aß40 en presència d'oligòmers covalents

Les malalties priòniques i la MA comparteixen alguns trets histopatològics tals com la mort neuronal o l'acumulació de proteïnes agregades en el cervell. És per això que en la última dècada s'han dedicat esforços en elucidar les connexions entre elles. El punt de connexió és la hipòtesi de que el mecanisme molecular subjacent és el mateix. En altres paraules, aquesta hipòtesi reivindica que la formació de plaques amiloides ve donada per la inducció del plegament *corrupte* d'Aß per part d'altres molècules d'Aß (llavors) que ja es troben plegades en la seva forma patològica. Aquesta connexió va emergir pel treball de Meyer-Luehmann *et al*, en el que s'injectava extractes de cervell de malalts de la MA o de ratolins transgènics adults amb plaques amiloides cerebrals, en el cervell dels mateixos ratolins transgènics, però joves i sans. Aquesta injecció induïa l'avançament de l'inici de la deposició de les plaques amiloides. De totes maneres, el que no explica aquesta hipòtesi és per què la resta de fenotips de la MA, com ara l'acumulació intracel·lular de cabdells neurofibril·lars o la pèrdua de les funcions cognitives, no es reprodueixen en aquests ratolins un cop han rebut la injecció.

Donada la possible rellevància dels nostres dímers covalents en la MA, es va plantejar si els nostres dímers covalents podien exercir de llavors d'agregació determinant una modulació de l'agregació d'Aß. És així com es van incubar dímers i trímers covalents d'Aß40 (Figura RC6-C) en quantitats subestequiomètriques en una solució monomèrica d'Aß40 acabada de purificar. Vam monitoritzar l'agregació

d'aquestes mostres per l'assaig de tioflavina (Figura RC6-B) i vam observar que efectivament dímers i trímers eren capaços de modular l'agregació d'Aß (Figura RC6-A). La presència de dímers covalents alentia la formació de fibres, mentre que la de trímers covalents frenava totalment la fibril·lació. Aquests resultats contrasten amb altres estudis en els que aquestes mateixes llavors, purificades mitjançant una altra metodologia, estimulen la fibril·lació. Es necessiten més assajos per confirmar els nostres resultats i per entendre per què no són consistents amb aquests altres estudis.

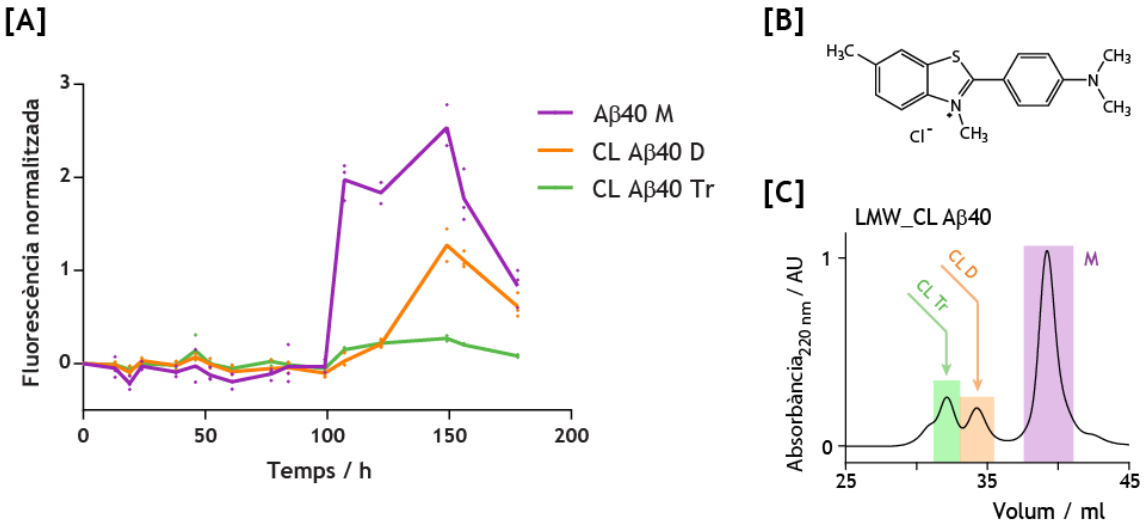


***Figura RC6.*** *Assaig de fluorescència de ThT.* **[A]** *Traces de fluorescència de ThT en funció del temps per la incubació de monòmer d'Aß40 en presència de dímers covalents d'Aß40 (D, taronja) i trímers covalents d'Aß40 (Tr, verd). L'addició de monòmer d'Aß40 (M, violeta) al mateix rati molar s'empra com a control negatiu. Cada mesura per triplicat s'indica amb punts i la línia uneix la mitjana de cada mesura.* **[B]** *Estructura molecular de la ThT.* **[C]** *Obtenció dels monòmers, dímers covalents i trímers covalents d'Aß40 mitjançant SEC amb tractament desagregant previ.*

# References

1. Haass, C. & Selkoe, D.J. Soluble protein oligomers in neurodegeneration: lessons from the Alzheimer's amyloid beta-peptide. *Nat Rev Mol Cell Biol* **8**, 101-12 (2007).

2. Jakob-Roetne, R. & Jacobsen, H. Alzheimer's disease: from pathology to therapeutic approaches. *Angew Chem Int Ed Engl* **48**, 3030-59 (2009).

3. Tanzi, R.E. The genetics of Alzheimer's disease. *Cold Spring Harb Perspect Med* **2**(2012).

4. Dementia: A public health priority. *World health organization and Alzheimer's disease international* (2012).

5. Small, D.H. & Cappai, R. Alois Alzheimer and Alzheimer's disease: a centennial perspective. *J Neurochem* **99**, 708-10 (2006).

6. Glenner, G.G. & Wong, C.W. Alzheimer's disease: initial report of the purification and characterization of a novel cerebrovascular amyloid protein. *Biochem Biophys Res Commun* **120**, 885-90 (1984).

7. Masters, C.L. et al. Amyloid plaque core protein in Alzheimer's disease and Down's syndrome. *Proc Natl Acad Sci U S A* **82**, 4245-9 (1985).

8. Grundke-Iqbal, I. et al. Abnormal phosphorylation of the microtubule-associated protein tau in Alzheimer cytoskeletal pathology. *Proc Natl Acad Sci U S A* **83**, 4913-7 (1986).

9. Hardy, J.A. & Higgins, G.A. Alzheimer's disease: the amyloid cascade hypothesis. *Science* **256**, 184-5 (1992).

10. Mandelkow, E.M. & Mandelkow, E. Tau as a marker for Alzheimer's disease. *Trends Biochem Sci* **18**, 480-3 (1993).

11. Jin, M. et al. Soluble amyloid beta-protein dimers isolated from Alzheimer cortex directly induce Tau hyperphosphorylation and neuritic degeneration. *Proc Natl Acad Sci U S A* **108**, 5819-24 (2011).

12. Ittner, L.M. et al. Dendritic function of tau mediates amyloid-beta toxicity in Alzheimer's disease mouse models. *Cell* **142**, 387-97 (2010).

13. Haass, C. Take five--BACE and the gamma-secretase quartet conduct Alzheimer's amyloid beta-peptide generation. *EMBO J* **23**, 483-8 (2004).

14. Masters, C.L. & Selkoe, D.J. Biochemistry of amyloid beta-protein and amyloid deposits in Alzheimer disease. *Cold Spring Harb Perspect Med* **2**, a006262 (2012).

15. McGowan, E. et al. Abeta42 is essential for parenchymal and vascular amyloid deposition in mice. *Neuron* **47**, 191-9 (2005).

16. Soscia, S.J. et al. The Alzheimer's disease-associated amyloid beta-protein is an antimicrobial peptide. *PLoS One* **5**, e9505 (2010).

17. Walsh, D.M. & Selkoe, D.J. A beta oligomers - a decade of discovery. *J Neurochem* **101**, 1172-84 (2007).

18. Ashe, K.H. & Zahs, K.R. Probing the biology of Alzheimer's disease in mice. *Neuron* **66**, 631-45 (2010).

19. Meyer-Luehmann, M. et al. Exogenous induction of cerebral beta-amyloidogenesis is governed by agent and host. *Science* **313**, 1781-4 (2006).

20. Selkoe, D.J. The molecular pathology of Alzheimer's disease. *Neuron* **6**, 487-98 (1991).

21. McLean, C.A. et al. Soluble pool of Abeta amyloid as a determinant of severity of neurodegeneration in Alzheimer's disease. *Ann Neurol* **46**, 860-6 (1999).

22. Lue, L.F. et al. Soluble amyloid beta peptide concentration as a predictor of synaptic change in Alzheimer's disease. *Am J Pathol* **155**, 853-62 (1999).

23. Price, J.L. et al. Neuropathology of nondemented aging: presumptive evidence for preclinical Alzheimer's disease. *Neurobiol Aging* **30**, 1026-36 (2009).

24. Blennow, K., Mattsson, N., Scholl, M., Hansson, O. & Zetterberg, H. Amyloid biomarkers in Alzheimer's disease. *Trends Pharmacol Sci* **36**, 297-309 (2015).

25. Brinkmalm, A. et al. Explorative and targeted neuroproteomics in Alzheimer's disease. *Biochim Biophys Acta* **1854**, 769-778 (2015).

26. Perrin, R.J., Fagan, A.M. & Holtzman, D.M. Multimodal techniques for diagnosis and prognosis of Alzheimer's disease. *Nature* **461**, 916-22 (2009).

27. Bennett, D.A. et al. Neuropathology of older persons without cognitive impairment from two community-based studies. *Neurology* **66**, 1837-44 (2006).

28. Rosen, C., Hansson, O., Blennow, K. & Zetterberg, H. Fluid biomarkers in Alzheimer's disease - current concepts. *Mol Neurodegener* **8**, 20 (2013).

29. Mangialasche, F., Solomon, A., Winblad, B., Mecocci, P. & Kivipelto, M. Alzheimer's disease: clinical trials and drug development. *Lancet Neurol* **9**, 702-16 (2010).

30. Selkoe, D.J. The therapeutics of Alzheimer's disease: where we stand and where we are heading. *Ann Neurol* **74**, 328-36 (2013).

31. Cummings, J.L., Morstorf, T. & Zhong, K. Alzheimer's disease drug-development pipeline: few candidates, frequent failures. *Alzheimers Res Ther* **6**, 37 (2014).

32. Doody, R.S., Aisen, P.S. & Iwatsubo, T. Semagacestat for treatment of Alzheimer's disease. *N Engl J Med* **369**, 1661 (2013).

33. Wisniewski, T. & Goni, F. Immunotherapeutic approaches for Alzheimer's disease. *Neuron* **85**, 1162-76 (2015).

34. Watt, A.D. et al. Do current therapeutic anti-Abeta antibodies for Alzheimer's disease engage the target? *Acta Neuropathol* **127**, 803-10 (2014).

35. Bemporad, F. & Chiti, F. Protein misfolded oligomers: experimental approaches, mechanism of formation, and structure-toxicity relationships. *Chem Biol* **19**, 315-27 (2012).

36. Knowles, T.P., Vendruscolo, M. & Dobson, C.M. The amyloid state and its association with protein misfolding diseases. *Nat Rev Mol Cell Biol* **15**, 384-96 (2014).

37. Lambert, M.P. et al. Diffusible, nonfibrillar ligands derived from Abeta1-42 are potent central nervous system neurotoxins. *Proc Natl Acad Sci U S A* **95**, 6448-53 (1998).

38. Walsh, D.M. et al. Amyloid beta-protein fibrillogenesis. Structure and biological activity of protofibrillar intermediates. *J Biol Chem* **274**, 25945-52 (1999).

39. Hoshi, M. et al. Spherical aggregates of beta-amyloid (amylospheroid) show high neurotoxicity and activate tau protein kinase I/glycogen synthase kinase-3beta. *Proc Natl Acad Sci U S A* **100**, 6370-5 (2003).

40. Walsh, D.M. et al. Naturally secreted oligomers of amyloid beta protein potently inhibit hippocampal long-term potentiation in vivo. *Nature* **416**, 535-9 (2002).

41. Lesne, S. et al. A specific amyloid-beta protein assembly in the brain impairs memory. *Nature* **440**, 352-7 (2006).

42. Shankar, G.M. et al. Amyloid-beta protein dimers isolated directly from Alzheimer's brains impair synaptic plasticity and memory. *Nat Med* **14**, 837-42 (2008).

43. Bernstein, S.L. et al. Amyloid-beta protein oligomerization and the importance of tetramers and dodecamers in the aetiology of Alzheimer's disease. *Nat Chem* **1**, 326-31 (2009).

44. Lasagna-Reeves, C.A., Glabe, C.G. & Kayed, R. Amyloid-beta annular protofibrils evade fibrillar fate in Alzheimer's disease brain. *J Biol Chem* **286**, 22122-30 (2011).

45. Jan, A., Hartley, D.M. & Lashuel, H.A. Preparation and characterization of toxic Abeta aggregates for structural and functional studies in Alzheimer's disease research. *Nat Protoc* **5**, 1186-209 (2010).

46. Bitan, G. et al. Amyloid beta -protein (Abeta) assembly: Abeta 40 and Abeta 42 oligomerize through distinct pathways. *Proc Natl Acad Sci U S A* **100**, 330-5 (2003).

47. Kloniecki, M. et al. Ion mobility separation coupled with MS detects two structural states of Alzheimer's disease Abeta1-40 peptide oligomers. *J Mol Biol* **407**, 110-24 (2011).

48. Clore, G.M. Seeing the invisible by paramagnetic and diamagnetic NMR. *Biochem Soc Trans* **41**, 1343-54 (2013).

49. Fandrich, M., Schmidt, M. & Grigorieff, N. Recent progress in understanding Alzheimer's beta-amyloid structures. *Trends Biochem Sci* **36**, 338-45 (2011).

50. Sachse, C. et al. Quaternary structure of a mature amyloid fibril from Alzheimer's Abeta(1-40) peptide. *J Mol Biol* **362**, 347-54 (2006).

51. Zhang, R. et al. Interprotofilament interactions between Alzheimer's Abeta1-42 peptides in amyloid fibrils revealed by cryoEM. *Proc Natl Acad Sci U S A* **106**, 4653-8 (2009).

52. Petkova, A.T. et al. Self-propagating, molecular-level polymorphism in Alzheimer's beta-amyloid fibrils. *Science* **307**, 262-5 (2005).

53. Paravastu, A.K., Leapman, R.D., Yau, W.M. & Tycko, R. Molecular structural basis for polymorphism in Alzheimer's beta-amyloid fibrils. *Proc Natl Acad Sci U S A* **105**, 18349-54 (2008).

54. Xiao, Y. et al. Abeta(1-42) fibril structure illuminates self-recognition and replication of amyloid in Alzheimer's disease. *Nat Struct Mol Biol* **22**, 499-505 (2015).

55. Johnson, R.D., Steel, D.G. & Gafni, A. Structural evolution and membrane interactions of Alzheimer's amyloid-beta peptide oligomers: new knowledge from single-molecule fluorescence studies. *Protein Sci* **23**, 869-83 (2014).

56. Serra-Vidal, B. et al. Hydrogen/deuterium exchange-protected oligomers populated during Abeta fibril formation correlate with neuronal cell death. *ACS Chem Biol* **9**, 2678-85 (2014).

57. Zhang, Y. et al. Pulsed hydrogen-deuterium exchange mass spectrometry probes conformational changes in amyloid beta (Abeta) peptide aggregation. *Proc Natl Acad Sci U S A* **110**, 14604-9 (2013).

58. Reinke, A.A. & Gestwicki, J.E. Insight into amyloid structure using chemical probes. *Chem Biol Drug Des* **77**, 399-411 (2011).

59. Rahimi, F., Shanmugam, A. & Bitan, G. Structure-function relationships of pre-fibrillar protein assemblies in Alzheimer's disease and related disorders. *Curr Alzheimer Res* **5**, 319-41 (2008).

60. Hayden, E.Y. & Teplow, D.B. Amyloid beta-protein oligomers and Alzheimer's disease. *Alzheimers Res Ther* **5**, 60 (2013).

61. Sohma, Y. et al. 'Click peptide': a novel 'O-acyl isopeptide method' for peptide synthesis and chemical biology-oriented synthesis of amyloid beta peptide analogues. *J Pept Sci* **12**, 823-8 (2006).

62. Zarandi, M. et al. Synthesis of Abeta[1-42] and its derivatives with improved efficiency. *J Pept Sci* **13**, 94-9 (2007).

63. Chemuru, S., Kodali, R. & Wetzel, R. Improved chemical synthesis of hydrophobic Abeta peptides using addition of C-terminal lysines later removed by carboxypeptidase B. *Biopolymers* **102**, 206-21 (2014).

64. Walsh, D.M. et al. A facile method for expression and purification of the Alzheimer's disease-associated amyloid beta-peptide. *FEBS J* **276**, 1266-81 (2009).

65. Finder, V.H., Vodopivec, I., Nitsch, R.M. & Glockshuber, R. The recombinant amyloid-beta peptide Abeta1-42 aggregates faster and is more neurotoxic than synthetic Abeta1-42. *J Mol Biol* **396**, 9-18 (2010).

66. Hellstrand, E., Boland, B., Walsh, D.M. & Linse, S. Amyloid beta-protein aggregation produces highly reproducible kinetic data and occurs by a two-phase process. *ACS Chem Neurosci* **1**, 13-8 (2010).

67. Saito, T. et al. Potent amyloidogenicity and pathogenicity of Abeta43. *Nat Neurosci* **14**, 1023-32 (2011).

68. Thal, D.R., Walter, J., Saido, T.C. & Fandrich, M. Neuropathology and biochemistry of Abeta and its aggregates in Alzheimer's disease. *Acta Neuropathol* **129**, 167-82 (2015).

69. Benilova, I., Karran, E. & De Strooper, B. The toxic Abeta oligomer and Alzheimer's disease: an emperor in need of clothes. *Nat Neurosci* **15**, 349-57 (2012).

70. Teplow, D.B. On the subject of rigor in the study of amyloid beta-protein assembly. *Alzheimers Res Ther* **5**, 39 (2013).

71. Marcoux, J. & Robinson, C.V. Twenty years of gas phase structural biology. *Structure* **21**, 1541-50 (2013).

72. Bernstein, S.L. et al. Amyloid beta-protein: monomer structure and early aggregation states of Abeta42 and its Pro19 alloform. *J Am Chem Soc* **127**, 2075-84 (2005).

73. Smith, D.P., Radford, S.E. & Ashcroft, A.E. Elongated oligomers in beta2-microglobulin amyloid assembly revealed by ion mobility spectrometry-mass spectrometry. *Proc Natl Acad Sci U S A* **107**, 6794-8 (2010).

74. Teplow, D.B. et al. Elucidating amyloid beta-protein folding and assembly: A multidisciplinary approach. *Acc Chem Res* **39**, 635-45 (2006).

75. Murray, M.M. et al. Amyloid beta protein: Abeta40 inhibits Abeta42 oligomerization. *J Am Chem Soc* **131**, 6316-7 (2009).

76. Pujol-Pina, R., and Vilaprinyó-Pascual, S. et al. SDS-PAGE analysis of Abeta oligomers is disserving research into Alzheimer's disease: a call for ESI-IM-MS. *Sci Rep* (under revisions).

77. Rappsilber, J. The beginning of a beautiful friendship: cross-linking/mass spectrometry and modelling of proteins and multi-protein complexes. *J Struct Biol* **173**, 530-40 (2011).

78. Fancy, D.A. & Kodadek, T. Chemistry for the analysis of protein-protein interactions: rapid and efficient cross-linking triggered by long wavelength light. *Proc Natl Acad Sci U S A* **96**, 6020-4 (1999).

79. Bitan, G. & Teplow, D.B. Rapid photochemical cross-linking--a new tool for studies of metastable, amyloidogenic protein assemblies. *Acc Chem Res* **37**, 357-64 (2004).

80. Bitan, G. Structural study of metastable amyloidogenic protein oligomers by photo-induced cross-linking of unmodified proteins. *Methods Enzymol* **413**, 217-36 (2006).

81. Ono, K., Condron, M.M. & Teplow, D.B. Structure-neurotoxicity relationships of amyloid beta-protein oligomers. *Proc Natl Acad Sci U S A* **106**, 14745-50 (2009).

82. Bitan, G., Fradinger, E.A., Spring, S.M. & Teplow, D.B. Neurotoxic protein oligomers--what you see is not always what you get. *Amyloid* **12**, 88-95 (2005).

83. Rangachari, V. et al. Amyloid-beta(1-42) rapidly forms protofibrils and oligomers by distinct pathways in low concentrations of sodium dodecylsulfate. *Biochemistry* **46**, 12451-62 (2007).

84. Watt, A.D. et al. Oligomers, fact or artefact? SDS-PAGE induces dimerization of beta-amyloid in human brain samples. *Acta Neuropathol* **125**, 549-64 (2013).

85. Fawzi, N.L., Ying, J., Torchia, D.A. & Clore, G.M. Probing exchange kinetics and atomic resolution dynamics in high-molecular-weight complexes using dark-state exchange saturation transfer NMR spectroscopy. *Nat Protoc* **7**, 1523-33 (2012).

86. Fawzi, N.L., Ying, J., Torchia, D.A. & Clore, G.M. Kinetics of amyloid beta monomer-to-oligomer exchange by NMR relaxation. *J Am Chem Soc* **132**, 9948-51 (2010).

87. Fawzi, N.L., Ying, J., Ghirlando, R., Torchia, D.A. & Clore, G.M. Atomic-resolution dynamics on the surface of amyloid-beta protofibrils probed by solution NMR. *Nature* **480**, 268-72 (2011).

88. Dukes, K.D., Rodenberg, C.F. & Lammi, R.K. Monitoring the earliest amyloid-beta oligomers via quantized photobleaching of dye-labeled peptides. *Anal Biochem* **382**, 29-34 (2008).

89. Ding, H., Wong, P.T., Lee, E.L., Gafni, A. & Steel, D.G. Determination of the oligomer size of amyloidogenic protein beta-amyloid(1-40) by single-molecule spectroscopy. *Biophys J* **97**, 912-21 (2009).

90. Narayan, P. et al. The extracellular chaperone clusterin sequesters oligomeric forms of the amyloid-beta(1-40) peptide. *Nat Struct Mol Biol* **19**, 79-83 (2012).

91. Calamai, M. & Pavone, F.S. Single molecule tracking analysis reveals that the surface mobility of amyloid oligomers is driven by their conformational structure. *J Am Chem Soc* **133**, 12001-8 (2011).

92. Narayan, P. et al. Single molecule characterization of the interactions between amyloid-beta peptides and the membranes of hippocampal cells. *J Am Chem Soc* **135**, 1491-8 (2013).

93. Chang, C.C. et al. Synergistic interactions between Alzheimer's Abeta40 and Abeta42 on the surface of primary neurons revealed by single molecule microscopy. *PLoS One* **8**, e82139 (2013).

94. Ganzinger, K.A. et al. Single-molecule imaging reveals that small amyloid-beta1-42 oligomers interact with the cellular prion protein (PrP(C)). *Chembiochem* **15**, 2515-21 (2014).

95. Kaminski Schierle, G.S. et al. In situ measurements of the formation and morphology of intracellular beta-amyloid fibrils by super-resolution fluorescence imaging. *J Am Chem Soc* **133**, 12902-5 (2011).

96. Esbjorner, E.K. et al. Direct observations of amyloid beta self-assembly in live cells provide insights into differences in the kinetics of Abeta(1-40) and Abeta(1-42) aggregation. *Chem Biol* **21**, 732-42 (2014).

97. Konermann, L., Vahidi, S. & Sowole, M.A. Mass spectrometry methods for studying structure and dynamics of biological macromolecules. *Anal Chem* **86**, 213-32 (2014).

98. Carulla, N., Zhou, M., Giralt, E., Robinson, C.V. & Dobson, C.M. Structure and intermolecular dynamics of aggregates populated during amyloid fibril formation studied by hydrogen/deuterium exchange. *Acc Chem Res* **43**, 1072-9 (2010).

99. Kheterpal, I. & Wetzel, R. Hydrogen/deuterium exchange mass spectrometry--a window into amyloid structure. *Acc Chem Res* **39**, 584-93 (2006).

100. Luhrs, T. et al. 3D structure of Alzheimer's amyloid-beta(1-42) fibrils. *Proc Natl Acad Sci U S A* **102**, 17342-7 (2005).

101. Olofsson, A., Sauer-Eriksson, A.E. & Ohman, A. The solvent protection of alzheimer amyloid-beta-(1-42) fibrils as determined by solution NMR spectroscopy. *J Biol Chem* **281**, 477-83 (2006).

102. Yu, L. et al. Structural characterization of a soluble amyloid beta-peptide oligomer. *Biochemistry* **48**, 1870-7 (2009).

103. Sanchez, L. et al. Abeta40 and Abeta42 amyloid fibrils exhibit distinct molecular recycling properties. *J Am Chem Soc* **133**, 6505-8 (2011).

104. Carulla, N. et al. Molecular recycling within amyloid fibrils. *Nature* **436**, 554-8 (2005).

105. Urbanc, B. et al. Neurotoxic effects of thioflavin S-positive amyloid deposits in transgenic mice and Alzheimer's disease. *Proc Natl Acad Sci U S A* **99**, 13990-5 (2002).

106. Busche, M.A. et al. Clusters of hyperactive neurons near amyloid plaques in a mouse model of Alzheimer's disease. *Science* **321**, 1686-9 (2008).

107. Meyer-Luehmann, M. et al. Rapid appearance and local toxicity of amyloid-beta plaques in a mouse model of Alzheimer's disease. *Nature* **451**, 720-4 (2008).

108. Spires-Jones, T.L. et al. Impaired spine stability underlies plaque-related spine loss in an Alzheimer's disease mouse model. *Am J Pathol* **171**, 1304-11 (2007).

109. Koffie, R.M. et al. Oligomeric amyloid beta associates with postsynaptic densities and correlates with excitatory synapse loss near senile plaques. *Proc Natl Acad Sci U S A* **106**, 4012-7 (2009).

110. Hong, S. et al. Dynamic analysis of amyloid beta-protein in behaving mice reveals opposing changes in ISF versus parenchymal Abeta during age-related plaque formation. *J Neurosci* **31**, 15861-9 (2011).

111. Xue, W.F. et al. Fibril fragmentation enhances amyloid cytotoxicity. *J Biol Chem* **284**, 34272-82 (2009).

112. Saido, T. & Leissring, M.A. Proteolytic degradation of amyloid beta-protein. *Cold Spring Harb Perspect Med* **2**, a006379 (2012).

113. Shen, Y., Joachimiak, A., Rosner, M.R. & Tang, W.J. Structures of human insulin-degrading enzyme reveal a new substrate recognition mechanism. *Nature* **443**, 870-4 (2006).

114. Malito, E., Hulse, R.E. & Tang, W.J. Amyloid beta-degrading cryptidases: insulin degrading enzyme, presequence peptidase, and neprilysin. *Cell Mol Life Sci* **65**, 2574-85 (2008).

115. Mukherjee, A. et al. Insulysin hydrolyzes amyloid beta peptides to products that are neither neurotoxic nor deposit on amyloid plaques. *J Neurosci* **20**, 8745-9 (2000).

116. Mok, Y.F. & Howlett, G.J. Sedimentation velocity analysis of amyloid oligomers and fibrils. *Methods Enzymol* **413**, 199-217 (2006).

117. Stine, W.B., Jr., Dahlgren, K.N., Krafft, G.A. & LaDu, M.J. In vitro characterization of conditions for amyloid-beta peptide oligomerization and fibrillogenesis. *J Biol Chem* **278**, 11612-22 (2003).

118. Hoshino, M., Hidenori, K., Yamaguchi, K. & Goto, Y. Dimethylsulfoxide-quenched hydrogen/deuterium exchange method to study amyloid fibril structure. *Biochim Biophys Acta* **1768**, 1886-1899 (2007).

119. Kheterpal, I., Zhou, S., Cook, K.D. & Wetzel, R. Abeta amyloid fibrils possess a core structure highly resistant to hydrogen exchange. *Proc Natl Acad Sci U S A* **97**, 13597-601 (2000).

120. Englander, S.W. & Kallenbach, N.R. Hydrogen exchange and structural dynamics of proteins and nucleic acids. *Q Rev Biophys* **16**, 521-655 (1983).

121. Hvidt, A. & Nielsen, S.O. Hydrogen exchange in proteins. *Adv Protein Chem* **21**, 287-386 (1966).

122. Chesneau, V. & Rosner, M.R. Functional human insulin-degrading enzyme can be expressed in bacteria. *Protein Expr Purif* **19**, 91-8 (2000).

123. Arimon, M., Grimminger, V., Sanz, F. & Lashuel, H.A. Hsp104 targets multiple intermediates on the amyloid pathway and suppresses the seeding capacity of Abeta fibrils and protofibrils. *J Mol Biol* **384**, 1157-73 (2008).

124. Berrow, N.S. et al. A versatile ligation-independent cloning method suitable for high-throughput expression screening applications. *Nucleic Acids Res* **35**, e45 (2007).

125. Neant-Fery, M. et al. Molecular basis for the thiol sensitivity of insulin-degrading enzyme. *Proc Natl Acad Sci U S A* **105**, 9582-7 (2008).

126. Copeland, R.A. *Enzymes: A practical Introduction to Structure, Mechanism, and Data Analysis*, (Wiley-VCH, New York (USA), 2000).

127. Leissring, M.A. et al. Kinetics of amyloid beta-protein degradation determined by novel fluorescence- and fluorescence polarization-based assays. *J Biol Chem* **278**, 37314-20 (2003).

128. Welzel, A.T. et al. Secreted amyloid beta-proteins in a cell culture model include N-terminally extended peptides that impair synaptic plasticity. *Biochemistry* **53**, 3908-21 (2014).

129. Klement, K. et al. Effect of different salt ions on the propensity of aggregation and on the structure of Alzheimer's abeta(1-40) amyloid fibrils. *J Mol Biol* **373**, 1321-33 (2007).

130. Bora, R.P. & Prabhakar, R. Elucidation of interactions of Alzheimer amyloid beta peptides (Abeta40 and Abeta42) with insulin degrading enzyme: a molecular dynamics study. *Biochemistry* **49**, 3947-56 (2010).

131. Kheterpal, I., Wetzel, R. & Cook, K.D. Enhanced correction methods for hydrogen exchange-mass spectrometric studies of amyloid fibrils. *Protein Sci* **12**, 635-43 (2003).

132. Fancy, D.A. Elucidation of protein-protein interactions using chemical cross-linking or label transfer techniques. *Curr Opin Chem Biol* **4**, 28-33 (2000).

133. Nickel, U. et al. Mechanisms and Kinetics of the Photocatalyzed Oxidation of p-Phenylenediamines by Peroxydisulfate in the Presence of Tri-2,2'-bipyridylylruthenium (II). *J Phys Chem* **98**, 2883-2888 (1994).

134. Teplow, D.B. Preparation of amyloid beta-protein for structural and functional studies. *Methods Enzymol* **413**, 20-33 (2006).

135. Walsh, D.M., Lomakin, A., Benedek, G.B., Condron, M.M. & Teplow, D.B. Amyloid beta-protein fibrillogenesis. Detection of a protofibrillar intermediate. *J Biol Chem* **272**, 22364-72 (1997).

136. Hackenberger, C.P. The reduction of oxidized methionine residues in peptide thioesters with NH4I-Me2S. *Org Biomol Chem* **4**, 2291-5 (2006).

137. Selkoe, D.J., Abraham, C.R., Podlisny, M.B. & Duffy, L.K. Isolation of low-molecular-weight proteins from amyloid plaque fibers in Alzheimer's disease. *J Neurochem* **46**, 1820-34 (1986).

138. Barghorn, S. et al. Globular amyloid beta-peptide oligomer - a homogenous and stable neuropathological protein in Alzheimer's disease. *J Neurochem* **95**, 834-47 (2005).

139. Pujol-Pina, R. Estudi d'espècies oligomèriques solubles de la proteïna beta-amiloide, relacionada amb la malaltia d'Alzheimer. *Doctoral thesis* (2012).

140. Reinke, A.A., Ung, P.M., Quintero, J.J., Carlson, H.A. & Gestwicki, J.E. Chemical probes that selectively recognize the earliest Abeta oligomers in complex mixtures. *J Am Chem Soc* **132**, 17655-7 (2010).

141. Petkova, A.T., Yau, W.M. & Tycko, R. Experimental constraints on quaternary structure in Alzheimer's beta-amyloid fibrils. *Biochemistry* **45**, 498-512 (2006).

142. Ahmed, M. et al. Structural conversion of neurotoxic amyloid-beta(1-42) oligomers to fibrils. *Nat Struct Mol Biol* **17**, 561-7 (2010).

143. Haupt, C. et al. Structural basis of beta-amyloid-dependent synaptic dysfunctions. *Angew Chem Int Ed Engl* **51**, 1576-9 (2012).

144. Arcella, A. et al. Structure and dynamics of oligonucleotides in the gas phase. *Angew Chem Int Ed Engl* **54**, 467-71 (2015).

145. Koistinen, V.U. Hepatitis B surface antigen polypeptides: artifactual bands in sodium dodecyl sulfate-polyacrylamide gel electrophoresis caused by aggregation. *J Virol* **35**, 20-3 (1980).

146. Serra-Bastiste, M. et al. Micelles promote Ab42 assembly into pore-forming oligomers. *In Preparation*.

147. Bitan, G. et al. A molecular switch in amyloid assembly: Met35 and amyloid beta-protein oligomerization. *J Am Chem Soc* **125**, 15359-65 (2003).

148. Seilheimer, B. et al. The toxicity of the Alzheimer's beta-amyloid peptide correlates with a distinct fiber morphology. *J Struct Biol* **119**, 59-71 (1997).

149. Varadarajan, S., Kanski, J., Aksenova, M., Lauderback, C. & Butterfield, D.A. Different mechanisms of oxidative stress and neurotoxicity for Alzheimer's A beta(1--42) and A beta(25--35). *J Am Chem Soc* **123**, 5625-31 (2001).

150. Hou, L., Kang, I., Marchant, R.E. & Zagorski, M.G. Methionine 35 oxidation reduces fibril assembly of the amyloid abeta-(1-42) peptide of Alzheimer's disease. *J Biol Chem* **277**, 40173-6 (2002).

151. Maiti, P., Lomakin, A., Benedek, G.B. & Bitan, G. Despite its role in assembly, methionine 35 is not necessary for amyloid beta-protein toxicity. *J Neurochem* **113**, 1252-62 (2010).

152. Mannini, B. et al. Toxicity of protein oligomers is rationalized by a function combining size and surface hydrophobicity. *ACS Chem Biol* **9**, 2309-17 (2014).

153. Lendel, C. et al. A hexameric peptide barrel as building block of amyloid-beta protofibrils. *Angew Chem Int Ed Engl* **53**, 12756-60 (2014).

154. Kondo, T. et al. Modeling Alzheimer's disease with iPSCs reveals stress phenotypes associated with intracellular Abeta and differential drug responsiveness. *Cell Stem Cell* **12**, 487-96 (2013).

155. Benilova, I. & De Strooper, B. Neuroscience. Promiscuous Alzheimer's amyloid: yet another partner. *Science* **341**, 1354-5 (2013).

156. Demuro, A. et al. Calcium dysregulation and membrane disruption as a ubiquitous neurotoxic mechanism of soluble amyloid oligomers. *J Biol Chem* **280**, 17294-300 (2005).

157. Demuro, A., Smith, M. & Parker, I. Single-channel Ca(2+) imaging implicates Abeta1-42 amyloid pores in Alzheimer's disease pathology. *J Cell Biol* **195**, 515-24 (2011).

158. Smith, D.P. et al. Copper-mediated amyloid-beta toxicity is associated with an intermolecular histidine bridge. *J Biol Chem* **281**, 15145-54 (2006).

159. Snyder, E.M. et al. Regulation of NMDA receptor trafficking by amyloid-beta. *Nat Neurosci* **8**, 1051-8 (2005).

160. Li, S. et al. Soluble oligomers of amyloid Beta protein facilitate hippocampal long-term depression by disrupting neuronal glutamate uptake. *Neuron* **62**, 788-801 (2009).

161. Townsend, M., Shankar, G.M., Mehta, T., Walsh, D.M. & Selkoe, D.J. Effects of secreted oligomers of amyloid beta-protein on hippocampal synaptic plasticity: a potent role for trimers. *J Physiol* **572**, 477-92 (2006).

162. Lauren, J., Gimbel, D.A., Nygaard, H.B., Gilbert, J.W. & Strittmatter, S.M. Cellular prion protein mediates impairment of synaptic plasticity by amyloid-beta oligomers. *Nature* **457**, 1128-32 (2009).

163. Kim, T. et al. Human LilrB2 is a beta-amyloid receptor and its murine homolog PirB regulates synaptic plasticity in an Alzheimer's model. *Science* **341**, 1399-404 (2013).

164. Kayed, R. & Lasagna-Reeves, C.A. Molecular mechanisms of amyloid oligomers toxicity. *J Alzheimers Dis* **33 Suppl 1**, S67-78 (2013).

165. Zempel, H., Thies, E., Mandelkow, E. & Mandelkow, E.M. Abeta oligomers cause localized Ca(2+) elevation, missorting of endogenous Tau into dendrites, Tau phosphorylation, and destruction of microtubules and spines. *J Neurosci* **30**, 11938-50 (2010).

166. Shipton, O.A. et al. Tau protein is required for amyloid {beta}-induced impairment of hippocampal long-term potentiation. *J Neurosci* **31**, 1688-92 (2011).

167. Deshpande, A., Mina, E., Glabe, C. & Busciglio, J. Different conformations of amyloid beta induce neurotoxicity by distinct mechanisms in human cortical neurons. *J Neurosci* **26**, 6011-8 (2006).

168. Noguchi, A. et al. Isolation and characterization of patient-derived, toxic, high mass amyloid beta-protein (Abeta) assembly from Alzheimer disease brains. *J Biol Chem* **284**, 32895-905 (2009).

169. Kuperstein, I. et al. Neurotoxicity of Alzheimer's disease Abeta peptides is induced by small changes in the Abeta42 to Abeta40 ratio. *EMBO J* **29**, 3408-20 (2010).

170. Matsumura, S. et al. Two distinct amyloid beta-protein (Abeta) assembly pathways leading to oligomers and fibrils identified by combined fluorescence correlation spectroscopy, morphology, and toxicity analyses. *J Biol Chem* **286**, 11555-62 (2011).

171. Wogulis, M. et al. Nucleation-dependent polymerization is an essential component of amyloid-mediated neuronal cell death. *J Neurosci* **25**, 1071-80 (2005).

172. Kayed, R. et al. Common structure of soluble amyloid oligomers implies common mechanism of pathogenesis. *Science* **300**, 486-9 (2003).

173. Jan, A. & Lashuel, H.A. Establishing the links between Abeta aggregation and cytotoxicity in vitro using biophysical approaches. *Methods Mol Biol* **849**, 227-43 (2012).

174. Liu, Y. & Schubert, D. Cytotoxic amyloid peptides inhibit cellular 3-(4,5-dimethylthiazol-2-yl)-2,5-diphenyltetrazolium bromide (MTT) reduction by enhancing MTT formazan exocytosis. *J Neurochem* **69**, 2285-93 (1997).

175. Jan, A., Gokce, O., Luthi-Carter, R. & Lashuel, H.A. The ratio of monomeric to aggregated forms of Abeta40 and Abeta42 is an important determinant of amyloid-beta aggregation, fibrillogenesis, and toxicity. *J Biol Chem* **283**, 28176-89 (2008).

176. Hartley, D.M. et al. Transglutaminase induces protofibril-like amyloid beta-protein assemblies that are protease-resistant and inhibit long-term potentiation. *J Biol Chem* **283**, 16790-800 (2008).

177. Cleary, J.P. et al. Natural oligomers of the amyloid-beta protein specifically disrupt cognitive function. *Nat Neurosci* **8**, 79-84 (2005).

178. Bezprozvanny, I. & Mattson, M.P. Neuronal calcium mishandling and the pathogenesis of Alzheimer's disease. *Trends Neurosci* **31**, 454-63 (2008).

179. Wu, H.Y. et al. Amyloid beta induces the morphological neurodegenerative triad of spine loss, dendritic simplification, and neuritic dystrophies through calcineurin activation. *J Neurosci* **30**, 2636-49 (2010).

180. Gotz, J., Chen, F., van Dorpe, J. & Nitsch, R.M. Formation of neurofibrillary tangles in P301l tau transgenic mice induced by Abeta 42 fibrils. *Science* **293**, 1491-5 (2001).

181. Stadtman, E.R. Protein oxidation and aging. *Free Radic Res* **40**, 1250-8 (2006).

182. Little, M.J., Aubry, N., Beaudoin, M.E., Goudreau, N. & LaPlante, S.R. Quantifying trifluoroacetic acid as a counterion in drug discovery by 19F NMR and capillary electrophoresis. *J Pharm Biomed Anal* **43**, 1324-30 (2007).

183. Narayan, P. et al. Rare individual amyloid-beta oligomers act on astrocytes to initiate neuronal damage. *Biochemistry* **53**, 2442-53 (2014).

184. Piper, J.D. et al. Characterization and application of controllable local chemical changes produced by reagent delivery from a nanopipet. *J Am Chem Soc* **130**, 10386-93 (2008).

185. Babakinejad, B. et al. Local delivery of molecules from a nanopipette for quantitative receptor mapping on live cells. *Anal Chem* **85**, 9333-42 (2013).

186. Klenerman, D., Shevchuk, A., Novak, P., Korchev, Y.E. & Davis, S.J. Imaging the cell surface and its organization down to the level of single molecules. *Philos Trans R Soc Lond B Biol Sci* **368**, 20120027 (2013).

187. O'Nuallain, B. et al. Amyloid beta-protein dimers rapidly form stable synaptotoxic protofibrils. *J Neurosci* **30**, 14411-9 (2010).

188. Walker, L.C. & Jucker, M. Neurodegenerative Diseases: Expanding the Prion Concept. *Annu Rev Neurosci* (2015).

189. Jucker, M. & Walker, L.C. Pathogenic protein seeding in Alzheimer disease and other neurodegenerative disorders. *Ann Neurol* **70**, 532-40 (2011).

190. Jucker, M. & Walker, L.C. Self-propagation of pathogenic protein aggregates in neurodegenerative diseases. *Nature* **501**, 45-51 (2013).

191. Walker, L.C. & Jucker, M. Seeds of dementia. *Sci Am* **308**, 52-7 (2013).

192. Walker, L.C., Diamond, M.I., Duff, K.E. & Hyman, B.T. Mechanisms of protein seeding in neurodegenerative diseases. *JAMA Neurol* **70**, 304-10 (2013).

193. Fritschi, S.K. et al. Abeta seeds resist inactivation by formaldehyde. *Acta Neuropathol* **128**, 477-84 (2014).

194. Stohr, J. et al. Purified and synthetic Alzheimer's amyloid beta (Abeta) prions. *Proc Natl Acad Sci U S A* **109**, 11025-30 (2012).

195. Aguzzi, A. & Calella, A.M. Prions: protein aggregation and infectious diseases. *Physiol Rev* **89**, 1105-52 (2009).

196. Watts, J.C. et al. Serial propagation of distinct strains of Abeta prions from Alzheimer's disease patients. *Proc Natl Acad Sci U S A* **111**, 10323-8 (2014).

197. Lu, J.X. et al. Molecular structure of beta-amyloid fibrils in Alzheimer's disease brain tissue. *Cell* **154**, 1257-68 (2013).

198. Langer, F. et al. Soluble Abeta seeds are potent inducers of cerebral beta-amyloid deposition. *J Neurosci* **31**, 14488-95 (2011).

199. Eisele, Y.S. et al. Induction of cerebral beta-amyloidosis: intracerebral versus systemic Abeta inoculation. *Proc Natl Acad Sci U S A* **106**, 12926-31 (2009).